UNIVERSITY OF HELSINKI REPORT SERIES IN PHYSICS

HU-P-D71

Study of Rare Decays of the b Quark with the DELPHI Detector at LEP

Marco Battaglia

Department. of Physics, University of Helsinki
and Helsinki Institute of Physics
P.O. Box 9, FIN-00014 University of Helsinki, Finland

ACADEMIC DISSERTATION

To be presented, with the permission of the Faculty of Science of the University of Helsinki, for public criticism in the Small Hall of the University Main Building, on March 11th, 1999, at 10 o'clock.

Helsinki 1999

ISBN 951-45-8183-0
ISSN 0356-0961

Helsinki 1999
Yliopistopaino

M. Battaglia: Study of Rare Decays of the b quark with the DELPHI detector at LEP, University of Helsinki, 1999, v, 124 p, University of Helsinki, Report Series in Physics, HU-P-D71, ISSN 0356-0961, ISBN 951-45-8183-0.

Abstract

The b quark is the heaviest fermion producing bound hadronic states. The study of their production and decays provides important data for the understanding of the processes responsible for the weak decays of fundamental fermions. In addition, due to the small value of the $|V_{cb}|$ element, suppressed and rare $b \to u$ and $b \to s$, d transitions are not completely obliterated by the CKM favoured $b \to c$ decays. This makes B hadrons an ideal laboratory for the study of rare decay processes. The sensitivity of these decays to the Standard Model structure, through suppressions proportional to the square of the elements in the quark mixing matrix and through loops that may reveal contributions of new particles, opens a new window on precision tests of the Standard Model and also on possible new physics beyond it.

The DELPHI detector, equipped with a precise silicon vertex tracker surrounding the beam interaction region and with Ring Imaging CHerenkov (RICH) detectors providing efficient hadron identification, at the LEP e^+e^- collider, is well suited for precise studies of B decays. This thesis presents the results of the analysis of the data collected with DELPHI at centre-of-mass energies around the Z^0 pole from 1990 to 1995 for the studies of rare decays of beauty hadrons. These studies have promoted the development of new techniques for the topological reconstruction of the B decay chain and for hadron identification based on the response of the RICH detectors.

Rare decays of the b quarks have been studied in several decay processes. Tree level $b \to u$ transitions have been studied mainly in the semileptonic $b \to u\ell\nu$ channel. A new technique that discriminate them from the favoured $b \to c$ transitions based on the reconstructed mass of the hadronic system recoiling against the lepton has been developed and applied. Evidence for the decay has been obtained and its rate has been used to extract an accurate determination of the $|V_{ub}|$ element in the quark mixing matrix. Hadronic charmless decays proceeding through both the tree level $b \to u$ but also the loop mediated $b \to s$ transitions have been studied in several exclusive final states. Evidence for rare hadronic charmless decays has been obtained by the observation of eight fully reconstructed candidate events in two body final states. The fraction of events with one charged kaon has been determined from a fit to the RICH and TPC dE/dx response and the total invariant mass. In addition the $B_{d,s} \to K^+\pi^-$ decay has been observed for the first time and its branching ratio has been measured. These results represent the first experimental evidence of the contribution of loop mediated $b \to s$ transition to B hadronic decays and acquires a special importance in the interpretation of CP violation in the B system at future dedicated B physics experiments. Signal for the $b \to sg$, $b \to s\gamma$ and $b \to s\nu\bar{\nu}$ transitions have also been searched for. No evidence for these decays has been obtained and upper limits have been derived. These upper limits set significant constraints on several scenarios for new physics beyond the Standard Model that are discussed also in relation to the direct searches being presently carried out in the high energy runs of the LEP collider (LEP 2).

Foreword

This thesis summarises the main results of my research activity, carried out as member of the DELPHI Collaboration, at CERN in Geneva (Switzerland) from 1993 to 1998. During these years I was associated to the Research Institute for High Energy Physics in Finland (SEFT), later become Helsinki Institute of Physics (HIP), under the direction of Risto Orava who followed and supported my activities and who has been my supervisor in the preparation of this dissertation. I would like to express my highest gratitude to him.

The studies discussed in this document range from the characterisation of the response of subsystems of the DELPHI detector to the physics analyses and the interpretation of their results. These subsystem are the silicon Vertex Detector and the Ring Imaging CHerenkov detector that became the key devices for the reconstruction and analysis of e^+e^- collision events in the study of rare decays of the b quark.

I devoted most of my time over the past years to these tasks. However I am conscious that I could not achieve these results without the cooperation with the many colleagues with whom I shared the interest and enthusiasm for particle physics and development of data analysis techniques. I am grateful to them all.

Peter M. Kluit, Dietrich Liko and Kenneth Österberg have been trusting me for working together on several of the analyses that are reported in this thesis. Over the years, I learned to appreciate them as friends at least as much as colleagues.

Peter Weilhammer first, Martyn Davenport and Olaf Ullaland later, taught me how to share expertise and responsibilities between the physics analysis and the detector operation groups. I remember the time shared between the DELPHI experimental hall for the detector maintenance and my office for the data analyses as, probably, the most inspiring and rewarding.

Walter Venus, Daniel Treille and Patrick Roudeau encouraged and followed my activities on rare B decays in DELPHI, also delegating me part of the responsibility for their organisation.

Ahmed Ali, Ikaros Bigi, Antonio Masiero and Matthias Neubert provided important theoretical background in the definition and interpretation of the physics analyses in several meetings and conversations.

I also would like to acknowledge the contributions and ideas from Wolfgang Adam, Gerald, Eigen, Gian Giudice, Christoph Greub, Katri Huitu, Alex Kagan, David Lange, Karen Lingel, Enrico Piotto, Ritchie Patterson, Michael Peskin, Anders Ryd, Achille Stocchi, Nikolai Uraltsev and Stephan Willocq.

While writing this thesis, I have greatly appreciated the suggestions from Risto Orava and the comments from Masud Chaichian, Heimo Saarikko, Katri Huitu and Kenneth Österberg. They all helped me in shaping this dissertation from a rather wide collection of published papers.

Despite all the advises and help by my supervisor, collegues and friends, I would not be in the position of submitting this Academic Dissertation without the constant love, care and support received from my family, despite our physical distance. It is therefore to my parents, Isa and Ignazio, that this thesis is dedicated.

Marco Battaglia

Geneva, 24 January 1999

Contents

Introduction 3

Theory of b quark Decays 5

1 Rare Decays of B hadrons in Standard Model 5
- 1.1 The CKM Mixing Matrix . . . 5
- 1.2 Rare B Decay Processes . . . 7
  - 1.2.1 Tree level B Decays . . . 10
  - 1.2.2 Loop mediated B Decays . . . 16

Experimental Techniques in the Study of B Decays 25

2 Heavy Flavour Physics with the DELPHI Detector at LEP 26
- 2.1 The DELPHI detector at LEP . . . 27
  - 2.1.1 Tracking Detectors . . . 28
  - 2.1.2 The Microvertex Detector . . . 29
  - 2.1.3 The Calorimeters . . . 32
  - 2.1.4 The Ring Imaging CHerenkov Detector . . . 33
- 2.2 B decay reconstruction . . . 39
  - 2.2.1 Track Impact Parameter and $Z^0 \to b\bar{b}$ Tagging . . . 39
  - 2.2.2 Topological reconstruction of B decays . . . 45
  - 2.2.3 Particle Identification with DELPHI . . . 47

Experimental Results on Rare b Decays 57

3 Semileptonic $b \to u$ Decays 58
- 3.1 Determination of $|V_{ub}|/|V_{cb}|$ . . . 60
  - 3.1.1 Data Analysis . . . 60
  - 3.1.2 Results and Discussion . . . 64

4 Hadronic Charmless b Decays 75
- 4.1 Exclusive $B \to n\pi$, $Kn\pi$ Decays . . . 76
  - 4.1.1 Data Analysis . . . 76
  - 4.1.2 Results . . . 78
  - 4.1.3 Discussion . . . 81
- 4.2 Inclusive $b \to sg$ Decays . . . 87
  - 4.2.1 The Kaon p_t Analysis . . . 88

4.2.2 The Impact Parameter Analysis 91
4.2.3 Conclusion 92

5 Radiative and Dincutrino Charmless b Decays **95**
5.1 $b \to s\gamma$ Decays 95
5.1.1 Data Analysis 96
5.1.2 Inclusive $b \to s\gamma$ 99
5.1.3 Exclusive $B^0 \to K^*\gamma$, $\phi\gamma$ 101
5.2 Dineutrino charmless decays 103
5.2.1 Event reconstruction 103
5.2.2 Results 104
5.2.3 Conclusion 106

6 Rare b Decays and New Physics beyond Standard Model **109**
6.1 Limits on Charged Higgs Bosons from $b \to s\gamma$ 110
6.1.1 Two Higgs Doublet Model (2HDM) 111
6.1.2 Charged Higgs Bosons in MSSM 112
6.1.3 Comparison with Limits from Direct Searches 114
6.2 Additional Constraints to SuperSymmetry from $b \to s$ *gluon* 116
6.3 Constraints on a new $U(1)$ Gauge Boson from $b \to s\nu\bar{\nu}$ 117

Conclusions **121**

Introduction

One century has passed since the first discovery of an elementary particle. The experiment of Thomson, giving the first experimental evidence for the electron in 1897, opened the way for modern science in the study of the fundamental constituents of matter. Inheriting, through Newton, the concept of the existence of indivisible building blocks of matter from the atomism of Democritus, today's high energy particle physics probes the mechanisms of production and decay of elementary particles and their electromagnetic, weak and strong interactions. Electromagnetic interactions have been well evident in the physics phenomenology since long and weak interactions were first revealed by radioactivity through β decays observed at the beginning of the century. Finally, strong interactions, responsible for the binding of quarks into protons and neutrons, have been probed only more recently with high energy particle accelerators.

An organic description of these interactions is presently encoded in the so-called Standard Model. The studies of cosmic rays first and of the interactions of beams of particles from accelerators later have revealed a complex spectrum of particles with masses ranging from vanishing values for the neutrinos up to more than 100 times the proton mass for the top quark. There are two groups of established elementary particles: the quarks and the leptons. Quarks carry fractional charge, in electron charge units, and are the constituents of protons and neutrons as well as of heavier hadrons as those considered in the following. Leptons, as the electron and the neutrinos, and quarks are spin 1/2 particles and are organised in three generations. Each generation consists of one charged lepton (e^-, μ^-, τ^-) and its neutrino (ν_e, ν_μ and ν_τ) and a doublet of quarks ((u,d), (c,s) and (t,b)) with increasing masses. Quarks and leptons interact by exchanging spin-1 gauge bosons. $W^\pm$ and Z^0 bosons mediate the weak interaction, photons carry the electro-magnetic interaction and gluons the strong interaction. The Standard Model is the gauge field theory describing these three fundamental forces acting on quarks and leptons based on the $SU(2) \times U(1) \times SU(3)$ group representation. The dimensions of the adjoint representation of the group correspond to the number of gauge bosons carrying the force. Strong interactions are described by quantum chromodynamics (QCD). The symmetry between electromagnetic and weak interactions is broken as manifested by the fact that photons are massless while the W and Z bosons are among the heaviest known particles. This symmetry breaking is realised by the so-called Higgs mechanism that introduces a scalar field developing a non-zero vacuum expectation value. The W and Z bosons acquire mass from their couplings with this field, while the photons and gluons are left massless. Quarks and leptons also acquire mass from their couplings with the scalar Higgs field.

The discoveries of the neutral currents mediated by Z bosons in 1973, of the W and Z bosons themselves in 1983, both performed at CERN, the recent direct observation of the top quark, at the mass predicted in the framework of the Standard Model, at Fermilab and the high precision tests performed in the study of Z and W boson decays, all represent a significant validation of the theory. However, despite all these successes the present picture of elementary particle physics remains incomplete. The origin of masses is described in terms of the electroweak symmetry breaking whose signature, the existence of the Higgs boson, has so far eluded the searches performed at LEP-2 and at the Tevatron. The hierarchy of fermion masses and of their weak couplings are also not yet understood. The questions about the underlying physics

of fermion mass generation are often referred to as the *"flavour problem"*. The Standard Model is also challenged by cosmological problems related with the nature of dark matter and with the apparent abundance of matter over antimatter in the Universe. Several extensions of the Standard Model have been proposed in order to answer these questions and also to incorporate the unification of the four known fundamental forces in the theory. In particular many elements of the Higgs mechanism for the electro-weak symmetry breaking can be retained when assuming the existence in Nature of a new symmetry between bosons and fermions known as Supersymmetry. Supersymmetric extensions of the Standard Model (SUSY) have received considerable attention, particularly in relation with the definition of unified theories. It has been shown that the coupling constants of electro-magnetic, weak and strong interactions cannot all come to coincide at a common value, at any energy scale, unless many new particles are added to the theory as in Supersymmetry. Massive supersymmetric partners of the known particles, may also represent the bulk of the mass of the Universe, thus solving the dark matter problem. In parallel with these theoretical developments, a broad range of experimental activities has been aimed to discover possible signals of new physics beyond the Standard Model. Every year, the international conferences on high energy physics provide increasingly precise tests of the validity of the Standard Model and limits derived from the searches for these so-far-unseen new phenomena. The study of decays of hadrons containing the heavy b quark represents a crucial part of this programme.

The beauty quark b is the heaviest fermion producing bound hadronic states. Whatever is the mechanism of generating fermion masses, it implies a stronger coupling to the heavy b quark, compared to the lighter u, d, s, and c quarks, making its study essential in the understanding of the flavour problem. Furthermore, the study of the production and decay of beauty hadrons provides important data for the understanding of the processes responsible for the weak decays of fundamental fermions. Finally, due to the small value of the $|V_{cb}|$ element, suppressed and rare $b \to u$ and $b \to s$, d transitions are not completely obliterated by the CKM favoured $b \to c$ decays. This makes B hadrons an ideal laboratory for the study of rare processes in Standard Model and for the search of possible signals of new physics beyond it.

In the perspective of fundamental tests of the Standard Model, the detailed study of CP violation in the B system acquires a special relevance. While the CPT symmetry is expected to be conserved in elementary particle interactions, CP asymmetries may result from the interference of phases that change sign under the CP operator. The only occurrence of CP violation observed so far concerns the K_L^0 decays, first reported in $K_L^0 \to \pi^+\pi^-$by Christenson, Cronin, Fitch and Turlay in 1964 at Brookhaven and still presently under study at CERN and at Fermilab . This feature of weak hadron decays shows that *"at some tiny level there is a fundamental asymmetry between matter and antimatter and (...) that interactions will show an asymmetry under the reversal of time"*. At present this *"cryptic message from nature"*, as in the words of one of its discoverers, still awaits to be fully deciphered. CP violation can be accommodated in the Standard Model by the appearance of a phase in the weak mixing matrix in presence of three or more generations of fermions. However CP violation may also be a signal of new physics. This can be in the form of a new superweak interaction or in that of either an extended Higgs sector consisting of two Higgs doublets or Supersymmetry. CP violation is one of the three conditions necessary to generate an asymmetry between the number of baryons and antibaryons in the early Universe, as first pointed out by Sakharov. However, the Standard Model mechanism for CP violation is not efficient enough to explain the manifest dominance of matter over antimatter in our Universe, making the introduction of new physics a suggestive scenario to solve the baryogenesis problem. The direct determination of the CP violating phases in the decays of beauty mesons, expected to be large, will clarify if the Standard Model fully accounts for the origin of CP asymmetries or if a new source of CP violation must be searched beyond it and if this is related with the matter-antimatter asymmetry in the Universe.

Studies in B physics have been actively carried out, since the end of the 70's, at low energy e^+e^- colliders. The ARGUS and CLEO experiments collected data at the $\Upsilon(4S)$ resonance, just above the threshold for $B\bar{B}$ production. MAC, MARK II and TASSO performed their studies at higher energies profiting of a moderate boost of the produced B hadrons. With the start of the LEP collider at CERN and SLC at SLAC, providing collisions at centre-of-mass energies corresponding to the Z^0 mass new perspectives in B physics were opened. The LEP collider delivered e^+e^- collisions at centre-of-mass energies around the Z^0 peak from 1989 to 1995. During this period more than 3 M Z^0 decays have been recorded by each of the experiments surrounding the four interaction regions of the collider corresponding to more than 1 M beauty hadron decays. The productions of all the B hadron species, the large boost of the B hadrons produced and the confinement of the B and $\bar{B}$ decay products in well separated hadronic jets, specific of $Z^0 \to b\bar{b}$ decays, represent significant advantages in B physics studies at LEP that are complementary to those performed at lower energy e^+e^- colliders like the CESR ring at Cornell. The DELPHI detector, equipped with a high resolution vertex detector and efficient particle identification ensured by its Ring Imaging Cherenkov detectors, has carried out a detailed programme of studies of the weak decays of beauty hadrons. The search and study of rare B decays, an important part of this programme, has provided with signals of rare B decays in semi-leptonic and hadronic modes, the world most precise determination of the $|V_{ub}|$ element in the quark mixing matrix and tight constraints on several decay modes sensitive to possible new physics beyond the Standard Model.

This thesis presents the results obtained in the studies of rare B decays to which I participated, together with the relevant event reconstruction and data analysis techniques that I contributed in developing as a member of the DELPHI Collaboration. These results have been the subject of several original publications referenced through the thesis. Selected papers are also summarised at the beginning of the relevant sections. While already interesting in themselves for the clarification of several aspects of weak b decays and the validation of new particle detection techniques, these results acquire a special relevance in the perspective of the next generations of dedicated B physics experiments at e^+e^- colliding B-factories, like PEP-II and KEK-B that are already being commissioned, or at hadron machines, like the LHC under construction at CERN.

The plan of this thesis is the following: the first chapter introduces the Cabibbo-Kobayashi-Maskawa quark mixing matrix and summarises the phenomenology of rare B decay transitions and their modelling. Chapter 2 reviews the experimental techniques developed for the analysis of the DELPHI data with special emphasis on the principles of operation of silicon microstrip sensors and Ring Imaging Cherenkov detectors and on the algorithms for the topological reconstruction of B decays. Chapters 3, 4 and 5 present the data analysis procedure and the results for three classes of rare decays. These are the measurement of $|V_{ub}|$ in semileptonic $b \to u$ decays, the study of hadronic charmless decays and the search for radiative $b \to s\gamma$ and dineutrino $b \to s\nu\bar{\nu}$ decays. These three classes of decays probe tree level $b \to u$ transitions, the magnitude of $|V_{ub}|$ and loop decays that are sensitive to the effects of both QCD corrections and possible new physics. The understanding of the contributions of tree level and loop transitions to hadronic charmless decays is also essential in the study of CP violation in the B system and the implications of the DELPHI results are discussed. The results obtained in these studies are compared with those reported by other collaborations both at LEP and at other accelerators. Finally, chapter 6 outlines the impact of all these results on the constraints on new physics beyond Standard Model also in comparison with the direct searches in the high energy program at LEP (LEP-2) and at the Tevatron at Fermilab.

Theory of b Quark Decays

Chapter 1

Rare Decays of B hadrons in Standard Model

1.1 The CKM Mixing Matrix

The Standard Model of electro-weak interactions (SM) describes flavour-changing quark transitions through a $V-A$ charged current operator coupled to the W boson according to the interaction Lagrangian:

$$L_{int} = -\frac{g}{\sqrt{2}}(\sum_{ij} \bar{u}_i \gamma^\mu \frac{1}{2}(1-\gamma_5) V_{ij} d_j W_\mu^+ + h.c.) \tag{1.1}$$

Quarks and leptons get their masses through Yukawa couplings Y_{jk}, Y'_{jk} involving a Higgs doublet field ϕ. After spontaneous symmetry breaking, the Lagrangian that couples the quarks to the Higgs field takes the form:

$$L_{Yukawa} = \sum_{j,k} [Y_{jk} \bar{u}_L^j u_R^k + Y'_{jk} \bar{d}_L^j d_R^k + h.c.] \frac{1}{\sqrt{2}}(v + H(x)) \tag{1.2}$$

where v is the Higgs vacuum expectation value, $H(x)$ the field corresponding to the Higgs boson and j,k are the flavour indexes. To determine the quark mass eigenstates it is necessary to diagonalise the mass matrices $m_{jk} = (-v/\sqrt{2})Y_{jk}$. Since the quark mass eigenstates d, s and b do not correspond to the weak interaction eigenstates d', s' and b', the V_{ij} elements of a $n_q \times n_q$ unitary matrix, where n_q is the number of quark families, relate these two bases through flavour non diagonal couplings:

$$\begin{pmatrix} d' \\ s' \\ b' \end{pmatrix} = \begin{pmatrix} V_{ud} & V_{us} & V_{ub} \\ V_{cd} & V_{cs} & V_{cb} \\ V_{td} & V_{ts} & V_{tb} \end{pmatrix} \begin{pmatrix} d \\ s \\ b \end{pmatrix} \tag{1.3}$$

This matrix is known as the Cabibbo-Kobayashi-Maskawa (CKM) mixing matrix [1, 2]. The flavour-changing charged current interactions of quarks are controlled by the entries of the CKM matrix. The diagonal elements that relate the favoured transitions $u \to d$, $c \to s$ and $t \to b$ are about unity. Elements away from the diagonal correspond to suppressed tree-level transitions, as the $b \to u$ process that is of special interest in the following. The values of the CKM elements, i.e. the strenght of the coupling between quarks of different species, are not predicted by the Standard Model similarly to the fermion masses and therefore they remain one of the SM features that still need to be fully understood. It can be shown that out of the $2n_q^2$ real parameters of the $n_q \times n_q$ matrix, only $(n_q-1)^2$ are independent. In the case of the 3×3 CKM matrix of

the Standard Model with three generations of fermions, there are four independent parameters. Together with the nine fermion masses, they account for 13 of the 18 free parameters of the theory. In the original parametrisation proposed by Kobayashi and Maskawa [2], these four parameters, three real rotation angles and a complex phase, have been expressed as the three angles θ_{12}, θ_{23}, θ_{13} and the phase δ_{13}. This extended to three quark families the parametrisation based on the introduction of the Cabibbo angle θ_C adopted for the 2×2 mixing matrix [1]. The appearence of a phase ensures that CP violating asymmetries, as observed in the neutral kaon system, can be accounted for in the Standard Model. Since the elements of the CKM mixing matrix are not predicted by the theory, it is of great importance to obtain precise determinations of their values. These are generally extracted by measuring decay rates that are proportional to the square of the $|V_{ij}|$ element of interest. The experimental status of the CKM matrix as of end of 1997, without assuming its unitarity, can be summarised as follows [3, 4]:

$$\begin{pmatrix} 0.9740 \pm 0.0010 & 0.2196 \pm 0.0023 & 0.0032 \pm 0.0008 \\ 0.224 \pm 0.016 & 1.04 \pm 0.16 & 0.0395 \pm 0.0017 \\ < 0.011 & \simeq 0.0395 & > 0.048 \end{pmatrix} \tag{1.4}$$

There have been alternative parametrisations of the 3×3 CKM mixing matrix; the one introduced by Wolfenstein [5] has recently become widely accepted for the representation of CP violation and of the matrix unitarity constraints. This parametrisation uses the four variables A, ρ, η and λ and takes $\lambda = \theta_C = |V_{us}|$ as an expansion parameter while η represents the CP-violating phase:

$$\begin{pmatrix} 1 - \frac{\lambda^2}{2} & \lambda & A\lambda^3(\rho - i\eta) \\ -\lambda & 1 - \frac{\lambda^2}{2} & A\lambda^2 \\ A\lambda^3(1 - \rho - i\eta) & -A\lambda^2 & 1 \end{pmatrix} + \mathcal{O}(\lambda^4) \tag{1.5}$$

The expansion can be continued to higher orders to obtain more accurate predictions [4]. The unitarity of the CKM matrix implies that the scalar product of a column with the complex conjugate of another column must vanish. Applying this prescription to the first and third columns of the CKM matrix gives:

$$V_{ud}V_{ub}^* + V_{cd}V_{cb}^* + V_{td}V_{tb}^* = 0 \tag{1.6}$$

Now, by using the Wolfenstein parametrisation and normalising each side by $|V_{cd}V_{cb}^*|$, this relation can be represented as a triangle in the ρ, η plane with vertices at $(0,0)$, $(1,0)$ and (ρ,η) with angles given by α, β and γ. For CP violation to be accomodated in Standard Model it is necessary that the area of the triangle is non zero or, in other words, that all the CKM elements are different from zero: in particular V_{ub} and V_{td} must be non zero. CP violation in the Standard Model arises when transitions i) with different phases or ii) with same phase but different amplitudes contribute to the same final state. If only one Standard Model decay amplitude dominates the decay channels, the three angles can be expressed as:

$$\alpha = arg(-\frac{V_{td}V_{tb}^*}{V_{ud}V_{ub}^*}) \tag{1.7}$$

$$\beta = arg(-\frac{V_{cd}V_{cb}^*}{V_{td}V_{tb}^*}) \tag{1.8}$$

$$\gamma = arg(-\frac{V_{ud}V_{ub}^*}{V_{cd}V_{cb}^*}) \tag{1.9}$$

Contribution from new physics to B transitions may shift the values of these angles and therefore being revealed by a careful analysis of CP asymmetries in B decays. Since quark mixing and CP violation are strictly connected with each other in the Standard Model, a detailed analysis

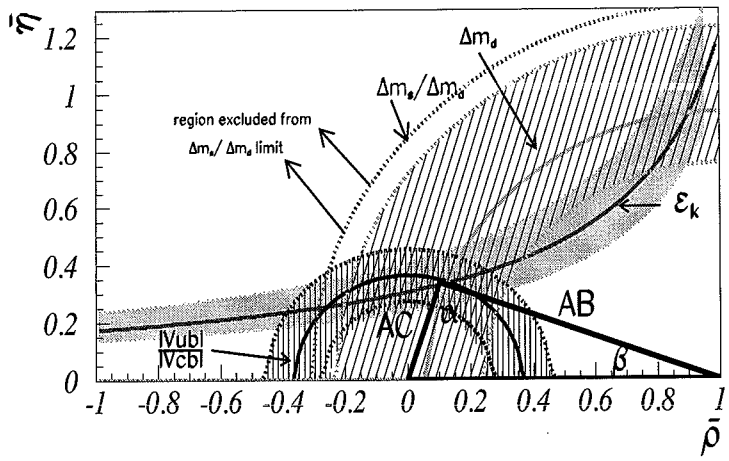

Figure 1.1: *The unitarity triangle and the constraints derived by present data on B and K decays (from ref. [8]).*

of the unitarity triangle will clarify if the non-zero value of the η phase in the CKM matrix is the only origin of CP violation and if the Standard Model offers a correct description of weak decays of hadrons. Present data on $|V_{ub}|$, $|V_{cb}|$, $B^0 - \bar{B}^0$ oscillations, CP violation in the K^0 system and rare K decays already provide significant constraints to the allowed region of the triangle vertex in the ρ, η plane (see Figure 1.1). There have been several of such analyses in recent years [6, 7, 8, 9]. Here these constraints are briefly discussed for the relevance of the measurements reported in the next chapters. The measurement of $|V_{cb}|$ sets the scale of the unitarity triangle $\lambda|V_{cb}| = \lambda^3 A$. The determination of $|V_{ub}|/|V_{cb}|$ defines the side AC of the triangle and its value represents a circle $\sqrt{\rho^2+\eta^2}$ in the ρ, η plane. The measurement of Δm_d from $B_d^0 - \bar{B}_d^0$ mixing and the limits on Δm_s from the search for $B_s^0 - \bar{B}_s^0$ oscillations can be used to constrain the value of $|V_{td}|$ and therefore of the side AB of the triangle. Finally the ϵ_K parameter derived by the observation of CP violation in $K^0 \to \pi\pi$ provides a further constraint on η in the form of a hyperbola in the ρ, η plane. The treatment of theoretical uncertainties in defining the allowed region of the triangle vertex is somehow controversial and different approaches have been proposed [8, 9].

Much of the studies in B physics of the present and future generation of experiments are devoted to the test of the unitarity triangle by determining its sides, as already discussed, and its angles (α, β and γ), measured at future experiments from the CP asymmetries in the B sector. These studies will clarify if the phenomenon of CP violation arises from the presence of a complex phase in the CKM matrix or has to be accounted as a signal of new physics beyond the Standard Model [10]

1.2 Rare B Decay Processes

The detailed study of the decay of b-flavoured hadrons provides data on the dynamics of the weak decay of the b quark and improves our knowledge of the couplings between quarks, formalised in the CKM mixing matrix. Decays of beauty hadrons proceed through three main mechanisms: i) tree level, ii) loop mediated and iii) annihilation and $W-$exchange. Decays of the first class

are pure spectator decays. This means that the light quark $\bar{q}$ in the B hadron does not play any direct role in the decay process that thus resembles that of a free b quark. Loop mediated $b \to s, d$ transitions are also mostly spectator processes, but gluonic decays may have interconnections between the gluon radiated and the light quark $\bar{q}$ as in the $b\bar{q} \to s\bar{q}$ processes discussed later. Finally annihilation and $W-$exchange diagrams are non-spectator processes in which the $b\bar{q}$ pair either annihilates into or exchanges a W boson.

Rare B decays are transitions either suppressed by the small coupling at the effective vertex or forbidden at tree level in Standard Model. The first category is exemplified by $b \to u$ tree level transitions suppressed by a $\frac{|V_{ub}|^2}{|V_{cb}|^2} \simeq 0.010$ factor compared to $b \to c$ decays while loop mediated decays exemplify a class of transitions, as $b \to s, d$, that are forbidden at tree level by the absence of flavour changing neutral currents in the Standard Model. These rare B decay modes are of great importance in the study of CP violation in the B sector and for their sensitivity to possible new physics that may reveal itself through its contribution to loop mediated transitions. The rare B decay modes that have been the subject of the experimental investigations reported in the following chapters belong to these two classes.

Rare decay modes are not exclusive of beauty hadrons and there exist important rare transitions of D and K mesons as well, as, for example, $K \to \pi\nu\bar{\nu}$. However the situation in the case of decays of B hadron is particularly favourable for their study. Since $m_t > m_b$, the b quark must decay into quarks outside its own generation. Therefore the CKM favoured B transition is $b \to c$ that proceeds proportionally to $|V_{cb}|^2 = 0.0016$. This is an exceptionally low value for a CKM allowed decay. For comparison in the charm sector, not only the CKM allowed $c \to s$ decays, that proceed within the same generation, are proportional to $|V_{cs}|^2 \simeq 1$ but also the off-diagonal $c \to d$ decays, with $|V_{cd}|^2 \simeq 0.048$, have a larger rate. This small value of $|V_{cb}|^2$ is also responsible for the long lifetime of B hadrons. As a consequence rare B decays are not completely obscured by the dominant $B \to DX$ decay modes. Having recorded samples of the order of 10^6 B decays each, CLEO at CESR and the ALEPH, DELPHI, L3 and OPAL experiments at LEP are sensitive to rare b decay channels with branching ratios in the range $10^{-4} - 10^{-5}$.

The relevance of experimental data on rare B decays for tests of the Standard Model and investigations of the dynamic of the weak decays of heavy hadrons largely depends on the reliability of the theoretical predictions in the framework of the Standard Model. There have been several different approaches for computing the expected branching ratios of exclusive and inclusive B decay modes including rare decays. To obtain the decay rate of a decay $B \to X$ it is necessary to compute the decay amplitude $M(B \to X)$. Computing this amplitude requires to consider the physics of processes at different energy scales μ, typically ranging from $\mu >> M_W$ down to $\mu \simeq \Lambda_{QCD}$ Since $m_b << M_W$, the typical exchanged momenta in the decay reaction are $p^2 << M_W^2$ and the decay can be described as a local interaction by an effective theory in which the masses of particles equal or larger than the M_W cut-off value have been removed. Following this approach, rates of many inclusive processes can be estimated by defining an effective Hamiltonian and using the operator product expansion (OPE) [11, 12] obtained by integrating away the top quark and the W heavy degrees of freedom. This effective hamiltonian H_{eff} can be written as:

$$H_{eff} = \frac{G_F}{\sqrt{2}}\left(\sum_{i=1}^{2} C_i(\mu)(V_{cb}^* V_{ud} Q_i^c + V_{ub}^* V_{ud} Q_i^u) - V_{tb}^* V_{ts} \sum_{i=3}^{8} C_i(\mu) O_i\right) + h.c. \qquad (1.10)$$

The four fermion operators O_1 and O_2 refer to tree level transitions while O_3 - O_8 describe penguin loop transitions. In this formulation the operators O_i represent the effective vertices and contain the long-distance effects while the Wilson coefficients $C_i(\mu)$ correspond to the effective couplings and encode the short-distance physics. In the full theory, the μ scale dependence in $C_i(\mu)$ is canceled out by that of the operators making $C_i O_i$ scale independent. In practice, the C_i coefficients are evaluated at a scale $\mu_W \simeq M_W >> m_b$ at the needed order in α_s. Since at

this scale the logaritms $log(\mu_W/M_W)$ are not large, the computation of the Wilson coefficients can be performed using perturbation theory. These coefficients need to be evolved from the scale μ_W down to the appropriate low energy scale $\mu \simeq m_b$. This is done by the renormalisation group equations. An exemplification of the application of this technique in the estimate of the decay branching ratio for the $b \to s\gamma$ transition is discussed in Section 1.2.2.

In exclusive B decays, bound state effects for semileptonic modes can be described by a single parameter, called form factor, as a function of the momentum transfer q^2 between the decaying and the produced hadrons. Heavy quark symmetry can be invoked in computing the form factors for $b \to c$ transitions [13]. Heavy quark symmetry is based on the observation that a beauty hadron consists of the heavy b quark and of quarks, antiquarks and gluons that can be considered as light degrees of freedom in the limit $m_b \to \infty$. In this limit, the light degrees of freedom only sense the heavy quark as a static colour source. At the time of the $b \to c\ell\nu$ transitions the heavy quark velocity changes from v to v', the leptons fly away undisturbed from the hadronic system and the light degrees of freedom rearrange themselves around the new colour source. This transition can be described by a form factor $\mathcal{F}(q^2)$ that is function of a universal probability function known as the Isgur and Wise function. In the zero recoil limit, the velocity of the b and c quark are the same $w = vv' = 1$ and the system is is seen as identical before and after the transition. This corresponds to the normalisation $\mathcal{F}(w = 1) = 1$. Heavy quark symmetry has been succesfully applied in the description of exclusive $b \to D\ell\nu$ decays. In the case of heavy-to-light transitions as $B \to \pi(\rho)\ell\nu$ decays, mediated by $b \to u\ell\nu$ transitions, heavy quark symmetry is less predictive since the u quark cannot be considered heavy in comparison to the QCD scale Λ_{QCD}. However significant progress has been recently made in the computation of the form factors for these reactions [14].

The treatment of exclusive hadronic decays is more heuristic since available QCD techniques do not yet allow computation of rates from first principles. In fact, the description of the final states for fully hadronic decays is complicated by non perturbative strong interaction effects. However, successful predictions of hadronic two body exclusive final states have been achieved by applying the factorization approximation. Factorization relies on the assumption that, due to the large energy release in the decay, the quark-antiquark pair produced in a colour singlet state by the virtual W and the quark coming from the b decay are emitted with large relative velocities so that they can be considered as two systems hadronising almost independently [15]. In this limit, the four quark matrix element for a decay like $B^0 \to D^{*+}\pi^-$, mediated by a $b \to c\bar{u}d$ transition, factorises in the product of two matrix elements, a heavy-to-heavy current matrix element $< D^{*+}|J_\mu|B^0 >$ and a vacuum-meson transition matrix element $< 0|A_\mu|\pi^- >$ similarly to the case of the semileptonic decay $B \to D^*\ell\nu$ that gives $< D^*|J_\mu|B^0 >< \nu|\gamma_\mu(1-\gamma_5)|\ell >$. A justification for this procedure comes from the observation that factorization follows to leading order in a $1/N_c$ expansion, where N_c is the number of colours [16]. Factorization can be invoked only for spectator decays. The model introduces two phenomenological parameters, denoted with a_1 and a_2, that replace the Wilson coefficients C_1 and C_2 of the OPE formalism. The two parameters a_1 and a_2 control processes that proceed through pure external or internal tree level level diagrams as in the case of $B \to D^{*+}\pi^-$ and $B \to J/\Psi K^-$ respectively. The values of a_1 and a_2 can be obtained from a fit to the measured branching ratios for exclusive hadronic two-body $b \to c$ transitions. Several tests of factorization have been performed and results have been found to be in reasonable agreement with the model predictions for a variety of B and D decay modes. A recent analysis of B decays gave the values $|a_1| = 1.07 \pm 0.07$ and $|a_2| = 0.23 \pm 0.02$ [17]. There is also indication that the sign of a_1 and a_2 are the same, i.e. internal and external diagrams have constructive interference. The factorization formalism has also been applied to heavy-to-light exclusive two-body transitions in which the B hadron decays into two light mesons as $B \to \pi\pi$. Multi-body final states cannot be easily treated with this formalism due to the presence of quark-antiquark pairs produced via gluons.

In the following, the estimates for rare tree level and penguin B decays in the Standard

model are discussed for the inclusive and exclusive final states that are the subject of the studies to be discussed in the following chapters.

1.2.1 Tree level B Decays

Rare tree level transitions are mostly represented by hadronic charmless decays as $B \to \pi\pi$ and semileptonic $b \to u\ell\nu$. Both of these decay modes are sensitive to the value of $|V_{ub}|^2$ in the CKM mixing matrix and the observation of either of those kinds of decays confirms the non-zero value of $|V_{ub}|$. However in hadronic decays the description of the final states is complicated by the non perturbative strong interaction effects. The extraction of $|V_{ub}|$ from hadronic decay modes is therefore affected by large theoretical uncertainties.

In semileptonic decays, bound state effects can be described by a single parameter, called form factor, as a function of the momentum transfer q^2 between the decaying and the produced hadrons. The study of inclusive semileptonic $b \to u\ell\nu$ decays provides with the most precise information on the $|V_{ub}|$ element in the CKM mixing matrix. Different descriptions of semileptonic decays of heavy quarks have been proposed starting with the ACCMM (Altarelli, Cabibbo, Corbo, Maiani and Martinelli) model [18] and developing in recent years model independent predictions based on OPE techniques [12]. A dedicated decay generator for $b \to u\ell\nu$ transitions has been developed by the author of this thesis to compare the decay descriptions of different models [19]. The main requirements are a definition for the kinematics of the b and spectator $\bar{q}$ quarks inside the B hadron, the description of the Q^2 distribution of the virtual W and of the kinematics in the $b \to uW$ and $W \to \ell\nu$ decays, and finally a model for the hadronisation of the $u\bar{q}$ system. In the following the implementation of this decay generator is discussed.

In the ACCMM model the B hadron consists of the b quark and the spectator $\bar{q}$ quark moving back-to-back in the B rest frame. Their momenta p are distributed according to the gaussian distribution:

$$\phi(p) = \frac{4}{\sqrt{\pi} p_F^3} e^{-\frac{p^2}{p_F^2}} \tag{1.11}$$

where the width p_F is known as Fermi momentum. The normalisation is chosen such that

$$\int_0^{+\infty} dp\ p^2 \phi(p) = 1. \tag{1.12}$$

The ACCMM model introduces two free parameters: *i)* the Fermi momentum p_F and *ii)* the spectator quark mass m_{sp}. There have been attempts to extract the values of these parameters from fits to experimental observables such as the momentum spectrum of leptons from $b \to c\ell\nu$ decay [20, 21], the photon spectrum in $b \to s\gamma$ decay [22] and the J/ψ momentum distribution in $B \to J/\psi\ X$ [23]. Most of these determinations point to a value of $p_F \simeq 0.5$ GeV/c (Table 1.1).

Table 1.1: *Experimental estimates of the p_F value in the ACCMM model*

Channel	p_F (GeV/c)	m_{sp} (GeV/c^2)	Ref.
$b \to c\ell\nu X$	0.27 ± 0.04	0.30	[20]
$b \to c\ell\nu X$	$0.51\ ^{+0.08}_{-0.07}$	0.0	[21]
$b \to s\gamma$	0.45	0.0	[22]
$B \to J/\psi X$	0.57	0.15	[23]

However it has been pointed out that the value of p_F obtained in a fit to $b \to c$ transitions may not be appropriate in the description of $b \to u$ decays [24]. At the same time it has also been shown that the ACCMM model is consistent with the QCD description of $b \to u\ell\nu$ and $b \to s\gamma$ transitions and that the corresponding parameters can therefore be related. This is the direction followed in recent studies.

The effective b quark mass m_b depends on p_F and m_{sp} as:

$$m_b^2 = m_b^2(p_b) = m_B^2 + m_{sp}^2 - 2m_B\sqrt{p_b^2 + m_{sp}^2} \tag{1.13}$$

where p_b is the momentum of the heavy quark in the hadron and m_B is the B hadron mass. The value of m_B can be taken as a parameter, tunable such that the ACCMM model corresponding to an average b mass $< m_b >$ can be compared with theory predictions obtained for a given value of m_b. Estimated values for the b quark pole mass are in the range $4.72\ \mathrm{GeV/c^2} < m_b < 4.92\ \mathrm{GeV/c^2}$ [20].

The value of p_F is proportional to the average kinetic energy of the b quark in the hadron since:

$$< p_b^2 >= \int_0^{+\infty} dp_b\ p_b^2\ (\phi(p_b)\ p_b^2) = \frac{3}{2}p_F^2 \tag{1.14}$$

where $\phi(p)$ is given by Eq. 1.11. Through the two above equations the ACCMM model parameters are related to those of the QCD description of the heavy quark inside the hadron discussed below. In this framework $< p_b^2 >$ corresponds to the value of the expectation value μ_π^2 of the kinetic operator. The value $p_F = 0.5$ GeV/c corresponds to $< p_b^2 > = 0.37\ \mathrm{GeV^2}$. Estimates of $< p_b^2 >$ have been obtained both from theory and fits to measured spectra in B decays as discussed below.

An alternative picture of the b quark kinematics has been proposed as an application of the parton model to heavy quark decays [25]. In this model the decay is considered in a frame where the B hadron moves with large momentum (infinite momentum frame or Breit frame). In this frame, the b quark behaves as a free particle carrying a fraction z of the B momentum, $p_b = zp_B$. The functional form of the probability density function $f(z)$ can be extracted from the b fragmentation function since the probability of finding the b quark carrying a fraction z of the hadron momentum corresponds to the probability for a b quark to produce a B hadron with a fraction z of its energy. This is usually described by the Peterson fragmentation function [26] that has the form:

$$f(z) = \frac{Nz(1-z)^2}{((1-z)^2 + \epsilon_b z)^2} \tag{1.15}$$

where ϵ_b is a free parameter. In this way, the parton model offers an advantage since the kinematics of the b quark is described by a function that can be directly related with experimental data on the fragmentation function for b quarks that has been measured at LEP. Averaging over the ALEPH, DELPHI and OPAL results, the fraction of the b quark energy taken by the beauty hadron is $< x_B >= 0.702 \pm 0.008$ [31]. Also the observed shape in the preliminary DELPHI analysis [32] was compatible with that of the Peterson function. These results point to a value for the ϵ_b parameter of $\epsilon_b = 0.0040$. In the simulation of decays with the parton model, the spectator quark mass m_q was set to zero and the b quark mass was varied in the range $4.72\ \mathrm{GeV/c^2} < m_b < 4.92\ \mathrm{GeV/c^2}$ as for the ACCMM model. It is interesting to notice that, by using the central value for ϵ_b, the parton model gave $< p_b^2 >= 0.35\ \mathrm{GeV^2}$ for $m_b = 4.72\ \mathrm{GeV/c^2}$, consistent with the value obtained in the ACCMM model for $p_F = 0.5$ GeV/c.

Recently there has been progress in defining the Fermi motion in the framework of QCD [27, 28]. This has been achieved in terms of a universal structure function describing the distribution of the light-cone residual momentum of the heavy quark inside the hadron. At leading order and

in the large m_b limit, the light-cone residual momentum k_+ can be expressed as the difference between the b quark pole mass and its effective mass m_b^* inside the hadron: $m_b^* = m_b + k_+$. As a consequence $k_+ < \bar{\Lambda} = m_B - m_b$. An ansatz for the shape of the universal structure function has been suggested [28] in the form:

$$F(w) = w^a(1 - cw)e^{-cw} \tag{1.16}$$

where $w = 1 - \frac{k_+}{\bar{\Lambda}}$, and the coefficients a and c depend on the values of $\bar{\Lambda}$ and of the kinetic energy operator.

The use of the QCD universal structure function F allows a consistent comparison with the results obtained in the framework of QCD and Heavy Quark expansion. The normalised moments $a_n = \frac{A_n}{\bar{\Lambda}^n}$ of F, given by

$$a_n = \frac{1}{\bar{\Lambda}^n} \int dk_+ k_+^n f(k_+) \tag{1.17}$$

relate the function parameters with that of the theory. In particular the first two moments define the function normalisation and the third is proportional to the expectation value of the kinetic energy operator [28]:

$$a_0 = 1 \tag{1.18}$$

$$a_1 = 0 \tag{1.19}$$

$$a_2 = \frac{3\mu_\pi^2}{\bar{\Lambda}^2} \tag{1.20}$$

These relationships define the values of the parameters a and c in Eq. 1.16 as a function of the values of μ_π^2 and $\bar{\Lambda}$. There have been several evaluations of μ_π^2 and a selection of recent results is given in Table 1.2. Results are scheme dependent and, depending on the method used in their derivation, they point to the values of μ_π^2 of 0.4 GeV^2 or 0.2 GeV^2.

Table 1.2: *Estimates of* μ_π^2

Method	μ_π^2 (GeV^2)	Ref.
QCD Sum Rules	0.50	[33]
Variational Method	0.44	[34]
Relativ. Potential	0.46	[35]
Virial Theorem	0.40 - 0.58	[36]
Virial Theorem	0.15 ± 0.03	[37]
$b \to c\ell\nu$	0.19 ± 0.10	[38]
$b \to c\ell\nu$	0.14 ± 0.03	[39]
$b \to s\gamma$	$0.71^{+1.16}_{-0.70}$	[40]

The two values of $\mu_\pi^2 = 0.2$ GeV^2 and 0.4 GeV^2 were chosen while $\bar{\Lambda}$ ranged between 0.36 GeV/c^2 and 0.56 GeV/c^2 for 4.72 GeV/c^2 $< m_b <$ 4.92 GeV/c^2 and $m_B = 5.28$ GeV/c^2. The masses of the light quarks, u and spectator quark, were set to zero.

The b quark decays as $b \to Wu$, the W and u being emitted back to back in the b rest frame with an isotropic distribution of their emission angle w.r.t the b direction. The virtual W is characterized by an effective mass q^2. The kinematics of the b and W decays correspond to that for two body decays. Therefore the model dependence that propagates to the final state

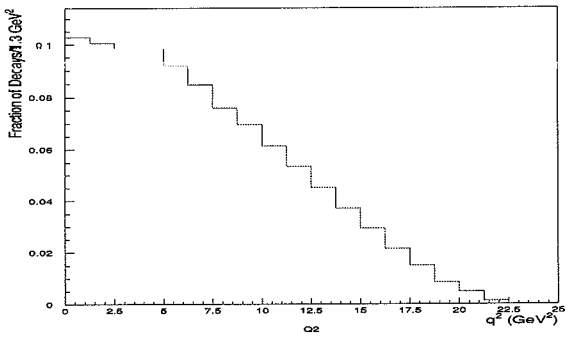

Figure 1.2: *The q^2 distribution in the decay $b \to u\ell\nu$ generated according to Eq. (1.21).*

kinematics depends on the choice of the values of p_F and m_q and of the q^2 distribution. By defining $x^2 = q^2/m_b^2$ the differential decay rate can be expressed as:

$$\frac{d\Gamma}{dx} = \frac{G_F^2 m_b^5 |V_{ub}|^2}{192\pi^3} F_0(x)(1 - \frac{2\alpha_s}{3\pi} F_1(x)) \tag{1.21}$$

The functions $F_0(x)$ and $F_1(x)$ describe the tree-level contribution and the QCD corrections terms. Following Ref. [29], they can be written, in the limit $m_u \to 0$, as:

$$F_0(x) = 2(1-x^2)^2(1+2x^2) \tag{1.22}$$

and

$$F_1(x) = (\pi^2 + 2S_{1,1}(x^2) - 2S_{1,1}(1-x^2)) + 8x^2(1-x^2-2x^4)ln(x) \tag{1.23}$$
$$+2(1-x^2)^2(5+4x^2)ln(1-x^2) - (1-x^2)(5+9x^2-6x^4) \tag{1.24}$$

where $S_{1,1}(x)$ is the Nielsen polylogarithm. The resulting Q^2 distribution is shown in Figure 1.2.

The virtual W is forced to decay into a lepton-neutrino pair. Due to the spin of the W, its decay is not isotropic and the angular distribution of the lepton varies as $1+cos^2\theta$. In computing the lepton and neutrino momenta in the W rest frame, the lepton mass is taken into account. After the decay the lepton and neutrino are boosted back to the B rest frame. The u quark is also boosted to the same system, and at this point the hadronic system is treated.

The energy and invariant mass of the hadronic system correspond to those of the $u\bar{q}$ quark pair. At the parton level these can be compared with the predictions obtained in QCD and heavy quark expansion. The observable final states are then generated by applying different prescriptions for describing the evolution of the quark fragmentation as shown in Figure 1.3. These include a fully inclusive hadronisation scheme according to the JETSET parton shower model [30] and exclusive descriptions of the final states in the $b \to u\ell\nu$ transition. At large enough recoil u quark energies, the $u\bar{q}$ system moves away fast and this picture is similar to that of the evolution of a jet initiated by a light quark q in $e^+e^- \to q\bar{q}$ annihilation. This is simulated by first arranging the $u\bar{q}$ system in a string configuration and then making it to fragment according to the parton shower model. Exclusive models compute the decay amplitudes from the heavy-to-light form factors and the quark hadronic wave functions. The so-called ISGW2 model [41] approximates the inclusive $b \to u\ell\nu$ decay width by the sum over resonant final states, taking into account leading corrections to the heavy quark symmetry limit.

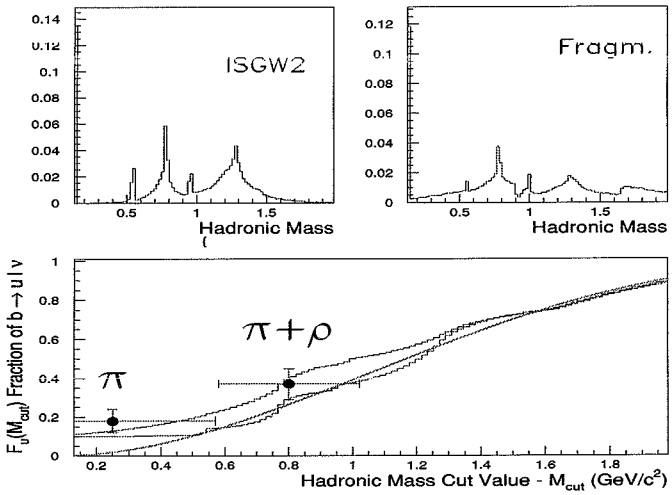

Figure 1.3: *Comparison of the invariant mass of the hadronic final state from the ISGW2 model (upper left) and from parton shower fragmentation (upper right). In the lower plot the corresponding fractions $F_u(M_{cut})$ of the $b \to u\ell\nu$ transitions resulting in a mass below a given cut value M_{cut} are shown as a function of M_{cut}. The curve refers to the invariant mass of the $u\bar{q}$ pair. The CLEO results for the branching ratios for the $\pi\ell\nu$ and $\rho\ell\nu$ channels are also shown.*

As already mentioned, the lepton spectrum is sensitive to the mass of the quark produced in the semileptonic b decay. While the lepton yield in the region of lepton energies above the kinematical limit $\simeq \frac{M_B^2 - M_D^2}{2M_B}$ for $b \to c\ell\nu$ transitions is subject to significant model dependences,

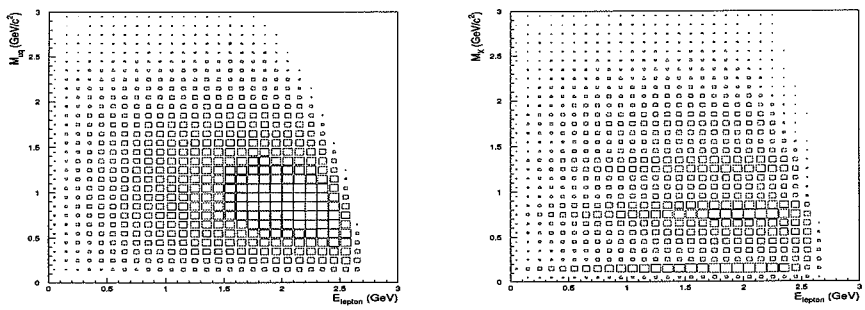

Figure 1.4: *Invariant mass of the hadronic system vs. lepton energy in $b \to u\ell\nu$ decays for the $u\bar{q}$ system (left) and the hadronic final state (right).*

a combined study of the mass of the hadronic system M_X and the energy of the lepton in the B rest frame E_ℓ^* may allow an extraction of the $|V_{ub}|$ with good sensitivity and improved control of the systematics. Figure 1.4 shows the correlation between the values of E_ℓ^* and M_X before and after the hadronisation of the $u\bar{q}$ system. By selecting decays with low hadronic invariant mass, the lepton spectrum is depleted in its lower end without significantly affecting the region of lepton energies above 1.5 GeV/c that are relevant for separating $b \to u\ell\nu$ from $b \to c\ell\nu$ decays. These characteristics of semileptonic $b \to u$ transitions have been exploited for a new determination of $|V_{ub}|$ with small model dependence as discussed in Chapter 3. The rate of semileptonic $b \to u$ transitions can be computed with quite good accuracy as a function of the ratio of the CKM elements $|V_{ub}|/|V_{cb}|$. A recent estimate gives [43]:

$$BR(B \to X_u\ell\nu) = (1.9 \pm 0.3) \times (\frac{|V_{ub}|/|V_{cb}|}{0.10})^2 \times 10^{-3} \tag{1.25}$$

The effective hamiltonian for the hadronic $b \to u$ transition including only the tree level contributions can be written as:

$$H = \frac{G_F}{\sqrt{2}} V_{ub}V_{ud}^*(C_1(\mu)[\bar{u}_i\gamma^\mu(1-\gamma_5)b^i][\bar{d}_j\gamma_\mu(1-\gamma_5)u^j] + C_2(\mu)[\bar{u}_i\gamma^\mu(1-\gamma_5)b^j][\bar{d}_j\gamma_\mu(1-\gamma_5)u^i] \tag{1.26}$$

where $C_1(\mu)$ and $C_2(\mu)$ are the Wilson coefficients evaluated at a scale $\mu \simeq m_b$. The inclusive rate of hadronic $b \to u$ decays has been estimated [43] to be:

$$BR(b \to u)_{hadr} = (0.73^{+0.16}_{-0.12}) \times (\frac{|V_{ub}|/|V_{cb}|}{0.10})^2 \times 10^{-2} \tag{1.27}$$

Exclusive charmless hadronic two-body final states are of special importance both for their role in the study of CP asymmetries and for the clear experimental signature of decays such as $B \to \pi\pi$ and $\rho\pi$. In order to evaluate the branching ratio for these exclusive decays, the factorization technique discussed in the previous section can be applied. The factorised hadronic matrix element for the decay $\bar{B}^0 \to \pi^+\pi^-$ reads:

$$< \pi^+\pi^-|O|\bar{B}^0 > = < \pi^+|\bar{u}\Gamma_u b|\bar{B}^0 >< \pi^-|\bar{d}\Gamma_u u|0 > \tag{1.28}$$

Several exclusive branching ratios of tree level dominated $b \to u$ decays have been computed using this technique. In particular the following predictions have been obtained [44]:

$$\mathrm{BR}(B_d^0 \to \pi^+\pi^-) = (2.6 \pm 1.2) \times (\frac{|V_{ub}|/|V_{cb}|}{0.10})^2 \times 10^{-5}$$

and

$$\mathrm{BR}(B_u^- \to \rho^0\pi^-) = (1.0 \pm 1.0) \times (\frac{|V_{ub}|/|V_{cb}|}{0.10})^2 \times 10^{-5}$$

The study of the time dependent rate asymmetry between $B^0 \to \pi^+\pi^-$ and its CP conjugate will play a central role in the study of CP violation in the B sector if the decay is dominated by the tree level weak amplitude. In fact the $B \to \pi\pi$ decay by penguin induced $b \to d$ transitions have a different phase and will confuse this measurement by introducing the so called "penguin pollution". The study of the interplay between tree level and penguin loop transitions in rare B decays is an essential prerequisite for the interpretation of the signals of CP violation in B decays.

1.2.2 Loop mediated B Decays

Loop mediated decays are responsible for effective flavour changing neutral current interactions that are forbidden at tree level in Standard Model. These induce $b \to s$ and $b \to d$ transitions that have recently attracted significant efforts both in theory and in the experiments, as the size of the available data sets has made their observations possible.

In Standard Model, the radiative decay $b \to s\gamma$ proceeds through a loop diagram in which a W boson and an up-type quark are emitted by the b quark and absorbed at the sWq vertex. The photon is radiated either by the boson or by the quark line. The $b \to s\gamma$ transition can be described by an effective Hamiltonian. In fact, the interactions mediated by the virtual W boson and quark appear point-like at the energy scale corresponding to the b quark mass of $\simeq 5$ GeV/c^2. By contracting the W and quark lines in the Feynman diagram to a point the Hamiltonian can be written in terms of effective operators O_i with Wilson coefficients that carry the information on the effective couplings as well as of QCD corrections. In the case of $b \to s\gamma$ this gives:

$$H_{eff}(B \to s\gamma) = \frac{4G_F}{\sqrt{2}} V_{tb}V_{ts}^* \sum_{i=1} C_i(\mu)O_i(\mu) \tag{1.29}$$

where G_F is the Fermi constant, $C_i(\mu)$ the Wilson coefficients evaluated at the scale μ and O_i the relevant operators. $O_i, (i = 1, 6)$ represent the quark operators while O_7 and O_8 are the magnetic and chromo-magnetic operators respectively. The Wilson coefficients incorporate the dependance on the mass of the bosons and quarks contributing to the loop. In the Standard Model, the dominant contributions to $b \to s\gamma$ are due to the operators O_2 O_7 and O_8 given by:

$$O_2 = -\frac{V_{cb}V_{cs}^*}{V_{tb}V_{ts}^*}(\bar{c}_{L\alpha}\gamma^\mu b_{L\alpha})(\bar{s}_{L\beta}\gamma_\mu c_{L\beta}) \tag{1.30}$$

$$O_7 = \frac{em_b}{16\pi^2}\bar{s}_{L\alpha}\sigma^{\mu\nu}b_{R\alpha}F_{\mu\nu} \tag{1.31}$$

and

$$O_8 = \frac{gm_b}{16\pi^2}\bar{s}_{L\alpha}\sigma^{\mu\nu}T_{\alpha\beta}b_{R\beta}G_{\mu\nu} \tag{1.32}$$

Since $\frac{|V_{ub}|}{|V_{cb}|} \simeq 0.1$ the u quark contribution in the loops is small and has been neglected in the expressions above.

As mentioned above, the coefficients $C_i(\mu)$ are defined such that, at the scale $\mu = m_W$, they correspond to the matrix elements of the Standard Model at the zeroth order in α_s. From this scale they are evolved down to the scale $\mu = m_b$ characteristics of the decays of B hadrons. This procedure allows to incorporate in the values of the Wilson coefficients the large logarithms $log(m_W^2/m_b^2)$ arising from the QCD corrections. The evolution of the coefficients is obtained using the renormalization group equation:

$$\mu\frac{dC_i(\mu)}{d\mu} - \sum_j(\gamma^T)_{ij}C_j(\mu) = 0 \tag{1.33}$$

where γ is the (8×8) anomalous dimension matrix of the eight operators O_i and

$$\mu\frac{dg_c}{d\mu} = \beta(g_c) = -(11 - \frac{2}{3}n_f)\frac{g_c^3}{16\pi^2} \tag{1.34}$$

In order to evolve the coefficients C_i to the scale $\mu = m_b$ we replace μ with g_c in the above expression use the number of quark flavours $n_f = 5$ obtaining:

$$\frac{dC_i(g_c)}{dg_c} = -\frac{6}{23g_c}\sum_j(\gamma'^T)_{ij}C_j(g_c) \tag{1.35}$$

The decay width $\Gamma(b \to s\gamma)$ can be computed from the Wilson coefficient $C_7(\mu)$ as:

$$\Gamma(b \to s\gamma) = \frac{G_F^2 \alpha m_b^5}{32\pi^4} |V_{tb}V_{ts}|^2 \, |C_7(\mu)|^2 K(\mu) \tag{1.36}$$

where $\alpha = \frac{e^2}{4\pi}$ and $K(\mu)$ contains the correction due to the $b \to s\gamma g$ bremsstrahlung process. It is possible to partially cancel the uncertainties from the fifth power of the b quark mass m_b by expressing the branching ratio $BR(b \to s\gamma)$ in terms of the semileptonic branching ratio $BR(b \to c\ell\nu)$:

$$BR(b \to s\gamma) = \frac{\Gamma(b \to s\gamma)}{\Gamma(b \to c\ell\nu)} BR(b \to c\ell\nu) \tag{1.37}$$

with

$$\Gamma(b \to c\ell\nu) = \frac{G_F^2 m_b^5}{192\pi^3} |V_{cb}|^2 f(\frac{m_c}{m_b})(1 - \frac{2}{3}\frac{\alpha_s}{\pi} g_{QCD}) \tag{1.38}$$

where $f(x) = 1 - 8x^2 + 8x^6 - x^8 - 24x^4 \, ln \, x$ is the phase space coefficient and g_{QCD} is the one-loop QCD correction factor. Thus:

$$\frac{BR(b \to s\gamma)}{BR(b \to c\ell\nu)} = \frac{6\alpha}{\pi} \frac{|V_{tb}V_{ts}|^2}{|V_{cb}|^2} |C_7(\mu = m_b)|^2 \frac{K(\mu = m_b)}{f(\frac{m_c}{m_b})(1 - \frac{2}{3}\frac{\alpha_s}{\pi} g_{QCD})} \tag{1.39}$$

Since $V_{ts} \simeq V_{cb}$ and $V_{tb} \simeq 1$ also the dependence on the CKM mixing matrix elements cancels out in the ratio.

The contributions from the particles in the loop can be expressed explicitely by rewriting the same relation in terms of the A_γ and A_g coefficients of the $bs\gamma$ an bsg operators in the effective Lagrangian:

$$L_{eff} = G_F \sqrt{\frac{\alpha}{8\pi^3}} V_{tb}V_{ts}^* m_b \Big(A_\gamma \bar{s}_L \sigma^{\mu\nu} b_R F_{\mu\nu} + A_g \bar{s}_L \sigma^{\mu\nu} T^\alpha b_R G^\alpha_{\mu\nu} \Big) + h.c. \tag{1.40}$$

The relation 1.39 becomes:

$$\frac{BR(b \to s\gamma)}{BR(b \to ce\nu)} = \frac{6\alpha}{\pi} \frac{\Big(\eta^{\frac{16}{23}} A_\gamma + \frac{8}{3}(\eta^{\frac{14}{23}} - \eta^{\frac{16}{23}}) A_g + K \Big)^2}{f(\frac{m_c}{m_b})\Big(1 - \frac{2}{3}\frac{\alpha_s(m_b)}{\pi} g_{QCD}\Big)} \tag{1.41}$$

where now $\eta = \alpha_s(m_Z)/\alpha_s(m_b)$ and K is computed at the leading order [46]. In the SM the only contribution to the loop is the one due to the $W^\pm$ emission that is described by the coefficients:

$$A^{SM}_{\gamma,g} = \frac{3}{2}\Big(\frac{m_t}{m_W}\Big)^2 f^{(1)}_{\gamma,g}\Big(\frac{m_t^2}{m_W^2}\Big) \tag{1.42}$$

where the $f^{(1)}_{\gamma,g}(x)$ terms have been computed analytically and are given in ref. [46]. Taking the top quark mass $m_t = 180$ GeV/c^2, $\alpha_s(m_Z) = 0.118$, $\alpha_s(m_b) = 0.215$, $m_c = 1.5$ GeV/c^2, $m_b = 4.8$ GeV/c^2 and $BR(b \to ce\nu) = 0.107$, the $b \to s\gamma$ rate in the Standard Model is $BR(b \to s\gamma)_{SM} = (2.9 \pm 0.8) \times 10^{-4}$. The sources of uncertainties of this estimate have been studied in details and a detailed discussion is given in ref. [47]. The dominant uncertainty depends on the next-to-leading order contributions (see Figure 1.5). This is shown by a strong dependance of the result on choice of the scale μ [47]. The full next-to-leading order corrections have been recently computed [45] giving:

$$BR(b \to s\gamma)_{SM} = (3.3 \pm 0.3) \times 10^{-4}.$$

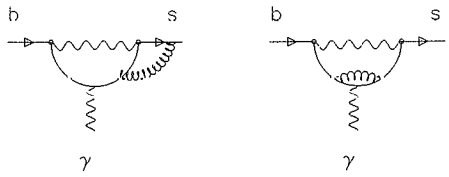

Figure 1.5: *Two diagrams of the next-to-leading order QCD corrections for the $b \to s\gamma$ transition.*

The second class of loop transitions of interest is that of hadronic penguin decays. These are responsible for decays like $B \to K\pi$. Hadronic penguin decays proceed through loop diagrams where a gluon is radiated instead of a photon. Hadronic penguin $b \to s$ transitions can be classified in the following processes: i) $b \to sg$, ii) $b \to sgg$, iii) $b \to sq\bar{q}$ and iv) non-spectator $b\bar{q} \to s\bar{q}$.

The $b \to sg$ decay is described by the effective Hamiltonian:

$$H_{eff}(B \to sg) = \frac{4G_F}{\sqrt{2}} V_{tb}V_{ts}^* C_8(\mu) O_8(\mu) \tag{1.43}$$

where O_8 is the chromomagnetic operator already introduced above and given by:

$$O_8 = \frac{g m_b}{16\pi^2} \bar{s}_{L\alpha} \sigma^{\mu\nu} T_{\alpha\beta} b_{R\beta} G_{\mu\nu} \tag{1.44}$$

In analogy to the case of $b \to s\gamma$ the branching ratio for $b \to sg$ can be expressed in terms of the semileptonic branching ratio to cancel the dependence on the b quark mass m_b obtaining:

$$\frac{BR(b \to sg)}{BR(b \to ce\nu)} = \frac{|V_{ts}^* V_{tb}|^2}{|V_{cb}|^2} \frac{2\alpha_s(\mu)}{\pi} \frac{|C_8^{eff}(\mu)|^2}{f(\frac{m_c}{m_b})\Big(1 - \frac{2}{3}\frac{\alpha_s(m_b)}{\pi} g_{QCD}\Big)} \tag{1.45}$$

At leading order QCD the BR($b \to sg$) has been estimated to be 1.7×10^{-2} [49]. However, the BR($b \to sg$) receives large QCD corrections and, from a partial NLO computation, it has been estimated to be $(1.57^{+0.90}_{-0.65}) \times 10^{-3}$ [45]. This can be extended to the four processes contributing to hadronic $b \to s$ penguin decays obtaining [48]:

$$\frac{BR(b \to s)}{BR(b \to ce\nu)} = \frac{|V_{ts}^* V_{tb}|^2}{|V_{cb}|^2} \frac{\alpha_s^2(\mu)}{\pi^2} \frac{(\frac{2\pi}{\alpha_s(\mu)} A_2^2) + (\frac{1}{4} A_1^2) + (\frac{17}{72} A_1^2 + \frac{5}{3} A_1 A_2) + (\frac{32\pi^2 f_B^2}{9 m_b} A_1^2)}{f(\frac{m_c}{m_b})\Big(1 - \frac{2}{3}\frac{\alpha_s(m_b)}{\pi} g_{QCD}\Big)} \tag{1.46}$$

where $A_1 = \frac{2}{3} ln \frac{m_c^2}{\mu^2} C_9(\mu) + C_7(\mu)$ and $A_2 = C_8(\mu)$ and the four terms in brackets at the numerator refer to the four processes i) - iv).

The full NLO computation for $b \to s$ hadronic decays, contrary to the case of $b \to s\gamma$, has not been completed yet. The inclusive $b \to s$ hadronic branching ratio has been estimated using the part of the NLO corrections available to be:

$$BR(b \to s)_{hadr} = (0.98^{+0.51}_{-0.30}) \times 10^{-2} \tag{1.47}$$

where the error comes mainly from the residual μ scale and scheme dependence [43]. This has to be compared with the estimated $b \to u$ hadronic branching ratio of $(0.73^{+0.16}_{-0.12})(\frac{|V_{ub}|/|V_{cb}|}{0.10})^2 \times$

10^{-2} [43]. From these predictions, the expected contribution of $b \to s$ loop transitions to the total charmless hadronic decay rate results to be:

$$\frac{BR(b \to s)_{hadr}}{BR(b \to u)_{hadr} + BR(b \to s)_{hadr}} = 0.57^{+0.36}_{-0.23} \tag{1.48}$$

assuming $|V_{ub}|/|V_{cb}| = 0.10 \pm 0.02$.

Decays rates for exclusive final states involving hadronic penguin loops as $B_s^0 \to K^+\pi^-$ have also been estimated. This is important since exclusive final states can be reconstructed with good efficiency and purity and thus represent an important source of experimental data on rare B decays as discussed in Chapter 4. The branching ratio for $B_d^0 \to K^+\pi^-$ has been estimated using the factorization technique and the result is:

$$\mathrm{BR}(B_d^0 \to K^+\pi^-) = (0.06(\tfrac{V_{ub}/V_{cb}}{0.10})^2 + 1.06) \times 10^{-5}$$

where the first contribution is due to the tree level diagram and the second to the penguin loop mediated transition [50].

The importance of penguin graphs relative to tree level $b \to u$ transitions can be estimated from the data by comparing decays as $B_d^0 \to K^+\pi^-$ with $B_d^0 \to \pi^+\pi^-$. The first decay proceeds mostly by penguin $b \to s\bar{u}u$ transition, tree level $b \to us\bar{u}$ being suppressed by the small value of the $|V_{us}|$ element. On the contrary the $\pi^+\pi^-$ final state is dominated by the tree level $b \to u\bar{u}d$ decay due to the analogous CKM suppression of $b \to d$.

Recently it has been pointed out that the determination of the ratio

$$R = \frac{\Gamma(B_d^0 \to \pi^\mp K^\pm)}{\Gamma(B_u^\pm \to \pi^\pm K^0)} \tag{1.49}$$

can provide further information on the phase η in the CKM matrix [51]. In fact the decay at the numerator is a mixture of penguin and Cabibbo suppressed tree level decays, while the denominator has a pure penguin component since the K^0 cannot be produced by the $W^\pm$. Now a value of $R < 1$ would be a signal of destructive interference between the tree level and penguin amplitudes in the $B_d^0 \to \pi^\mp K^\pm$ decay. This can be used to set a constrain on the CKM parameters in the Wolfenstain parametrisation discussed in section 1.1 in the form $\frac{\eta^2}{\rho^2+\eta^2} < R$ that is known as the Fleischer-Mannel bound. The study of these decays using the DELPHI data set is presented in Chapter 4.

Bibliography

[1] N. Cabibbo, *Phys. Rev. Lett.* **10** (1963), 531.

[2] M. Kobayashi and K. Maskawa, *Prog. Theor. Phys.* **49** (1973), 652.

[3] C. Caso *et al.*, Particle Data Group, *Review of Particle Physics* Eur. Phys. J. **C 3** (1998).

[4] A.J. Buras, *CKM Matrix: Present and Future*, TUM-HEP-299/97.

[5] L. Wolfenstein, *Phys. Rev. Lett.* **51** (1983), 1945.

[6] A. Ali and D. London, *CP violation and flavour mixing in the standard model*, DESY 95-148.

[7] A.J. Buras, M.E. Lautenbacher and G. Ostermaier, *Phys. Rev.* **D 50** (1994), 3433.

[8] P. Paganini, F. Parodi, P. Roudeau and A. Stocchi, *Phys. Scripta* **58** (1998), 556 and F. Parodi, P. Roudeau and A. Stocchi, *Constraints on the parameters of the V_{CKM} matrix at the end of 1997*, LAL-98-49 and hep-ph/9802289.

[9] Y. Grossman *et al.*, *Nucl. Phys.* **B 511** (1998), 69.

[10] For recent reviews of CP violation and future perspectives see:
M. Neubert, *Int. J. Mod. Phys.* **A 11** (1996) 4173,
A.J. Buras and R. Fleischer, in A.J. Buras and M. Lindner (editors), *Heavy Flavours*, 2^{nd} edition, World Scientific (1997),
T. Nakada, to appear in the *Proceedings of the XXIX International Conference on High Energy Physics ICHEP-98*, Vancouver B.C. (Canada), July 1998 and
D. Boutigny *et al.* (BaBar Collaboration), *The BaBar Physics Book*, SLAC, October 1998,

[11] K. Wilson, *Phys. Rev.* **179** (1969), 1499.

[12] I. Bigi, M. Shifman and N. Uraltsev, *Aspects of Heavy Quark Theory*, TPI-MINN-97/02-T, hep-ph/9703290.

[13] M. Neubert, in *Heavy Flavours* (A.J. Buras and M Lindner editors), 2nd edition, World Scientific, Singapore, 1998, 239 and

[14] P. Ball and V.M. Braun, *Phys. Rev.* **D 58** (1998), 1094.

[15] M. Bauer, B. Stech and M. Wirbel, *Z. Phys.* **C34** (1987), 103.

[16] A.J. Buras, J.M. Gerard and R. Ruckl, *Nucl. Phys.* **B 268** (1986), 16.

[17] T.E. Browder and K. Honscheid, *Prog. Part. Nucl. Phys* **35** (1995).

[18] G. Altarelli *et al.*, *Nucl. Phys.* **B 208** (1982), 365.

[19] M. Battaglia, *Study of $b \to u\ell\nu$ Decays with an Inclusive Generator*, DELPHI 98-42 PHYS 772 and HIP-1998-32/EXP.

[20] M.S. Alam *et al.* (CLEO Collaboration), *Phys. Rev. Lett.* **74** (1995), 2885.

[21] D.S. Hwang, C.S. Kim and W. Namgung, *Average Kinetic Energy of Heavy Quark in Semileptonic B Decay*, KEK-TH-473, March 1996.

[22] A. Ali and C. Greub, *Photon Energy Spectrum in $B \to X_s\gamma$ and Comparison with Data*, DESY 95-117.

[23] W.F. Palmer, E.A. Paschos and P.H. Soldan, *Phys. Rev.* **D 56** (1997), 5794.

[24] I. Bigi, M. Shifman, N. Uraltsev and A. Vainshtein, *Phys. Lett.* **B 328** (1994), 431.

[25] A. Bareiss and E.A. Paschos, *Nucl. Phys.* **B 327** (1989), 353.

[26] C. Peterson *et al.*, Phys. Rev. **D 27** (1983), 105.

[27] M. Neubert, *Phys. Rev.* **D 49** (1994), 4623 and
M. Neubert, *Phys. Rev.* **D 50** (1994), 2037.

[28] R.D. Dikeman, M. Shifman and N.G. Uraltsev, *Int. J. Mod. Phys.* **11** (1996), 571.

[29] M. Jezabek and J.H. Kühn, *Nucl. Phys.* **B 314** (1989), 1.

[30] T. Sjöstrand, *Comp. Phys. Comm.* **82** (1994), 74.

[31] The LEP Electroweak Working Group, LEPHF/96-01

[32] M. Feindt and O. Podobrin, *Inclusive Measurement of the b Fragmentation Function*, DELPHI 95-103 PHYS 538.

[33] P. Ball and V.M. Braun, *Phys. Rev.* **D 49** (1994), 2472.

[34] D.S. Hwang, C.S. Kim and W. Namgung, *Phys. Lett.* **B 406** (1997), 117.

[35] F. de Fazio, *Mod. Phys. Lett.* **A 11** (1996), 2693.

[36] D.S. Hwang, C.S. Kim and W. Namgung, *Phys. Rev.* **D 54** (1996), 5620.

[37] M. Neubert, private communication.

[38] M. Gremm *et al.*, Phys. Rev. Lett. **77** (1996), 20.

[39] V. Chernyak, *Nucl. Phys.* **B 457** (1995), 96;
V. Chernyak, *Phys. Lett.* **B 387** (1996), 173.

[40] H. Li and H.L. Yu, *Phys. Rev* **D 55** (1997), 2833.

[41] D. Scora and N. Isgur, *Phys. Rev.* **D 52** (1995), 2783.

[42] C. Ramirez, F. Donoghue and G. Burdman, *Phys. Rev.* **D 41** (1990), 1496.

[43] A. Lenz, U. Nierste and G. Ostermayer, *Determination of the CKM angle γ and $|V_{ub}/V_{cb}|$ from inclusive direct CP asymmetries and branching ratios in charmless B decays*, DESY 97-208.

[44] A. Deandrea *et al. Phys. Lett.* **B 318** (1993), 549.

[45] M. Ciuchini *et al.*, *Phys.Lett.* **B 334** (1994) 137.

[46] R. Barbieri and G.F. Giudice, CERN-TH.6830/93.

[47] A.J. Buras *et al.*, *Nucl. Phys.* **B 424** (1994), 374.

[48] R. Grigjanis *et al.*, Phys. Lett. **B 224** (1989), 209.

[49] P.J. O'Donnell, in *Proc. of Les Recontres de Physique del la Vallee d'Aoste*, La Thuile (Italy), March 1990.

[50] N.G. Deshpande and J. Trampetic, *Phys. Rev.* **D 41** (1990), 895.

[51] A.J. Buras, R. Fleischer and T. Mannel, *Nucl. Phys.* **B 533** (1998), 3.

Experimental Techniques in the Study of B Decays

Brief Summaries of Selected Original Papers

Paper i)
M. Battaglia with W. Adam *et al.*, *Performance of the ring imaging Cherenkov detector of DELPHI, Nucl. Instr. and Meth. in Phys. Res.* **A 367** (1995), 253.

Paper ii)
M. Battaglia with W. Adam *et al.*, *Current achievements of the DELPHI ring imaging cherenkov detector, Nucl. Instr. and Meth. in Phys. Res.* **A 371** (1996), 12.

These papers summarise the design, performances and operation of the Ring Imaging Cherenkov detector installed in the DELPHI experiment. The author of this thesis contributed to the testing and commissioning of the Barrel RICH gas system, to the study of the performances of the MWPC's and to the characterisation of the cross-talk effects induced by the large ionisation collected on the chambers from charged particle tracks crossing the photon detecting volume and to the pattern recognition, reconstruction and analysis of the Cherenkov rings.

Paper iii)
M. Battaglia with W. Adam *et al.*, *Particle Identification Algorithms for the DELPHI RICH Detector, Nucl. Instr. and Meth. in Phys. Res.* **A371** (1996) 240.

This paper summarises the particle identification algorithms based on the RICH detector response developed for the analysis of the DELPHI data. The author of this thesis has introduced, in collaboration with P.M. Kluit of NIKHEF (Amsterdam), an original iterative algorithm based on photo-electron clustering and determination of the average Cherenkov angle associated to each particle track. This algorithm has been used first for the study of the RICH detector performance, calibration and comparison of real data to Monte Carlo simulation. Later the algorithm has been developed in a complete particle identification package, combining also with the response from the TPC detector, by the same authors. This package has become the standard tool of particle identification in DELPHI and it is presently included in the DELPHI official software releases.

Chapter 2

Heavy Flavour Physics with the DELPHI Detector at LEP

B particles are characterized by their large masses and relatively long lifetimes. At LEP centre-of-mass energies, B hadrons are produced with an average energy of about 32 GeV due to the hard b quark fragmentation (Figure 2.1). This has two main experimental consequences.

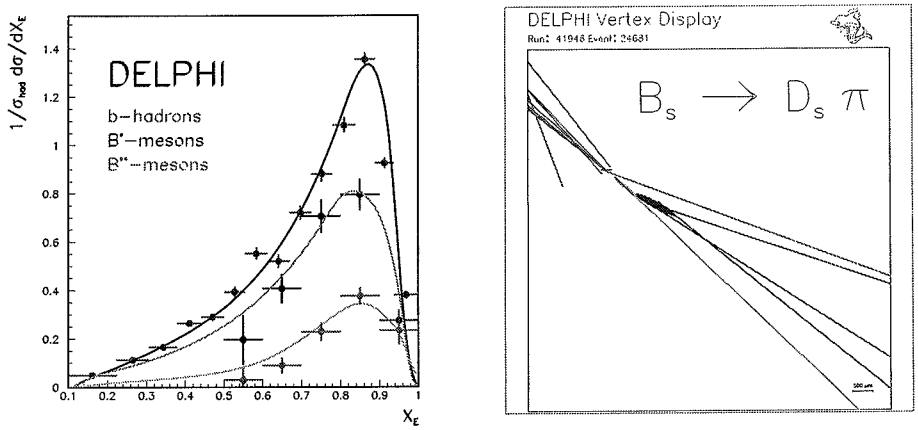

Figure 2.1: *Fragmentation function for inclusive B hadrons and mesons produced in B^* and B^{**} excited states (left) (from ref. [1]). The histogram shows the fraction of the beam energy taken by the B particle, the points with error bars are the DELPHI measurements and the line the best fit using the Peterson parametrisation. An example of reconstructed B_s decay with the secondary and tertiary vertices well separated from the Z^0 production point (right).*

First, the B decay products carry a large fraction of the beam energy, second the B hadrons fly significantly far from the e^+e^- interaction point before decaying, due to the large Lorentz boost. These characteristics are at the basis of most of the techniques, used at LEP, for identifying and reconstructing the decays of the b quark. The reconstruction and classification of B decays is possibly the most demanding type of data analysis in terms of its requirements on the performances of the experimental apparatus. In fact, the identification of the B decay

products requires efficient and accurate reconstruction of the particle track trajectories in space. This is achieved by the use of high precision silicon detectors surrounding the beam-pipe. Good momentum resolution is also important for a precise measurement of invariant masses. An efficient identification of hadrons (π, K and p) and leptons (e, μ) allows to classify the B decay modes. In addition, the study of several decay channels requires the use of neutral particles, as photons and neutral pions, detected in the electromagnetic calorimeter. The DELPHI detector, equipped with a high resolution silicon vertex tracker and using Ring Imaging Cherenkov (RICH) detectors for hadron identification, is particularly suited for these studies in B physics.

2.1 The DELPHI detector at LEP

DELPHI (DEtector with Lepton, Photon and Hadron Identification (Figures 2.2 and 2.3) is one of the four large experiments built around the four interaction regions of the LEP e^+e^- collider at CERN. In this chapter the principle of operation and performances of the detector sub-systems

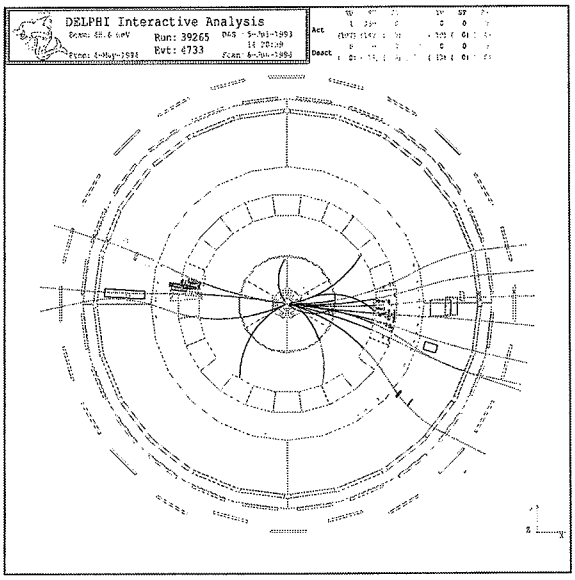

Figure 2.2: *An event display showing the response of the DELPHI apparatus to a $Z^0 \rightarrow b\bar{b}$ decay. The view is shown on a plane normal to the LEP beam axis. From the inside to ouside there are the VD, the ID, the TPC, the RICH and the calorimeters. The outermost detector layers are the muon chambers.*

of the DELPHI apparatus most used in these studies are briefly reviewed; more details can be found in [2]. Special emphasis is given to the silicon Microvertex (VD) and to the RICH detectors because of their major role in the studies of B physics with DELPHI. The techniques, based on the response of these detectors developed, for the identification and reconstruction of B decays and for the tagging of stable particles in DELPHI are then discussed in section 2.2.

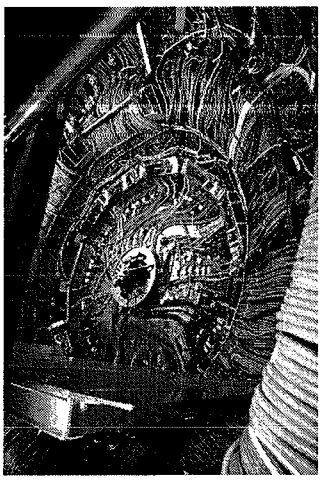

Figure 2.3: *A view of the barrel region of the DELPHI detector during a LEP shutdown period. The LEP beam pipe has been removed. At the center, the outer flange of the Inner Detector is visible followed by the TPC end wall covered by the cables from the VD and ID. On the outside are the cables of the RICH and HPC detectors. (CERN Photo)*

2.1.1 Tracking Detectors

Charged particles produced in the e^+e^- interactions are detected by the ionization created in solid state and gaseous detectors. These detectors are the **Microvertex Detector (VD)**, the **Inner Detector (ID)**, the **Time Projection Chamber (TPC)**, and the **Outer Detector (OD)**. In the forward regions the reconstruction of charged particles relies also on the response of the **Forward Chambers (FCA** and **FCB)**.

Moving from the interaction region outwards, the first sensitive elements of DELPHI are the three layers of silicon detectors of the **Microvertex detector** that is is presented in details in the next section.

Further away from the interaction region, the VD is followed by the **ID** that consists of a jet-chamber providing up to 24 $R-\phi$ points measured with a resolution of of 75 - 125 μm, depending on the drift distance, at radii from 12 cm to 23 cm for polar angles $23° < \theta < 157°$. The two track resolution of the Inner Detector is about 1 mm.

The main tracking device of DELPHI is the **TPC**. The TPC is a cylinder of 2.4 m diameter and 3.3 m length with two drift volumes, separated by a high voltage plate producing an electric drift field of 187 Volts cm^{-1}. The trajectory of a charged particle crossing the TPC is reconstructed from the electrons released in the 80% Ar 20% CH_4 gas mixture. Around 70 e^- cm^{-1} are produced by ionisation and drifted to the end-plates where their charge is collected by the proportional chambers. 192 sense wires and 16 circular pad rows provide space points at radii from 40 cm to 110 cm. Grid wires are used to collect the positive ions produced in the multiplication of the charge carriers at the level of the sensitive wires, thus avoiding distortions of the drift field in the main TPC volume. The z coordinate is measured by the drift time over a length of up to 150 cm. Single point resolution of 250 μm and 880 μm have been measured in the $R-\phi$ and z coordinates respectively. The TPC also provides information on the specific energy loss dE/dx sampled at the sense wires. This information is used for particle identification, in combination with the RICH response as discussed in section 2.2.3.

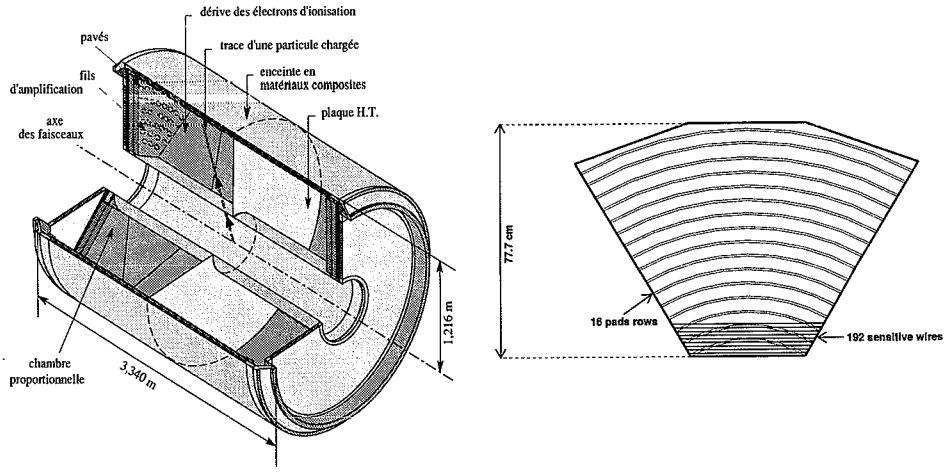

Figure 2.4: *A schematic view of the* DELPHI *TPC (left) and the layout of one of the sector endplates (right). Each of the 2 × 6 TPC sectors have 16 rows of pads. In each sectors there are 1680 pads. In front of the pad plates there are three levels of grids. The one closest to the pad (with the anode at a HV of 1430 volts) contains 192 sensitive wires per sector performing the dE/dx measurement.*

The outermost tracking device in the barrel region is represented by the **OD** that consists of drift tubes, operated in limited streamer mode, located outside the Cherenkov detector, at radial position from 197 cm to 206 cm. The OD provides single point resolutions of 110 μm in $R-\phi$ and 3.5 cm in z where the position is determined by the timing of the anode signals.

Charged particle tracks are reconstructed by a track fit that includes the points measured in all tracking detectors. The momentum and charge are determined by the curvature, in the 1.23 T magnetic field provided by the DELPHI superconducting solenoid, of the projected helix describing the particle trajectory. The resulting momentum resolution, measured for muons from tagged $Z^0 \rightarrow \mu^+\mu^-$ decays, has been found to be $\sigma(1/p) = 0.6 \times 10^{-3}$ $(\mathrm{GeV/c})^{-1}$ (see Figure 2.5). The resolution for extrapolating a charged particle track back to its production vertex is expressed as the impact parameter resolution. This resolution defines the ability of the detector to identify particles produced in the decay of short-lived hadrons and to reconstruct their production vertices. Therefore precise impact parameter resolution is essential in the study of B decays. Accurate extrapolation of charged particle tracks is ensured in DELPHI by the use of a vertex tracker based on high resolution silicon microstrip detector technology.

2.1.2 The Microvertex Detector

The **VD** [3] consists of three concentric layers of AC coupled silicon microstrip detectors located at average radii of 6.3 cm, 9 cm and 11 cm. The detector was originally equipped with single-sided silicon microstrip sensors installed with the strips parallel to the LEP beam direction and therefore measuring the $R-\phi$ coordinate of impact of charged particle tracks. In 1994 the VD was upgraded by replacing the silicon sensors on the innermost and outermost layers with double-sided microstrip detectors, with sensitive strips implanted both parallel and orthogonal to the beam line, thus reconstructing space points of passage of charged particles. The VD covers polar angles in the range $25° < \theta < 155°$. The extrapolation resolution σ_{extr} of a particle

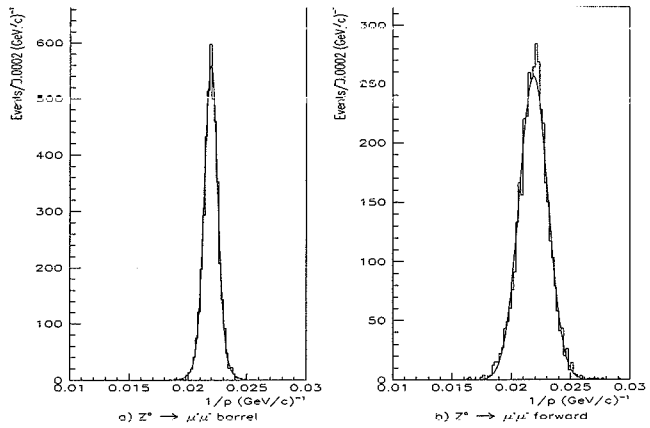

Figure 2.5: *Inverse momentum distributions for collinear muons from $Z \rightarrow \mu^+\mu^-$ decays: barrel tracks containing hits from VD, ID, TPC and OD (left) and forward tracks containing hits from VD and FCB at least (right) (from ref. [2]).*

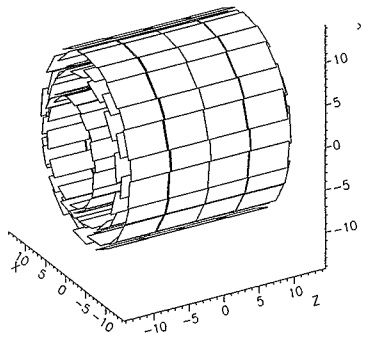

Figure 2.6: *Schematic layout of the DELPHI Vertex Detector in its configuration used for the 1994 and 1995 LEP runs.*

measured with accuracy σ_{point} at radii R_{in} and R_{out} separated by a lever arm $d = R_{out} - R_{in}$ can be approximated as:

$$\sigma_{extr} = \frac{\sigma_{point}}{d}\sqrt{R_{out}^2 + R_{in}^2} \tag{2.1}$$

in absence of multiple scattering. The multiple scattering term, important at low particle momentum, varies with the thickness x_T of material traversed as $\sqrt{x_T}$.

In DELPHI, the inner and outer radii have been dictated respectively by the LEP beampipe

radius, optimised by considering the accelerator induced backgrounds, and by the ID inner radius. In the design of the VD upgrade, emphasis was put on achieving accurate single point reconstruction σ_{point} in both the $R-\Phi$ and z coordinates. A possible solution for obtaining space points with conventional silicon microstrip detectors is to glue two detectors back to back with strips in orthogonal directions. This approach has been followed, for example, by the OPAL experiment [4]; however the disadvantage of such a design comes from the doubling of the amount of material crossed by the particle tracks. It is important to keep this material to the minimum in order to maintain good extrapolation resolution also at low momenta, where the multiple scattering term dominates the tracking accuracy. The solution chosen by DELPHI has been to

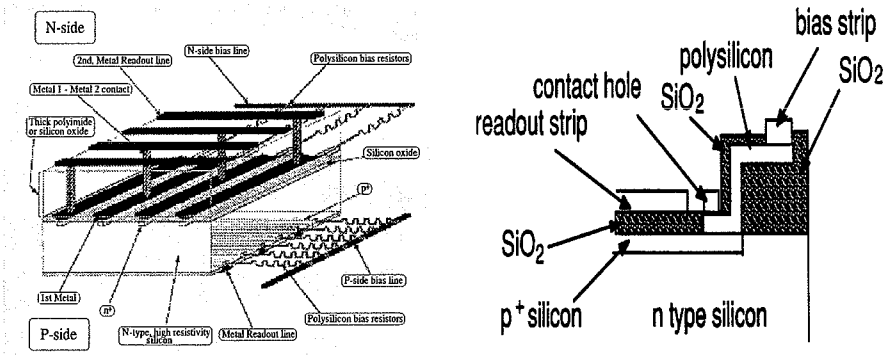

Figure 2.7: *A cross section view of the double-sided silicon microstrip detector developed for the DELPHI VD showing the n and p implants (left) and a detail of the implant of a p^+ strip (right) (from ref. [3]).*

develop a new design of capacitively coupled microstrip detectors with double-sided readout [5]. These detectors provide space points with the same amount of material as single-sided microstrip devices.

Double-sided silicon microstrip detectors are obtained by implanting strips, in orthogonal directions, on both the p- and n- sides of the silicon junction (see Figure 2.7). The signal induced by the electron-hole pairs produced in the depleted region is readout through capacitively coupled metallization strips connected with front-end preamplifiers. The use of a double metal layer makes possible to route the readout lines of both sides at the same detector edge, where a readout chip is bonded. With this design the readout chips are installed outside the detector sensitive region thus further reducing the amount of material traversed by the particles. The bias voltage is applied on both sides by polysilicon resistors connecting each strip to a common bias bus. Finally p^+ type implantations or field plates, added between the n^+ strips, are used to disrupt the accumulation of electrons at the oxide-Si interface and to prevent the signal to spread over several contiguous strips thus compromising the detector resolution. The detector thickness is 300 μm with strip pitch of 25 μm for the p side and 50 μm for the n side implantations with readout pitch of 50 μm for both sides. The readout is performed by Microplex MX6 readout chips, each with a 128 input channel amplifier produced in 3 μm CMOS technology. The output is multiplexed and read out at 2.5 MHz.

The passage of charge particle tracks through the active layers generate signals produced on the strips adjacent to the particle position of impact. These signals are characterised by their positions and measured pulse heights. Due to the inter-strip capacitive coupling and the finite size of the ionisation column, two or more adjacent strips are usually fired by a single charged

particle forming a so called *cluster*. Since a particle creates the same number of electrons and holes, the signals induced on the p and n strips have the same pulse height. This feature of double-side microstrip detectors can be exploited in the pattern recognition to solve ambiguities in associating the $R-\phi$ and z hits originating from a particle. The most probable signal to noise ratio for strip clusters has been measured to be 17:1 for the outermost layer and 11:1 for the innermost layer.

The centre of gravity of the charge collected on contiguous strips has been used to determine the point of impact of a charged particle. The single hit resolution has been measured using the regions of overlaps of detectors in a layer used for the detector internal alignment. From the residues of hits of particle tracks, single point resolutions of 7.6 μm in the $R-\Phi$ projection and 9 μm in the z coordinate for perpendicular tracks have been measured (see Figure 2.8). The track extrapolation resolution is quantified by the so called impact parameter resolution,

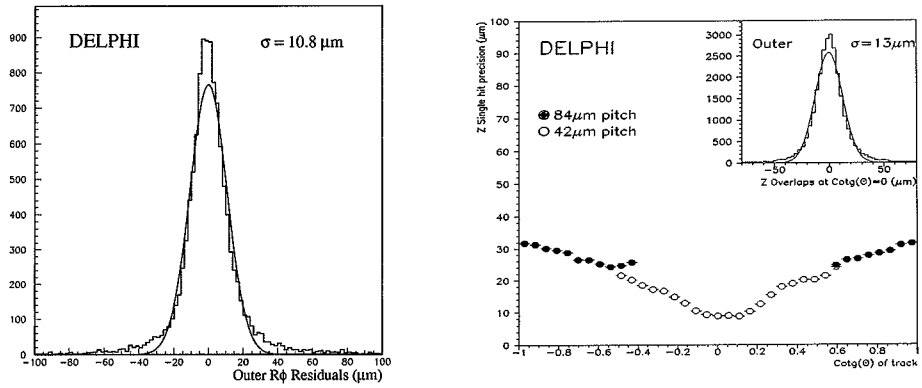

Figure 2.8: *The residual distributions in $R-\Phi$ (left) and, as a function of the incidence angle, z (right). The single point resoluton is given by the gaussian width of the distributions divided by $\sqrt{2}$. The inset in the right plot shows the z residual distribution for tracks at normal incidence (from ref. [2]).*

i.e. the accuracy in reconstructing the point of closest approach of a track to the Z^0 production point as discussed in details in section 2.2.1.

2.1.3 The Calorimeters

Detection of the energy carried by the particles produced in the e^+e^- annhilations is performed by the electromagnetic calorimeters, mainly located inside the DELPHI coil, and by the hadron calorimeter that instruments the return yoke of the superconducting solenoid.

The electromagnetic calorimeter system is composed of the barrel calorimeter **High Density Projection chamber (HPC)** and the forward **Forward ElectroMagnetic Calorimeter (FEMC)** complemented by the very forward **STIC** and **VSAT** mainly used for luminosity measurements.

The **HPC** consists of 144 modules, each with 41 layers of lead wires mounted on a thin fiberglass-epoxy support. These act as converters while also defining the drift field in the gas volume. Electrons, produced in the electromagnetic shower initiated by either a photon or an

energetic electron, are drifted to rows of read-out pads where they induce signals, similarly to the case of the TPC. In this way both the energy released and the shower profile are measured in the calorimeter. This feature of the HPC detector has been the basis of the γ/π^0 separation and electron identification techniques used in the analysis of B decays as discussed in section 2.2.3. The total converter thickness is 18 $X_0/\sin\theta$. The response to photons has been parametrised as $\sigma(E)/E = 0.043 \oplus 0.32/\sqrt{E}$ for the relative energy resolution while the angular resolution has been measured to be $\pm$ 1.7 mrad in the azimuthal angle Φ and $\pm$ 1.0 mrad in the polar angle θ.

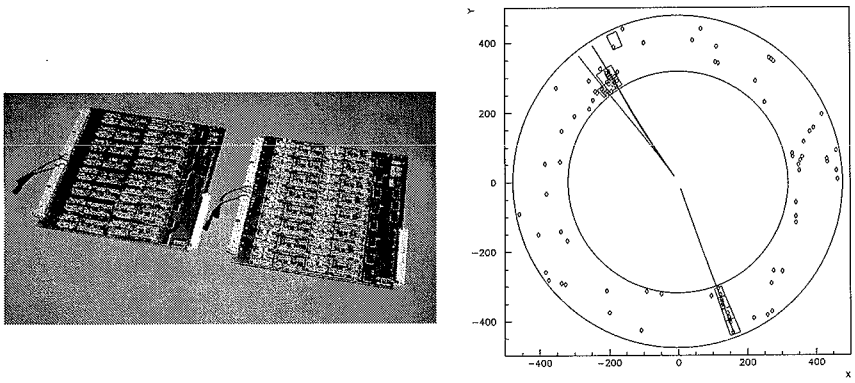

Figure 2.9: *A read-out board for the HCAL cathode readout designed and tested by the Helsinki group (left). Display of the HCAL response to a* $Z^0 \to \tau^+\tau^-$, $\tau^+ \to \mu\nu\nu$, $\tau^- \to \pi^+\pi^-\pi^-\nu$ *decay. The diamonds show the points reconstructed from the cathode signals and the boxes the energy depositions measured in the pads (right).*

The **Hadron Calorimeter (HCAL)** consists of limited streamer tubes interleaved in the 50 cm thick iron plates of the return yoke of the solenoid. It covers the polar angles from 11° to 169°. In the barrel region, five pads in the radial direction are read-out on the same channel, defining a tower. The relative energy resolution has been measured to be $\sigma(E)/E = 0.21 \oplus 1.12/\sqrt{E}$ in the barrel region. In order to increase the granularity of the detector, the cathode signals of the individual streamer tubes are also read-out. The cathode read-out information provides energy information independent from the pad response, improves the matching of the hadronic showers with reconstructed charged particle tracks and the detection of neutral hadrons and muons.

Outside the HCAL, the **MUon Chambers (MUC)** identify weakly interacting charged particles penetrating through the iron of the calorimeter. Three modules of drift chamber detectors, the first embedded in the return flux iron and the two outermost staggered, in the barrel and two planes in the forward region ensure the full solid angle coverage. The point resolution is about 2 mm for the barrel and 5 mm for the forward part, matching the requirements from the accuracy on the track trajectory extrapolation due to multiple scattering.

2.1.4 The Ring Imaging CHerenkov Detector

The DELPHI **Ring Imaging Cherenkov Detector (RICH)** has been the first example of RICH detector installed in a collider experiment [6]. The aim of the RICH is to detect the Cherenkov light [7] emitted by a particle when travelling in the radiator at a speed v_p larger

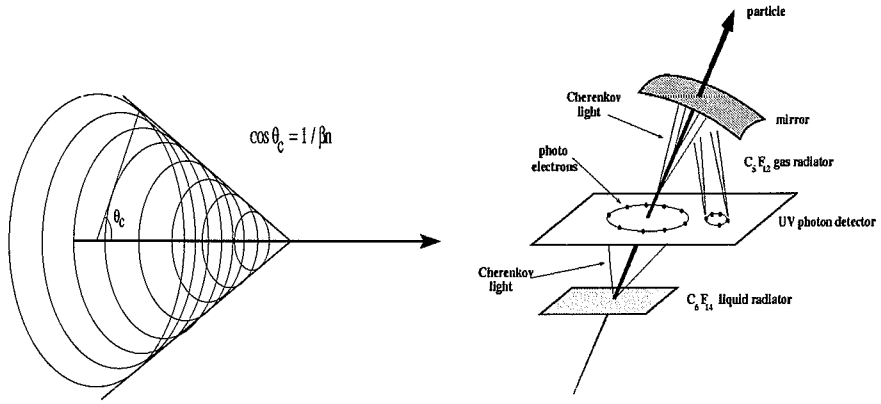

Figure 2.10: *Huygens construction showing the build-up of a coeherent spherical wave front for radiation emitted by a particle at $v_p > c/n$ (left) and the principle of formation of Cherenkov rings in a RICH detector (right).*

than that of light in the same medium $v_\gamma = 1/n$ and to determine the mass of that particle by measuring the angle of emission of the radiation. The emission of radiation along the particle path forms a front of coherence that propagates as a cone at an angle θ_c with the particle direction, known as Cherenkov angle. From the construction of Figure 2.10 it follows that:

$$\cos\theta_c(\lambda) = \frac{1}{\beta n(\lambda)} = \frac{\sqrt{p^2+m^2}}{pn(\lambda)} \tag{2.2}$$

where p and m are the particle momentum and mass and β its velocity v_p/c and $n(\lambda)$ is the refractive index of the radiator for a given photon wavelength λ. Once the particle momentum p is measured independently and the refractive index n is known, the measurement of the Cherenkov angle provides a determination of the particle mass as $m = p\sqrt{n^2\cos^2\theta_c - 1}$. There is a minimum velocity $\beta_{min} = 1/n$ below which no Cherenkov ligh is emitted, while for $\beta \to 1$ the Cherenkov angle approaches a saturation value $arcos(1/n)$. Finally it can be shown [8] that the number of photons emitted per unit of particle path and of photon energy is given by: $d^2N_{ph}/dLdE = 370\sin^2\theta_c$, for particles of unit charge. The particle energy radiated for a particle with $\beta = 1$ is about 1% of the energy loss for ionisation. The number of photons is thus proportional to $sin^2\theta_c$ and therefore to the particle velocity and to its mass. All these features of the emission of Cherenkov light are used in the RICH detector to identify stable particles. The principle of the Ring Imaging Cherenkov technique [9] is to detect the Cherenkov photons on the focal plane of a set of mirrors reflecting the Cherenkov light back to a photon detector. Once the cone of radiation intercepts the detecting plane, the photons are seen as a ring (Cherenkov ring) with radius R_c proportional to $\tan\theta_c$ (see Figure 2.11).

In the DELPHI RICH detectors two different radiators have been chosen, one gaseous (C_5F_{12}) with low refractive index ($n = 1.00172$ for 7 eV photons) to identify high momentum hadrons and one liquid (C_6F_{14}) with higher refractive index ($n = 1.283$ for 7 eV photons) to complement the identification at low momenta. The liquid and gaseous Cherenkov radiators are separated by a photosensitive TPC volume delimited by UV transparent quartz walls. In the gas radiator, photons are produced over an average useful path of 40 cm and are reflected by a total of 408 mirrors on the photon detector. Cherenkov photons produced in the 1 cm thick liquid radi-

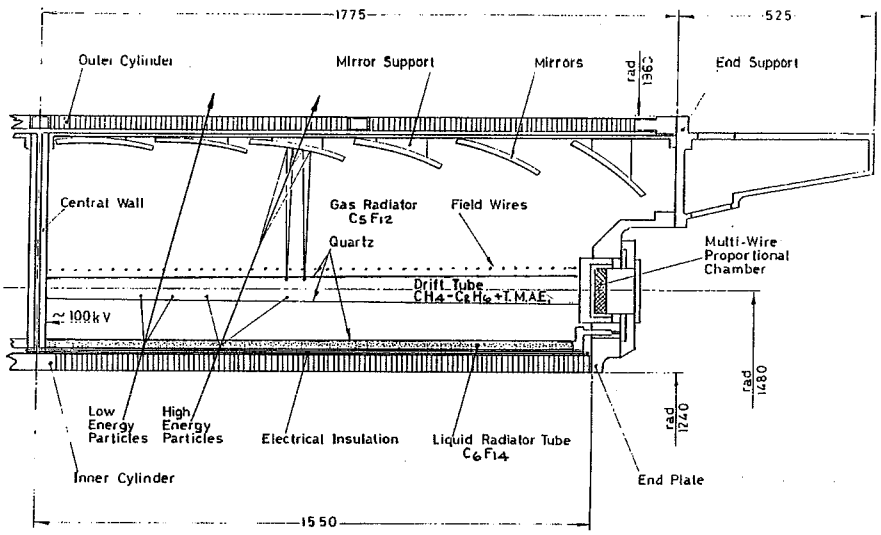

Figure 2.11: *Schematics of the DELPHI Barrel RICH detector.*

ator propagate up to the photon sensitive TPC by proximity focusing. The Cherenkov angle is computed by measuring the radius of the resulting ring with center given by the extrapolated particle trajectory. For tracks at large angles, part of the Cherenkov photons are totally reflected at the quartz interface and are therefore lost for detection. The geometry provides separation between the charged particle ionisation in the detector and the reflected ring from the gas radiator in order to reduce the background and dead-time due to the primary ionisation. The system runs at constant pressure of 1030 hPa and at $40°C$ temperature to avoid risk of perfluorocarbon condensation. The full solid angle coverage is provided by three independent detectors, two equipping the forward regions and one the barrel section of DELPHI.

Each photon detector consists of a TPC filled with $CH_4 + C_2H_6$ drift gas added with vapours of the photosensitive Tetrakis diMethyl Amino Ethylene (TMAE) agent [10]. Cherenkov photons are converted into electrons (called *photoelectrons*) by the photoionisation process. The TMAE has a ionisation threshold of 5.5 eV matching well both the typical energy of Cherenkov photons, in the UV range, and the transparency curve of the fused quartz walls of the photon detector. Photons are converted according to $N_{ph}(x) = N_{ph}(0)e^{-\mu x}$ where the absorption coefficient μ depends on the photon energy and TMAE concentration in the drift gas. Now the mean free path for a photon has to be kept small compared with the thickness of the detector active volume to maximise its efficiency. This implies a high TMAE concentration that may reduce the electron lifetime in the drift field due to the presence of electronegative TMAE oxidation products. At an optimal working point, photons from the liquid radiator are converted in the lower half of the detector and those from the gas radiator in the upper half, thus helping the Cherenkov ring pattern recognition.

At the operational TMAE temperature of 28°, the photon mean free path is 1.6 cm, that is small compared with the active detector thickness, and the electron attenuation length is larger than 10 m for 1.5 m of maximum drift length. Photoelectrons are drifted along the volume defined by a drift field directed along the beam axis at the outer end of the detector where they are collected and multiplied in a Multi Wire Proportional Chamber (MWPC) [11]. The photon

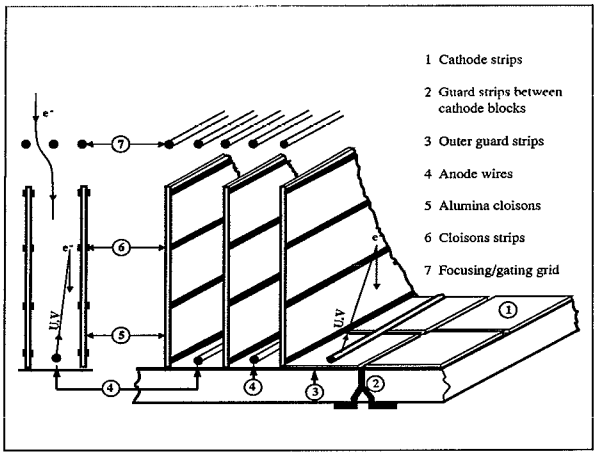

Figure 2.12: *Layout of a MWPC of the RICH photon detector.*

detector is optimised for single electron detection requiring a high gain MWPC (2×10^5). The generation of columns of dense ionisation by the energy loss of charged particle (corresponding to 300 - 500 e^-) imposes special care to achieve a stable detector operation. In fact UV photons produced in the gas amplification process may reach the photosensitive gas where they would be converted in the photosensitive gas and induce spurious signals. At the DELPHI RICH operation condition the probability for an incoming electron to create a feedback avalanche by this process is of the order of 10%. This corresponds to 30-50 spurious electrons per track that would obscure the 8 Cherenkov photoelectrons expected from the gas radiator. Therefore blinds were added to separate the anode wires, thus suppressing these feedback effects by one order of magnitude by reducing the solid angle seen by the photosensitive volume. The layout of the DELPHI RICH MWPC is shown in Figure 2.12. There are 48 drift tubes in the barrel and 24 in each of the two forward sections.

The resolution on the reconstruction of the Cherenkov angle of a single detected photon is determined by the accuracies on the photon conversion point, on the photon emission point and on the particle direction. The MWPC measures the *photon conversion point* by the signal induced by the avalanche, providing two coordinates of the position of the photon conversion by the wire number and the centre of gravity of the induced signal on the cathode strips. The third coordinate, as in a TPC, is given by the measured drift time. This provides spatial reconstruction of the photon conversion point. With anode pitch of 2.62 mm, cathode pitch of 4.0 mm and drift time resolution of 8 ns the detector has point resolutions of $\sigma_x = 0.8$ mm, $\sigma_y = 1.2$ mm and $\sigma_z = 1.2$ mm. The overall resolution on the reconstruction of the photon conversion point is given by the convolution of the detector resolution with the contribution from the diffusion in the drift gas as: $\sigma^2_{rec} = \sigma^2_{det} + \sigma^2_{diff}$. This resolution depends on the actual drift length as shown in Figure 2.13. Performances of the DELPHI RICH detectors are summarised in [12] In order to derive the resolution on the individual Cherenkov angle the effect of the geometric and chromatic resolutions have also to be taken into account. In the RICH detector the point of emission of the Cherenkov photon is not measured and has to be approximated as the centre of the particle trajectory in the radiator. This approximation contributes to the geometrical error. Also the trajectory of the particle is known only with a finite accuracy depending on the tracking detectors resolution and on the multiple scattering in the RICH

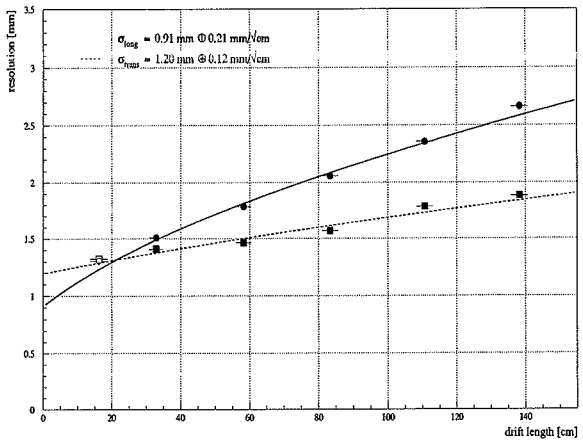

Figure 2.13: *The longitudinal and transverse single photon resolution as a function of the drift length z. Points show measured values in the RICH detector. The curves correspond to the fit of the expected dependence* $\sigma_z = \sqrt{(\sigma_t v_d)^2 + (\sigma_L^2 z)}$ *and* $\sigma_{x,y} = \sqrt{s/12 + (\sigma_T^2 z)}$ *where* $\sigma_{T,L}$ *are the transverse and longitudinal diffusion coefficients,* σ_t *the time resolution,* v_d *the drift velocity and s the MWPC read-out pitch. The resolution extrapolated at zero drift corresponds to the intrinsic detector resolution* σ_{det} *[13].*

detector itself. Finally the *chromatic error* is due to the dependence of the radiator refractive index $n(\lambda)$ on the wavelength of the produced photon. Cherenkov photons are produced over a continuum of energies and the region of interest of this spectrum depends on the radiator and quartz transmission curves and on the photosensitive agent ionisation potential and quantum efficiency curve. The chromatic error is given by $\Delta\theta_c = \Delta n/n \tan\theta_c$. The relative contributions of these effects to the overall single photon θ_c resolution depends on the detector design. In the case of the DELPHI RICH gas radiator response, the MWPC resolution dominates in the experimental resolution, the mirror focusing diminishing the geometrical effects. In the liquid radiator, the three components have comparable contributions to the overall resolution. Single photoelectron resolutions can be measured by using high momentum particles, as, for example, from $Z^0 \to \mu^+\mu^-$ events, for which the Cherenkov angle saturates [12]. Typical values for the resolution and of the number of detected photoelectrons are given in Table 2.1 and the related distributions are shown in Figure 2.14.

Table 2.1: *Measured number of photoelectrons and single photon resolution in the barrel and forward DELPHI RICH detector.*

Barrel RICH	Nb. of p.e.	$\sigma(\theta_c)$ (mrad)	Forward RICH	Nb. of p.e.	$\sigma(\theta_c)$ (mrad)
Liquid Radiator	13.3	14.0	Liquid Radiator	7.5	11.4
Gas Radiator	8.3	4.3	Gas Radiator	8.0	2.5

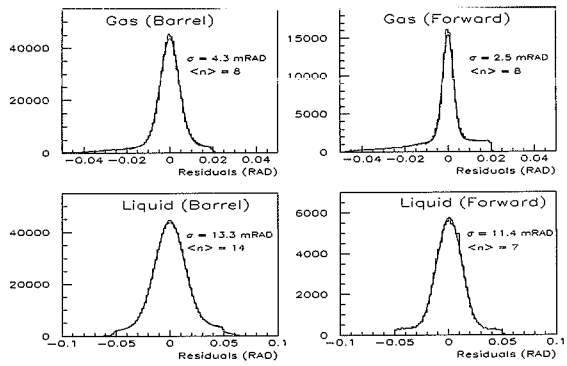

Figure 2.14: *The Cherenkov angle reconstructed for tracks from $Z^0 \rightarrow \mu^+\mu^-$ events in the Gas (upper plots) and Liquid (lower plots) radiators of the Barrel (left) and Forward (right) RICH detectors.*

The typical response of the RICH detector to an energetic charged particle is shown in Figure 2.15 for a $Z^0 \rightarrow \tau^+\tau^-$ decay from the DELPHI 1994 real data.

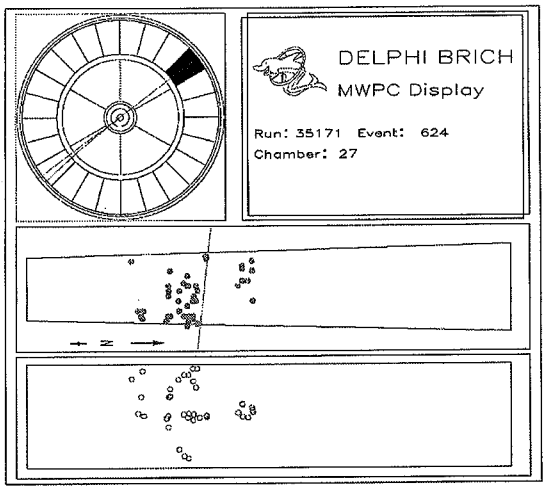

Figure 2.15: *Display of the Barrel RICH response to an energetic particle from a $Z^0 \rightarrow \tau^+\tau^-$ event. The dots show the detected electrons from side (center display) and top views (lower display) of the drift tube. The MWPC is at the right end of the drift volume. It is possible to distinguish the primary ionisation along the extrapolated track direction, the complete small gas Cherenkov ring and a portion of the larger liquid ring. Electrons detected behind the primary ionisation column are mostly due to feed-back and cross-talk in the MWPC.*

2.2 B decay reconstruction

The response of the different detector systems is at the basis of the techniques for B decay reconstruction. These require to first select $Z^0 \rightarrow b\bar{b}$ events, then to identify the particles originating from the heavy hadron decay and finally to classify its decay mode.

2.2.1 Track Impact Parameter and $Z^0 \rightarrow b\bar{b}$ Tagging

In $Z^0 \rightarrow q\bar{q}$, a $b\bar{b}$ pair is produced in about one every five decays. Due to the high luminosity obtained by LEP in its running around the Z^0 peak from 1990 to 1995, a sample of about 1.5×10^6 b quark decays was recorded by each of the four experiments. However their study requires an efficient procedure for separating the $b\bar{b}$ events from the hadronic decays of the Z^0 boson into lighter quark pairs and to identify the B decay products. The first method employed to select b quark events was the use of the semileptonic decays of heavy quarks.

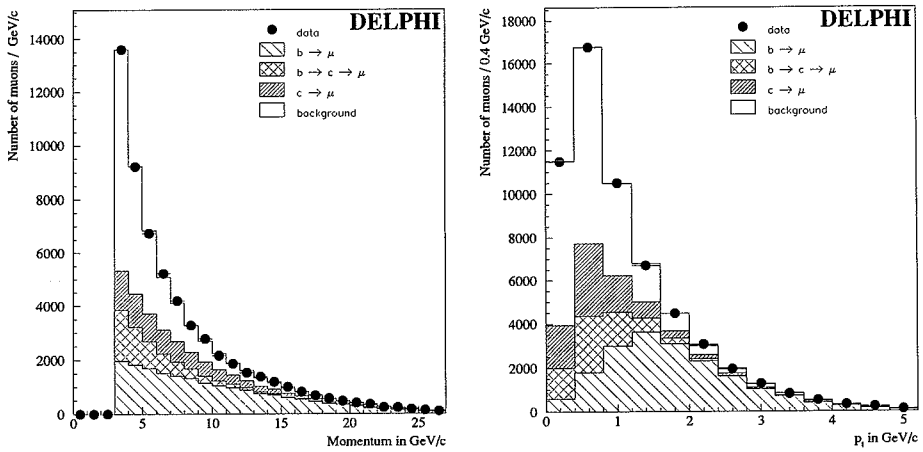

Figure 2.16: *The distribution of the momentum p (left) and the momentum component transverse to the jet thrust axis p_t (right) for candidate muons from the DELPHI data. The different muon sources as predicted by the simulation are also shown. At large p and p_t values, the sample is enriched in muons from $b \rightarrow X\mu\nu_\mu$ decays.*

In fact, in B decays, a lepton can be emitted as a result of either the direct semileptonic $b \rightarrow cl\nu$ decay or the cascade decay $b \rightarrow c$ followed by $c \rightarrow sl\nu$. The main background sources are due to the direct semileptonic charm decay and to hadrons misidentified as leptons. Both these backgrounds can be reduced by using the fact that, due to the large B mass, the component of the momentum of the lepton from the B decay, transverse to the B direction, is large. The B direction can be approximated by the jet axis and the distribution of the transverse momentum p_t from the different sources contributing to the tagged lepton sample is shown in Figure 2.16. By choosing leptons with large values of p_t, a sample highly pure in B events can be obtained. This method was already used by experiments at lower energy colliders, in particular for the measurement of the B hadron lifetime [14]. The main drawback in using high p_t leptons for selecting B decays is the small tagging efficiency. This is due to the fact that only about 20% of B particles decay by emitting either an electron or a muon.

Other techniques using event or hemisphere shape variables have been also applied but the use of high resolution silicon vertex detectors and the favourable kinematics have made the use of the track and vertex topology the best mean for identifying and reconstructing B decays at LEP.

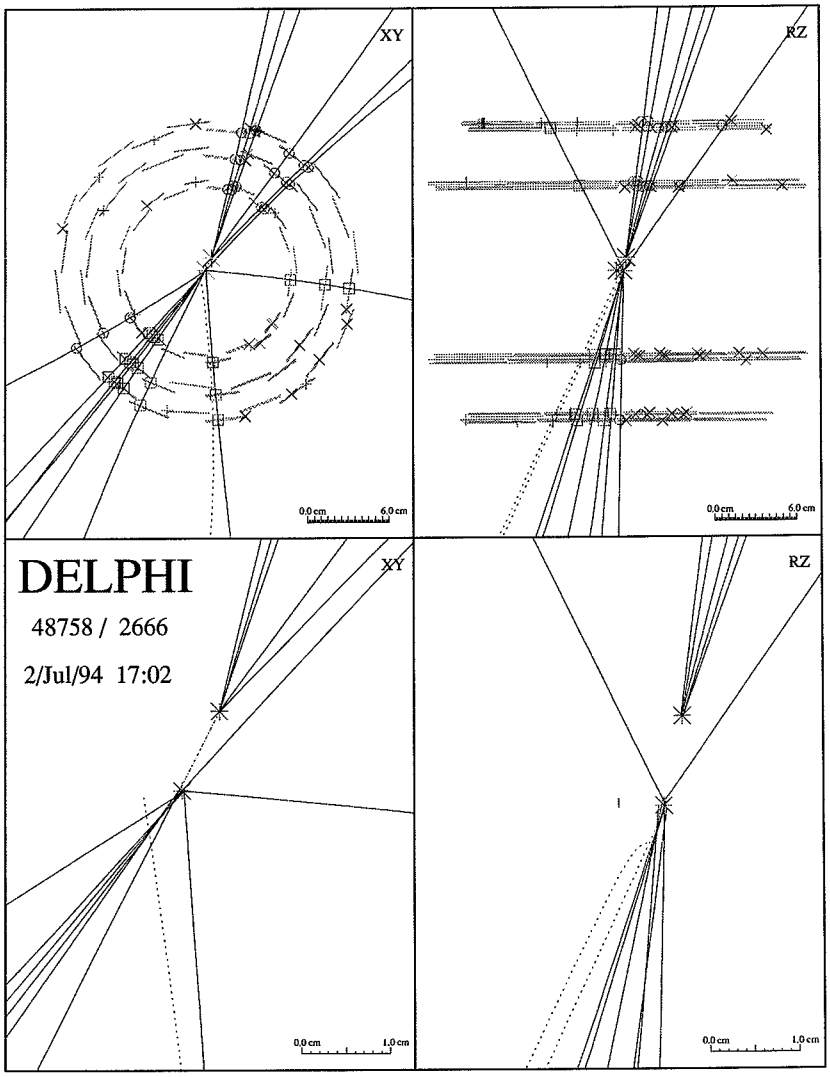

Figure 2.17: *Display of an identified $Z^0 \to b\bar{b}$ decay showing the $R-\phi$ (left) and $R-z$ (right) view in the DELPHI Microvertex detector and a magnification of the vertex region (below). The displaced secondary vertex from the decay of a long flying B particle is clearly visible in both the projections.*

The average boost $\gamma = \frac{1}{\sqrt{1-\beta^2}}$ for a B hadron is about 7. Since the B hadron lifetime is $\tau_B = 1.55$ ps, this gives an average decay distance in space $< l_{space} >= \beta\gamma c\tau_B = 2.1$ mm. In addition the average charged decay multiplicity for a B particle is 5.5, to be compared with the average jet multiplicity of about ten. If the resolution in extrapolating the reconstructed particle tracks to their production vertex is high enough, $Z^0 \rightarrow b\bar{b}$ decays can be characterised as events with a significant fraction of particles originating at vertices distinct from the Z^0 production point at the LEP interaction region. It is more useful to discuss the compatibility of tracks with the Z^0 production point introducing a new track variable called impact parameter. The impact parameter d is defined as the distance of closest approach of a particle to the Z^0 production point. Because the track reconstruction accuracy in the $R-\phi$ plane is higher, the projection of the impact parameter to this plane is generally used. This can be expressed as:

$$d = \beta\gamma c t_B \sin\alpha \sin\theta \tag{2.3}$$

where t_B is the proper decay time of the B particle, α is the angle of the track with respect to the direction of the parent particle, projected in the $R-\phi$ plane and θ the polar angle of the parent particle. It is interesting to notice that, for large values of $\beta\gamma$, this factor is on average cancelled by the decrease of the angle α, so that the ratio $< d > /c\tau_B$ becomes independent on the decay kinematics. This characteristic has made the use of the impact parameter an important technique in the determination of the B lifetime [14, 15, 16]. The average impact parameter for B decay products is about 300 μm. Secondary particle tracks, originating from the decay of B hadrons, or of other long-lived particles, are characterised by non-zero values of their impact parameters. On the contrary particles directly originating from the fragmentation process or from promptly decaying resonant states have impact parameters compatible with zero, within the measurement accuracy. This accuracy σ_{IP} is the convolution of the resolution in extrapolating charged particle tracks from the first measured point in the vertex detector to the production vertex inside the beam pipe σ_{extr} with the accuracy in reconstructing the Z^0 production point σ_{vtx}. The extrapolation resolution σ_{extr} can be parametrised in terms of the intrinsic resolution σ_{asympt} and the multiple scattering term σ_{ms}. This is due to the small angle deflections suffered by the particle in its Coulomb interactions with the nuclei of the traversed medium and it contributes with a term dependent on the momentum p and on the amount of material traversed as:

$$\sigma_{ms} = \frac{\alpha_{ms}}{p \sin^{3/2}\theta} \tag{2.4}$$

where α^2_{ms} is proportional to the material thickness expressed in units of radiation length x/X_0 with $X_0 = 9.36$ cm in silicon. Therefore $\sigma_{extr} = \sqrt{\sigma^2_{asympt} + \sigma^2_{ms}}$. The particle trajectory resolution performances, achieved including the VD, are summarised in Figure 2.18.

The Z^0 production point can be obtained by an event-by-event fit of the primary vertex position using the constrain of the LEP beam-spot position. A two step procedure is used for determining the primary vertex. First, primary vertices are reconstructed for all hadronic events. The primary vertex fit is based on the Kalman Filter algorithm [17]. This algorithm allows single tracks to be added or removed from the fit easily. Tracks are tested for compatibility with the primary vertex by calculating their individual χ^2 contributions to the vertex fit. After scaling the track reconstruction errors appropriately, the χ^2 probability distribution is flat, except for a peak due to tracks at low probabilities. Such tracks, having a probability of less than 1%, are removed and the vertex refitted. The vertex reconstruction error depends on the number of tracks used in the vertex fit and on the event topology. Its typical value, in the direction orthogonal to the event thrust axis, is ± 110 μm. The vertices obtained by this procedure have been used to measure the average position and the width of the interaction region for each LEP fill. The mean beam position in a fill has been reconstructed to better than 20 μm in both x

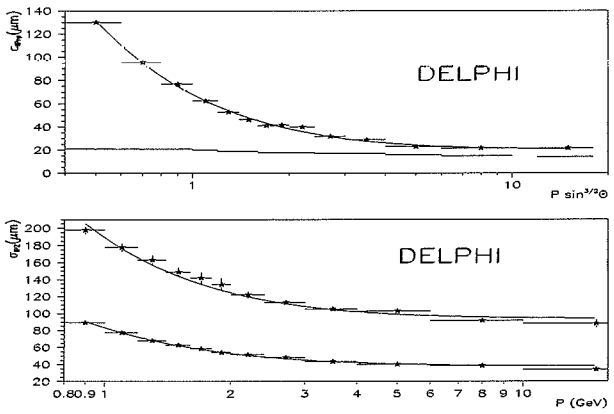

Figure 2.18: *Track extrapolation resolution as a function of the particle momentum in the $R-\phi$ (upper plot) and z coordinates. This resolution has been obtained by subtracting in quadrature from the impact parameter resolution the primary vertex resolution also shown by the line in the upper plot. The full line corresponds to $(65/p\sin^{3/2}\theta \oplus 20)\mu m$. The two set of values in the lower plot refer to tracks with $45° < \theta < 55°$ and $80° < \theta < 90°$; the full lines correspond to $(71/p \oplus 39)\mu m$ and $(151/p \oplus 96)\mu m$ respectively. Tracks close to normal incidence have better resolution due to the smaller amount of traversed material. Similarly, the degradation of the resolution at low particle momenta is due to multiple scattering in the beam-pipe and in the first silicon layers of the VD (from ref. [3]).*

and y. Due to the small vertical size of the interaction region ($\approx$ 15 μm), the reconstruction accuracy achieved in this first step has been deduced from the apparent vertical size while the horizontal size of the beam spot has been determined by unfolding this reconstruction error from the apparent horizontal size. This has been measured for all fills with sufficient statistics. As these mean beam positions have been reconstructed using a large number of vertices, they are essentially independent of any individual event. Therefore, in a second step, an optimal estimate of the Z^0 production point has been obtained by re-evaluating the vertex including the beam constraint for each event. The mean beam position in the fill has been used to initialize the fit. Subsequently, tracks were tested for compatibility with this vertex position before being included in the final primary vertex estimate. After this procedure, the small vertical beam size dominates the y value but the fitted x value is more accurate than the average beam position. The impact parameter has been therefore computed with respect to this fitted vertex. To avoid the bias due to the inclusion of the track in the fit, each track has been removed from the vertex fit before computing its impact parameter. The compatibility of a particle track with the event primary vertex can be obtained by the impact parameter significance $S = d/\sigma_{IP}$.
The track impact parameter is attributed a sign depending on the position of the intersection of the particle track with the jet thrust axis. The sign is positive if the intersection point corresponds to a positive decay length. Particle with negative impact parameter appear as they originated behind the primary vertex. Since this configuration is unphysical, the impact parameter sign becomes negative due to the finite reconstruction accuracy. Therefore the resolution σ_d can be studied on the negative part of the signed impact parameter distribution. In Figure 2.19

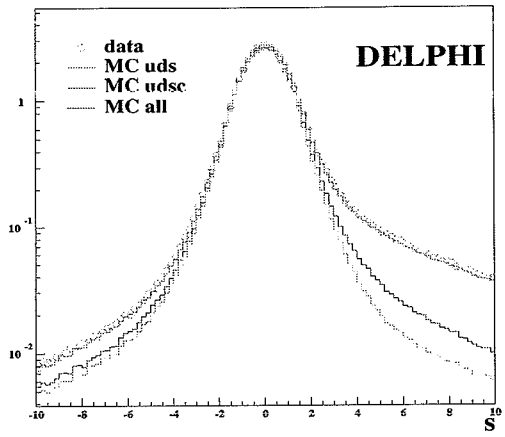

Figure 2.19: *The impact parameter significance S for tracks in $Z^0 \to q\bar{q}$ events recorded by DELPHI (left). The continuous lines represent the different components as obtained from simulation while the open dots show the data. The asymmetry produced by $b\bar{b}$ events at large positive values of significance is well visible.*

the impact parameter significance is plotted for particle tracks from real and simulated events showing that the region at large positive values of S is highly enriched in B decay products. $Z^0 \to b\bar{b}$ events have been selected by a tagging algorithm that uses the probability that all the tracks in the event are compatible with originating from the primary vertex [18]. For a given set of N tracks having impact parameter significances S_i, the probability that they all originate from the primary vertex is given by:

$$P_N = \Pi \sum_{j=0}^{N-1} (-ln\Pi)^j / j! \tag{2.5}$$

where $\Pi = \prod_{i=1}^{N} P(S_i)$. It can be shown that P_N has the correct behaviour of a probability [19]. In particular P_N has an uniform distribution between zero and one for tracks originating from the primary vertex while it peaks at small values for those sets of tracks including secondary particles as shown in Figure 2.20. This algorithm can be applied to both event tagging and to restricted track samples as in the case of the tag of a single jet or hemisphere. By varying the value of the cut on the N track probability P_N, the purity of the selected sample can be varied as shown in Figure 2.21 in the case of event tagging. In the case of B decay reconstruction, further enrichment in $b\bar{b}$ events can be obtained by the requirements on vertex topology and kinematics in the different analyses. For this reason rather loose b tagging requirements have been applied to hadronic events. Typical cut values have been set to 0.03 - 0.01 on the event probability from the b-tagging algorithm. These cuts give an efficiency of 0.85 - 0.75 for $Z^0 \to b\bar{b}$ events and a purity of 0.67 - 0.80.

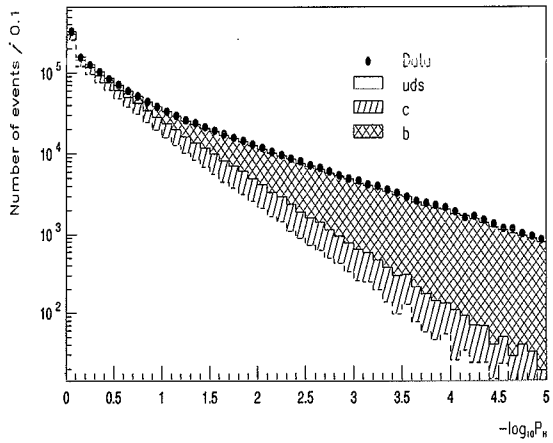

Figure 2.20: *The b-tagging probability for tracks in one hemisphere in $Z^0 \rightarrow q\bar{q}$ events. The $b\bar{b}$ pairs have an excess of events at low values of probability due to the presence of secondary particles from the B decay chain. This is also the case for $c\bar{c}$ events but the effect is less pronounced due to the shorter lifetime of charm hadrons.*

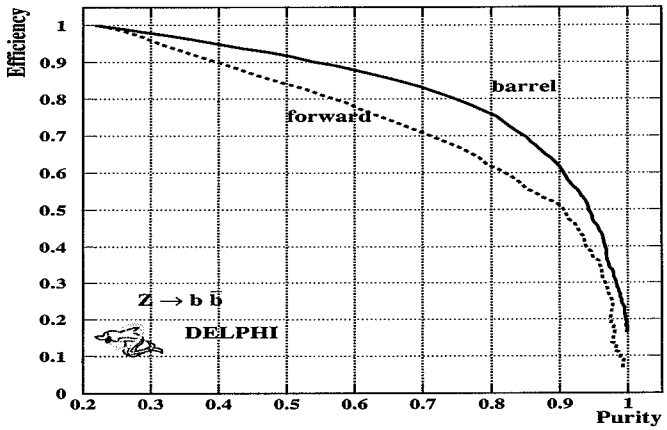

Figure 2.21: *The b-tagging efficiency as a function of the purity of the tagged sample for different values of the cut on the event probability (upper plot). The full lines show the tag performances for events fully contained in the barrel region and the dashed line for events in the forward region.*

2.2.2 Topological reconstruction of B decays

The b-tagging techniques described in the previous section separate the $Z^0 \to b\bar{b}$ events from most of other decays modes of the Z^0. Nevertheless they do not provide information on the B decay mode. A detailed study of weak decays of beauty particles needs the reconstruction of the B decay chain. This can be performed both by inclusive techniques and partial reconstruction or by selecting fully reconstructed exclusive final states [20]. The first approach leads to relatively large samples containing a mixtures of different B decay modes while in the second case the significantly lower reconstruction efficiency is compensated by higher purity and by a more direct interpretation.

Techniques of inclusive B recostruction are based on the use of discriminating variables for separating particles that are B decay products from those produced in the hadronisation. Discriminating variables exploit the B decay kinematics as the p, p_t and rapidity, the particle mass and its topology as the particle impact parameter. Topological properties of B decays are further exploited for bundling candidate secondary particles and to fit a common secondary vertex. Primary particles can be identified and rejected iteratively. The original B energy, direction, decay multiplicity and charge can be estimated on a decay-by-decay basis from the identified decay products. Since the decay is usually not fully reconstructed, missing particles have to be accounted in the B energy estimate. This can be done effectively by introducing a scaling function based on the ratio of the measured to nominal B mass M_X/M_B whose functional dependence is optimised using simulation. B energy resolutions of 10% have been achieved in hadronic B decays and of 13% in semileptonic decays. This is important for those analysis requiring to reconstruct the B rest frame and to boost the decay particles to this frame. The efficiency for inclusive reconstruction of B decays is of the order to 50 - 70%, eventually lowered by additional requirements in order to improve the reconstruction of the B energy and direction. Examples of inclusive B decay reconstruction are those developed for the $b \to u\ell\nu$ and $b \to s\gamma$ analyses.

The study of fully reconstructed exclusive B decays proceed by selecting secondary particles consistent with forming the decay chain of interest. The reconstruction of exclusive B decays implies several constraints useful in rejecting background events. Firstly, in hadronic decays, the secondary particles must be consistent with the B mass and subsets of those with possible intermediate resonant states. Hadron identification is important at this stage since it reduces the combinatorial background due to the assignment of different mass hypotheses to the same particle. The candidate secondary particles are fitted at one or more secondary detached vertices according to the decay of interest. In order to further suppress the combinatorial, a minimum decay distance from the event primary vertex is required. Finally all particles not assigned to the B decay must come from the same primary vertex, being fragmentation particles. Fully reconstructed decay candidates with unassigned particles not consistent with originating at the primary vertex may be rejected as ambiguous. Typical reconstruction efficiencies for fully reconstructed exclusive B decays vary inversely with the final state multiplicity from 20% to a few %. These techniques have been effectively applied in several analyses as the determination of the mass of the B_s^0 [21] and Λ_b^0 [22] beauty hadrons and in the search for hadronic charmless decays as discussed in Chapter 4.

An important tool in the study of exclusive B decays is a versatile interactive graphic program visualising the trajectories of the particles in the vicinity of the primary vertex. The program VTXGRA has been developed for the needs of the analyses presented in the following and used to validate the response of the reconstruction program for the candidate exclusive decays [23].

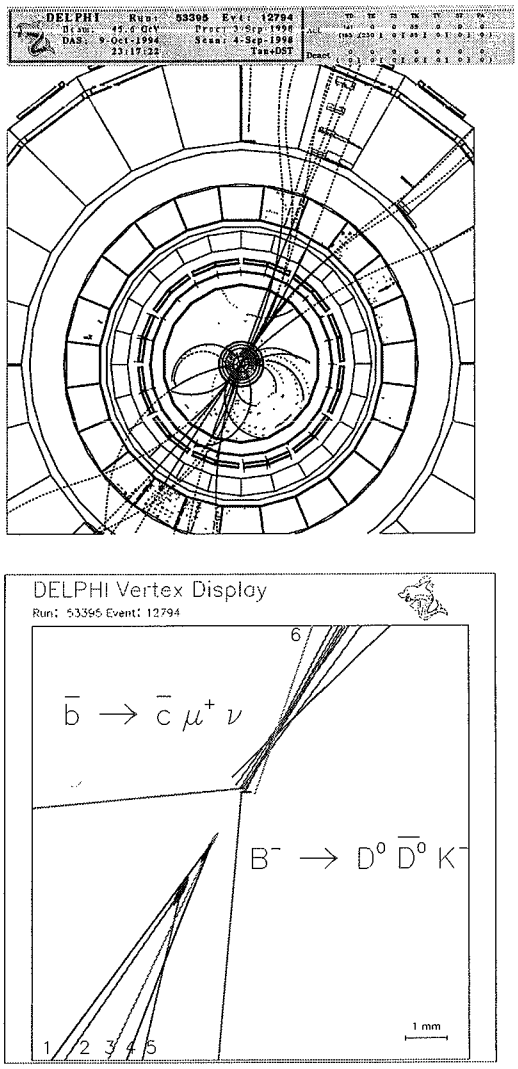

Figure 2.22: *Display of a $Z^0 \rightarrow b\bar{b}$ decay with a magnification of the vertex region obtained with the VTXGRA program. The combination of topological reconstruction and particle identification allowed to reconstruct the two decays, one inclusively and the second exclusively. In the upper hemisphere the $\bar{b} \rightarrow c\mu^+\nu$ decay is tagged by the observation of a μ^+ (labelled with 6 in the display) and an inclusively reconstructed secondary vertex. In the lower hemisphere a double charmed B^- decay is signalled by the presence of three kaons coming from the fully reconstructed decay $B^- \rightarrow D^0\bar{D}^0K_3^-X$; $D^0 \rightarrow K_2^-\pi_5^+$, $\bar{D}^0 \rightarrow K_1^+\pi_4^-(\pi^0)$. This is the first reconstructed unambiguous $B \rightarrow D\bar{D}K$ decay and proved that the $b \rightarrow c\bar{c}s$ decay rate is not saturated by $D_s\bar{D}$ final states [24].*

2.2.3 Particle Identification with DELPHI

Particle identification plays an important role in the reconstruction of B decays [25]. The CKM favoured $b \to c \to s$ decay chain produces a strange particle in the final state of decays of all B hadrons. In addition another strange hadron is produced, from the spectator s quark, in the decay of strange beauty B_s mesons. This feature can be used for tagging B_s decays. Similarly beauty baryons can be identified by the presence of a secondary proton.

The design of the DELPHI apparatus, as already highlighted by the experiment name, emphasises the importance of identifying the stable particles detected in e^+e^- annihilations. A key component for this task are the Ring Imaging Cherenkov detectors already described in details in the previous section. In the following the techniques developed in the identification of stable hadrons are discussed.

The **identification of charged hadrons** is based on the combined response of the TPC and RICH detectors. As already mentioned, the TPC provides with up to 192 measurements of the specific energy loss dE/dx of a charged particle while travelling through its drift gas volume. These measurements follow a Landau distribution centered around the most probable value,

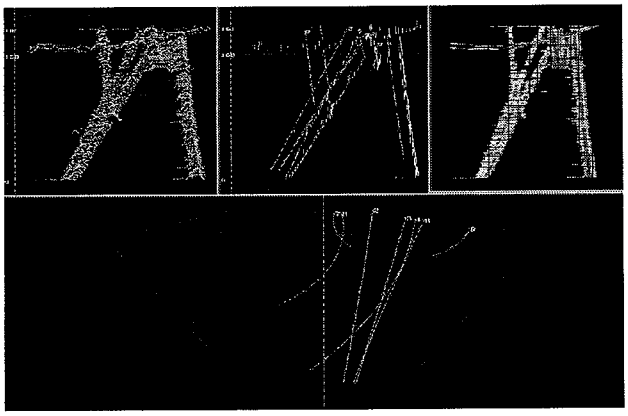

Figure 2.23: *The response of the TPC to three charged particles from a* $\tau^+ \to \pi^+\pi^-\pi^+\nu$ *decay. The upper central plot shows the pulse height measured on the TPC sensitive wires used to determine the* dE/dx *of the particles [26].*

depending on the mass of the particle, as given by the Bethe and Bloch formula:

$$\frac{dE}{dx} = K\frac{Z}{A}\frac{1}{\beta^2}[\frac{1}{2}ln\frac{2m_ec^2\beta^2\gamma^2T_{max}}{I^2} - \beta^2 - \frac{\delta}{2}] \tag{2.6}$$

where β is the particle velocity, T_{max} the maximum kinetic energy transferable in a single collision, I the mean excitation energy of the medium and δ a density correction effect. At low momenta π, K and p are separated by their dE/dx in the $1/\beta^2$ region. At energies above the minimum of ionisation, the identification is performed in the region of $ln\beta\gamma$ relativistic rise of the specific ionisation, due to the contribution of long distance collisions. To achieve the best separation between different mass hypoteses, in the analysis of the DELPHI TPC data, the dE/dx is estimated by the truncated mean on this distribution where 80% of the lowest measurements are considered. In addition, measurements affected by overlaps of different tracks are also rejected. The resulting distribution of dE/dx shows clearly the bands due to particles of different mass as a function of the particle momentum as shown in Figure 2.24. The resolution

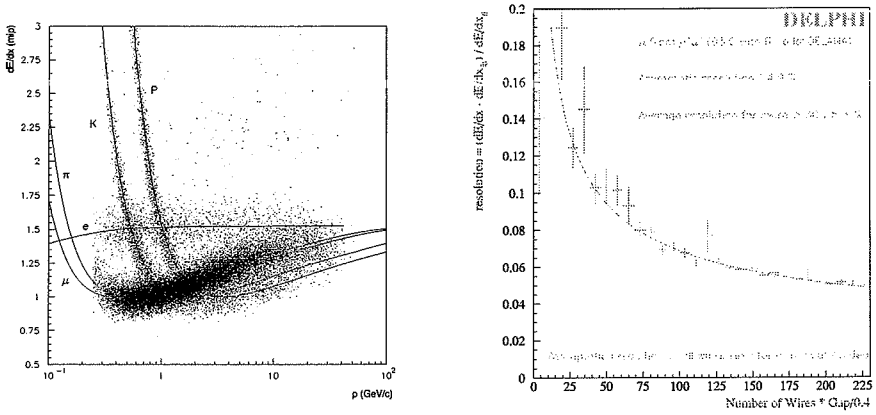

Figure 2.24: *The measured dE/dx as a function of the particle momentum p showing the bands due to particles of different masses (left) and the dE/dx resolution as a function of the number of wires used (right) [26].*

on dE/dx depends on the number of samplings available as shown for the case of isolated, high momentum tracks in Figure 2.24. In hadronic events the typical average resolution for accepted dE/dx measurement is 7%. This corresponds to a 1.5 σ π/K separation in the region of the dE/dx relativistic rise above 3.0 GeV/c.

Hadron identification with the RICH detectors is based on the measured Cherenkov angles and observed number of photoelectrons for particles traversing its active volume. Both the Cherenkov angle θ_c and the number of photoelectrons n_{pe} give information on the mass m of a particle of momentum p on the basis of the formulae:

$$m = p\sqrt{n^2 \cos^2 \theta_c - 1} \tag{2.7}$$

$$n_{pe} = N^0 Z^2 \sin^2 \theta_c \tag{2.8}$$

Below the threshold for Cherenkov light, given by $\beta = 1/n$, no photons are emitted by the particle. This region is called *veto region* and the identification is achieved on the basis of the observed number of photoelectrons. Above the veto region, kaons and protons can be separated from lighter particles (e,μ or π) using the Cherenkov angle of the detected radiation (*ring region*). The extension of these regions in the DELPHI Barrel RICH detector is summarised in Figure 2.25 and Table 2.2.

The resolution on the Cherenkov angle from the single photoelectron measurement is not accurate enough for efficient identification over a large momentum interval. In addition background may bias the mass determination and an optimal procedure defining the Cherenkov angle and the number of signal photoelectrons needs to be defined. The photons associated to a track are characterised by the Cherenkov angle, its expected error, the photon absorption depth in the photon detector and ambiguity information from the pattern recognition. There have been different estimators of the Cherenkov angle and number of photoelectrons, developed for particle identification with the RICH detectors [27]. An ambitious approach is to define likelihood functions, including mass dependant signal and background terms, and to extract the most likely particle mass and the amount of background from a fit to all the observed photoelectrons [28].

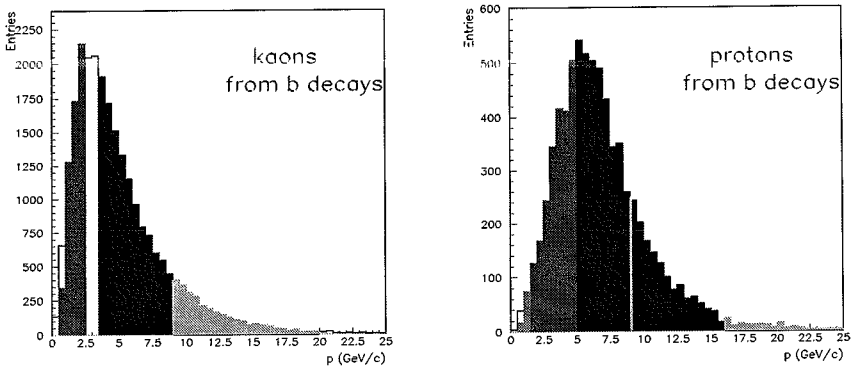

Figure 2.25: *The coverage of kaon (left) and proton (right) identification with the different techniques used in the RICH analysis. The spectra correspond to those of kaons and protons produced in B hadron decays.*

Table 2.2: *The kinematic regions (expressed in p (GeV/c)) of relevance of the different identification techniques for kaons and protons in the RICH.*

	Kaons	Protons
Liquid Veto	-	0.7 - 1.5
Liquid Ring	0.7 - 2.5	1.5 - 5.0
Gas Veto	3.5 - 9.0	3.5 - 17.
Gas Ring	9.0 - 25.	17. - 35.

However this method is sensitive to the precise background description and therefore suffers of systematic uncertainties when simulated events have to be used to estimate its efficiency and misidentification probability. The computation of the average Cherenkov angle with an iterative procedure of outlier rejection results in a more robust estimator. It improves the θ_c resolution by a $1/\sqrt{n_{pe}}$ factor compared with that of individual photons and allows rejection of spurious measurements. The iterative algorithm RIBMEAN has been therefore developed and used in DELPHI [29]. RIBMEAN computes the average Cherenkov angle in four main steps. First photons are grouped into clusters and attributed weights w_i according to their expected measurement errors, conversion depth and ambiguity information. Secondly the average Cherenkov angle is computed as $< \theta_c >= (\sum_{i=1}^{n} w_i\theta_i)/W$ and the compatibility of all the photons to belong to a common Cherenkov ring is estimated from the observed χ^2. If this probability is below a preset cut value, the photon with largest χ^2 contribution is dropped and the procedure iterated. Ambiguities due to photons compatible with more than one particle track are solved by choosing the photon configuration minimising the χ^2 of both Cherenkov rings, for ambiguities for the same radiator, and by using also the measured photon conversion depth for gas-liquid radiator ambiguities. Quality criteria, based on the number of rejected photons and final χ^2, are finally applied to reject badly reconstructed rings. The efficiency for reconstructing a Cherenkov ring has been studied on simulation and real data and found to be (92 $\pm$ 1) % in low multiplicity events and (89 $\pm$ 0.5) % in dense hadronic jets.

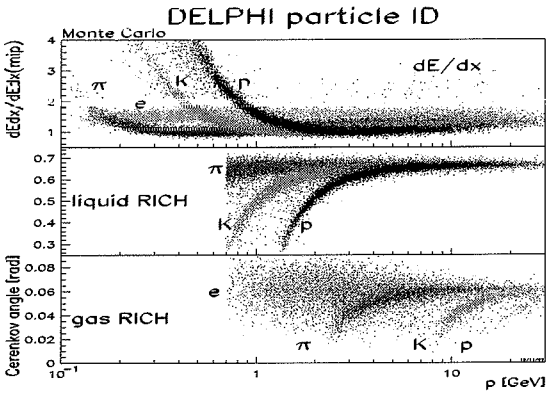

Figure 2.26: *The average Cherenkov angle θ_c in the DELPHI RICH Gas (upper) and Liquid (center) radiator as a function of the measured particle momentum. The dE/dx response is also shown (lower plot). The components due to particles of different masses are clearly visible. The combined use of the two RICH radiators and the dE/dx measurements in the TPC allow to identify particles over the full momentum spectrum.*

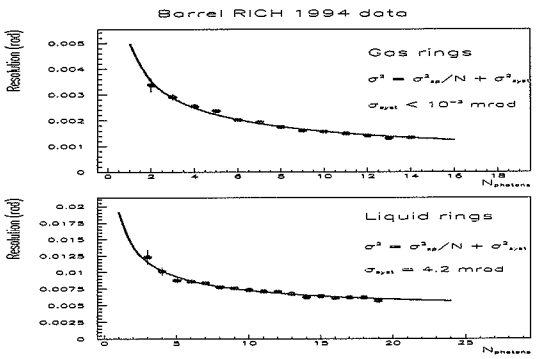

Figure 2.27: *The average Cherenkov angle resolution as a function of the number of accepted photons for the gas (upper plot) and liquid (lower plot) rings in the Barrel RICH. The good agreement observed with the expected $1/\sqrt{n}$ scaling shows that the background contribution after the outlier removal is small. The appearence of a fixed term for liquid radiator rings depends on the track reconstruction and extrapolation resolution.*

The measured resolutions are given in Table 2.3. The statistical behaviour of the error on the average Cherenkov angle has also been verified and results are shown in Figure 2.27. In the case no ring is detected, it is important to ensure that the RICH photon detector performed properly at the time the event was recorded. This is done by either applying geometrical cuts defining a detector fiducial volume and run quality selection based on the operational conditions of the RICH detector or by directly verifying that either primary ionisation from a track or other

Table 2.3: *Average Cherenkov angle resolutions*

	Liquid Radiator (mrad)	Gas Radiator (mrad)
Barrel RICH	1.4	1.8
Forward RICH	1.4	0.7

rings have been detected in the same drift tube.

Probabilities for five particle hypotheses (e, μ, π, K and p) have been evaluated for the liquid and gas radiators using the average Cherenkov angle and the number of accepted photoelectrons. Each probability contains a Gaussian term:

$$P_i^{Gauss} = \frac{e^{-(<\theta_c>-\theta_c^i)^2/2\sigma^2}}{\sqrt{2\pi}\sigma} \tag{2.9}$$

and a Poissonian term:

$$P_i^{Poisson} = \frac{N_i^n e^{-N_i}}{N!} \tag{2.10}$$

where θ_c^i and N_i are the expected Cherenkov angle and number of photoelectrons for each mass hypothesis. The total probability is defined as the product of the Gaussian and the

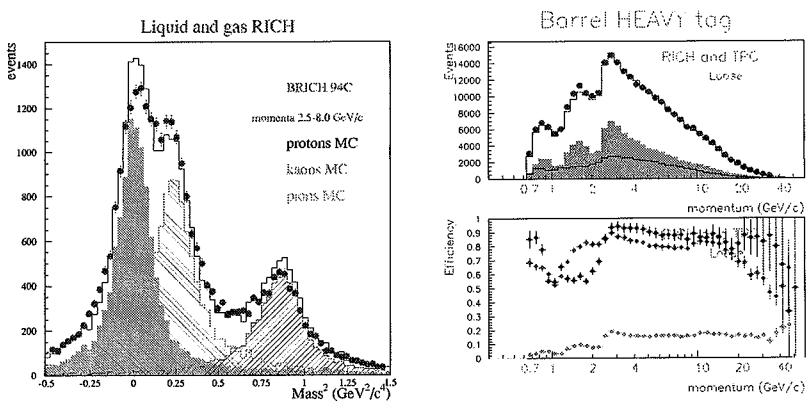

Figure 2.28: *Squared particle masses derived from the measured average Cherenkov angle and measured momentum (left). The contributions from pions, kaons and protons are clearly visible. The histograms represent the simulated RICH response and the points with error bars the DELPHI data.*
Performances for heavy (K and p) identification using the combination of the TPC and RICH response in Z^0 hadronic decays (right). The upper plot shows the number of tagged events as a function of the particle momentum in data (points with error bars) and simulation (histograms). The grey area corresponds to the pions in the sample. The lower plot gives the proton (dark grey), kaon (mid grey) and pion (light grey) tag efficiencies.

Poissonian terms properly normalised. The probabilities for π, K and p have been used for particle identification in both the veto and the ring region and combined with those obtained from the dE/dx response by defining a probability for each mass hypothesis given by the product of the TPC and RICH probabilities properly normalised. Quality flags are also set taking into account the number of measurements in the TPC, the RICH flags and the containment in the fiducial volumes of the detectors. The performances in terms of efficiency and misidentification probability of this tagging algorithm have been adapted according to the requirements of the analysis by varying the working point of the probability cuts and the quality flag criteria. This flexibility allowed to use the same hadron identification algorithm for several analyses with different requirements in terms of efficiency and background rejection. Typical performances of the working point chosen in the analysis of exclusive B decays where a high efficiency and a moderate misidentification probability are required are shown in Figure 2.2.3.

Neutral hadrons produced in the decay of B particles include K^0 and Λ^0 particles and π^0's. The **identification of K_s^0 and Λ^0** is performed by reconstructing their decays, into $\pi^+\pi^-$ and $p\pi^-$ respectively, inside the fiducial volume of the tracking detectors. π^0's are identified by the response of the HPC. At energies up to about 6 GeV the two photons from the $\pi^0 \to \gamma\gamma$ decay are separated enough to produce two distinct electromagnetic showers in the calorimeter. Photon pairs with total energy below 6 GeV and with invariant mass compatible with the π^0 hypothesis are accepted as π^0 candidates. At larger π^0 energies, the two photons are too close in space to be resolved by the calorimeter. π^0's can still be discriminated from energetic photons by the electromagnetic cluster shape reconstructed in the HPC calorimeter as shown in Figure 2.29.

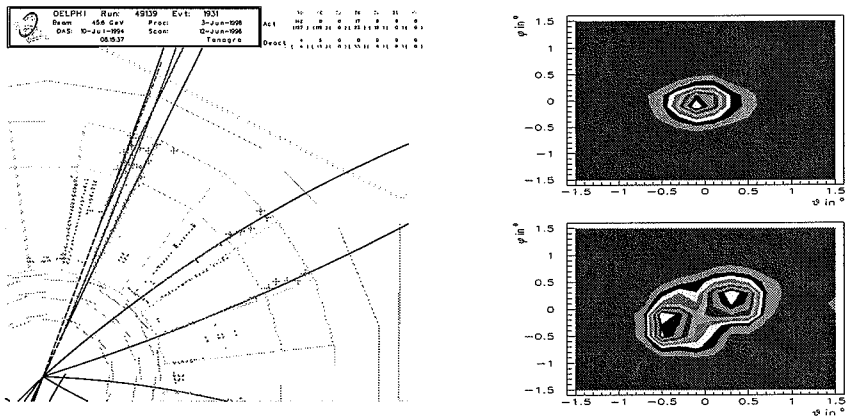

Figure 2.29: *Examples of identification of neutral hadrons in DELPHI. The display of an event with two reconstructed Λ^0 decays is shown on the left. The two baryons decay in two $p\pi$ pairs, visualised as the four tracks at the top. On the left are shown the shower shapes for an energetic photon (upper) and π^0 (lower) detected in the HPC calorimeter.*

High accuracy in reconstructing the production point of stable charged particles coupled with an efficient hadron identification have been obtained with the DELPHI detector. They provide an effective tool in the study of B physics at LEP. The following chapters describe the details of the analysis methods and the results obtained in the study of rare B decay modes. Further, these techniques acquire special relevance in the perspective of the next generation of B physics experiments at particle colliders.

Bibliography

[1] O. Podobrin and M. Feindt, *Inclusive Measurement of the b Fragmentation Function*, DELPHI 95-103 PHYS 538.

[2] P. Abreu,..., M. Battaglia *et al.*,*Nucl. Instr. and Meth. in Phys. Res.* **A 378** (1996) 57.

[3] N. Bingefors,..., M. Battaglia *et al.*, *Nucl. Instr and Meth. in Phys. Res.* **A 328** (1993), 447 and
V. Chabaud *et al.*, Nucl. Instr. and Meth in Phys. Res. **A 368** (1996), 314.

[4] P.P. Allport *et al.* Nucl. Instr. and Meth in Phys. Res. **A 346** (1994), 476.

[5] B. S. Avset, ..., M. Battaglia *et al.*, A new microstrip detector with double sided readout, in *Proc. of the IEEE Nucl. Sci. Symposium*, IEEE Trans. Nucl. Sci. **37** (1990), 1153.

[6] E.G. Anassontzis *et al.*,*Nucl. Instr. and Meth. in Phys. Res.* **A 323** (1992) 351 and
W. Adam *et al.*, *IEEE Trans. on Nucl. Science* **NS-40** (1993), 583.

[7] P.A. Cherenkov, *Doklady AN SSSR* **3** (1936), 413; **14** (1937), 103;
translated in *Phys. Rev* **52** (1937), 378.

[8] I.E. Tamm and I.M. Frank, *Doklady AN SSSR* **14** (1937), 107.

[9] A. Roberts, *Nucl. Instr. and Meth.* **9** (1960), 55 and
J. Seguinot and T. Ypsilantis, *Nucl. Instr. and Meth.* **142** (1977), 377.

[10] R. Arnold *et al.*, *Nucl. Instr. and Meth. in Phys. Res.* **A 252** (1986) 588.

[11] W. Dulinski *et al.*, *Nucl. Instr. and Meth. in Phys. Res.* **A 252** (1986), 418.

[12] W. Adam, ..., M. Battaglia *et al.*, *Nucl. Instr. and. Meth. in Phys. Res.* **A 367** (1995), 253 and
W. Adam, ..., M. Battaglia *et al.*, *Nucl. Instr. and Meth. in Phys. Res.* **A 371** (1996), 12.

[13] Courtesy of Wolfgang Adam (DELPHI Collaboration).

[14] N.S. Lockyer *et al.*, *Phys. Rev. Lett.* **51** (1983), 1316,
J.M. Brown *et al.*, *Phys. Lett.* **195 B** (1987), 301,
D.A. Klem *et al.*, *Phys. Rev.* **37 D** (1988), 41.

[15] M. Althoff *et al.*, *Phys. Lett.* **149 B** (1984), 524,
R.A. Ong, SLAC-320 (September 1987).

[16] D. Decamp *et al.*, *Phys. Lett.* **244 B** (1990), 551,
B. Adeva *et al.*, *Phys. Lett.* **261 B** (1991), 771,
M.Z. Akrawy *et al.*, *Phys. Lett.* **263 B** (1990), 311,
P. Abreu,...,M. Battaglia *et al.*, *Zeit. Phys.* **C 53** (1992), 567.

[17] P. Billoir, R. Frühwirt and M. Regler, *Nucl. Instr. and Meth.* **A 241** (1985) 115.

[18] G. Borisov, DELPHI 94-125, PROG 208.

[19] D. Brown and M. Frank, ALEPH 92-135.

[20] M. Battaglia, in *Proceedings of the First Arctic Workshop on Future Physics and Accelerators*, edited by M. Chaichian, K. Huitu and R. Orava, World Scientific, Singapore 1995, 35.

[21] P. Abreu, ..., M. Battaglia *et al.*, *Phys. Lett.* **B 324** (1994), 500.

[22] P. Abreu, ..., M. Battaglia *et al.*, *Phys. Lett.* **B 374** (1996), 351.

[23] M. Battaglia and D. Liko, *VTXGRA - The DELPHI Vertex Display package*, unpublished.

[24] M. Battaglia and P.M. Kluit, *First Measurement of the Inclusive Charmless B decay Branching Ratio and Precise Determination of the* $b \to c\bar{c}s$ *Rate*, DELPHI Note 97-80 CONF 66.

[25] M. Battaglia, *The role of RICH particle identification in B physics: Recent Results and Perspectives*, to appear in *Nucl. Instr. and. Meth. in Phys. Res.* **A**.

[26] Courtesy of Pierre Antilogus (DELPHI Collaboration).

[27] W. Adam, ..., M. Battaglia *et al.*, *Nucl. Instr. and. Meth. in Phys. Res.* **A371** (1996) 240.

[28] P. Baillon, *Nucl. Instr. and Meth. in Phys. Res.* **A 238** (1993), 341.

[29] W. Adam, ..., M. Battaglia *et al*, *Nucl. Instr. and Meth. in Phys. Res.* **A 371** (1996) 240, M. Battaglia and P.M. Kluit, *Particle identification using the RICH detectors based on the RIBMEAN package*, DELPHI 96-133 RICH 90 and
M. Battaglia and P. Kluit, *Particle Identification using the DELPHI RICH Detectors*, to appear in *Nucl. Instr. and. Meth. in Phys. Res.* **A**.

Experimental Results on Rare b Decays

Brief Summaries of Selected Original Papers

Paper iv)
M. Battaglia, *New Measurements of $|V_{ub}|$ and $|V_{cb}|$ with DELPHI at LEP*, HIP Preprint 1998-74/EXP, to appear on the *Proceedings of the XXIX Int. Conf. on High Energy Physics ICHEP-98* Vancouver B.C. (Canada), July 1998.

This recent conference paper summarises the preliminary results of the determination of $|V_{ub}|/|V_{cb}|$ based on a new technique proposed by several theoreticians to reduce the model dependent uncertainties in the extraction of $|V_{ub}|/|V_{cb}|$ from semileptonic decays. These results are presented in Chapter 3. The author of this thesis developed an original algorithm for the reconstruction of the secondary hadronic system emitted in the semileptonic decay, developed a dedicated decay generator for studying the model dependances of the method (already discussed in Chapter 1), studied the signal characterisation and background rejection to optimise the event reconstruction procedure and evaluated the systematic uncertainties from B and D decay models.

Paper v)
M. Battaglia with P. Abreu *et al.*, *Study of rare b decays with the DELPHI detector at LEP*, *Zeit. Phys.* **C 72** (1996), 207.

This paper reports the DELPHI result on the study of rare B decays in the charmless hadronic, radiative inclusive $b \to s\gamma$ and exclusive $B \to K^*\gamma$ and dineutrino exclusive $B \to K^*\nu\bar{\nu}$ modes. These studies are discussed in details in Chapters 4, 5 and 6. The author of this thesis coordinated the analyses and was responsible for the event reconstruction and background rejections, the extraction of the signal of charmless hadronic decays, of the fraction of loop mediated charmless decays, the limits for the dineutrino decays and their interpretation.

Paper vi)

M. Battaglia, *Study of the Inclusive $b \to c\bar{c}s$ and $b \to sg$ Transitions with the DELPHI detector at LEP*, DELPHI 97-80 CONF 66 and HIP Preprint 1998-05/EXP, paper submitted to the *Int. Europhysics Conference on High Energy Physics EPS-97*, Jerusalem (Israel), August 1997.

This conference paper reports the preliminary results obtained by the author of this thesis for the determination of the double charm B decay rate and the search for the rare $b \to sg$ transition. Both analyses are based on the study of the transverse momentum distribution of identified kaons. The limit derived from the search for $b \to sg$ is discussed in Chapter 4.

Paper vii)
M. Battaglia with P. Abreu *et al.*, *Measurement of the inclusive charmless and double-charm B branching ratios*, *Phys. Lett.* **B 426** (1998), 193.

This paper reports the studies the double charm B decay rate and the search for the inclusive charmless B transition with an inclusive method based on the event topology. The author contributed in the estimate of the systematic uncertainties and in the studies of the simulation models for the $b \to sg$ decay. These results can be combined with those of the previous paper since their systematic uncertainties are largely uncorrelated.

Chapter 3

Semileptonic $b \to u$ Decays

Semileptonic $b \to u\ell\nu$ decays represent the simpler realisation of a CKM suppressed b transition. The absence of final state interactions and of long distance corrections makes the measurement of this branching ratio for the decay the most precise way to determine the $|V_{ub}|$ element in the CKM mixing matrix. Evidence of the non-zero value of $|V_{ub}|$ has been first obtained by observing leptons produced in B decays with momentum exceeding the kinematical limit for $b \to c\ell\nu$ transitions by both ARGUS [1] and CLEO [2]. However the extraction of $|V_{ub}|$ from the

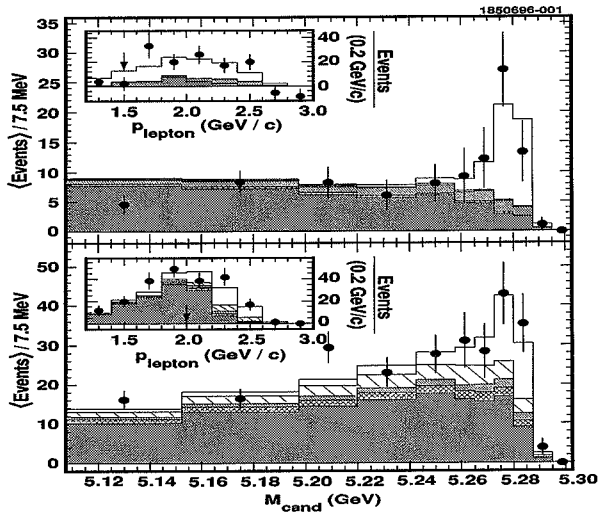

Figure 3.1: *The signal for exclusive $B \to \pi\ell\nu$ (upper plot) and $B \to \rho\ell\nu$ (lower plot) obtained from CLEO at CESR (from ref. [3]).*

yield of leptons above the $b \to c\ell\nu$ endpoint is subject to large systematical uncertainties. More recently, exclusive $B \to \pi\ell\nu$ and $B \to \rho\ell\nu$ decays have been observed by CLEO and their rates measured [3, 4]. Still the derivation of $|V_{ub}|$ from exclusive semileptonic decays, contrary to the case for $|V_{cb}|$ in $B \to D^*\ell\nu$, has a significant model dependence.

The precise determination of the $|V_{ub}|$ element in the CKM matrix is an essential part of the program of Standard Model tests in the study of CP violation in the B sector. As discussed

in detail in Chapter 1 the SM predictions on the value of the CP violating phases are based on the unitarity constraint of the CKM mixing matrix. This can be represented by the so called unitarity triangle. This constraint allows to compare the values of the measured phases, corresponding to the angles of the triangle, with the SM predictions once the relevant CKM elements, defining the triangle sides, are known. In particular, the triangle height is proportional to $|V_{ub}|$. The success of these SM tests therefore depends on the precise determination of the relevant CKM elements: $|V_{ub}|$, $|V_{cb}|$ and $|V_{td}|$. It is possible to reverse the argument and study the effect of other unitarity triangle contraints on the predicted value of $|V_{ub}|$ [5]. Figure 3.2 shows the probability density function for the $|V_{ub}|$ value obtained from data on CP violation in the K sector and $B^0\bar{B}^0$ oscillations together with the unitarity constraint [6]. From the width of the 68% confidence region it is possible to conclude that a determination of $|V_{ub}|$ with accuracy better than 25% provides additional constraints to the unitarity triangle.

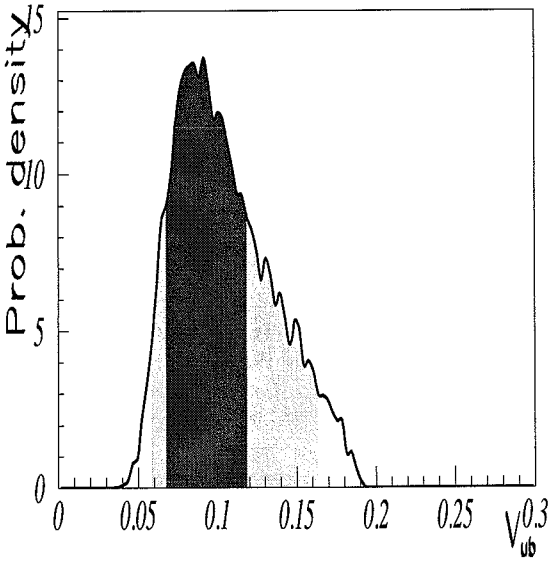

Figure 3.2: $|V_{ub}|/|V_{cb}|$ *p.d.f. from independent constraints on the unitarity triangle. The dark shaded area shows the 68% confidence region corresponding to an uncertainty of* $\pm$ *30% (from [6]).*

3.1 Determination of $|V_{ub}|/|V_{cb}|$

A novel technique for the extraction of $|V_{ub}|$ from the shape of the invariant mass of the hadronic system recoiling against the lepton in $b \to u\ell\nu$ transitions [7] has been the subject of recent theoretical calculations [8, 9]. The proposed method starts from the observation that the hadronic system recoiling against the lepton in the decay has an invariant mass lower than the charm mass for the majority of $b \to u\ell\nu$ decays. The model dependence in predicting the shape of this invariant mass distribution is expected to be smaller compared to that for estimate of the lepton spectrum end-point region and the exclusive final state branching ratios.

In this chapter the results on the first determination of $|V_{ub}|/|V_{cb}|$ obtained by a fit to the shape of the full spectrum of the lepton energy in the B rest frame for B semileptonic decays with reconstructed hadronic invariant mass significantly smaller than the D mass are discussed [10, 11]. Samples enriched and depleted in $b \to u$ transitions have been defined using the secondary vertex topology and identified kaons. This technique allowed to reduce the systematics due to the description of charm decays.

3.1.1 Data Analysis

The extraction of the value of the $|V_{ub}|$ element is based on the analysis of the secondary hadronic mass and of the lepton energy, computed in the B rest frame, for semileptonic B decays. In the following the analysis technique is discussed starting from the event preselection to continue with the particle identification, the reconstruction of the hadronic secondary system and the B energy and direction.

The analysis has been performed on the statistics collected by DELPHI at LEP at $\sqrt{s}$ energies around the Z^0 pole between 1993 and 1995, corresponding to 2.8 M Z^0 hadronic decay candidates. The backgrounds have been estimated using samples of Z^0 hadronic decays simulated with JETSET 7.3 [12] and passed through the full detector simulation. The simulated events corresponded to 4.9 times the real data and have been evenly divided in order to describe the DELPHI detector response in the different years of data taking. Events containing signal $b \to u\ell\nu$ decays have been simulated using the BTOOL decay generator discussed in Chapter 2 [13], interfaced with the JETSET program. Hadronic final states have been produced using a tuned version of the parton shower model. The branching ratios for the exclusive $B \to \pi\ell\nu$ and $B \to \rho\ell\nu$ decays have been forced to those measured by CLEO [3, 4]. The probability for the production of vector and axial resonances have been tuned to agree with the measurements of their inclusive cross-sections in Z^0 decays.

Hadronic events have been selected using the standard DELPHI criteria. These gave 2789419 events in the combined 1993-95 statistics. This sample has been enriched in $Z^0 \to b\bar{b}$ events by applying a b-tag algorithm based on the measured track impact parameters as discussed in Chapter 3. This algorithm computes the probability for all the reconstructed particles to originate at the event primary vertex [14]. This probability has been required to be smaller than 0.08 corresponding to an efficiency of 0.85 and 0.13 for $Z^0 \to b\bar{b}$ and $Z^0 \to c\bar{c}$, $s\bar{s}$, $d\bar{d}$ and $u\bar{u}$ events respectively. Events have been divided into two hemispheres by a plane perpendicular to the event thrust axis. Jets have been reconstructed using the LUCLUS clustering algorithm with a d_{join} value of 6.0 GeV. Only events with two or three jets have been used. For the two most energetic jets of each event, a search for a jet secondary vertex has been performed using charged particle tracks with significantly large impact parameters. This procedure allowed to define an inclusive jet secondary vertex in 60 % of the jets in events fulfilling the b-tagging criteria.

Candidate leptons from the semileptonic B decay have been tagged in the momentum interval 3.5 GeV/c $< p <$ 25 GeV/c.

Muons have been identified by the hits associated in the muon chambers [15]. The efficiency has been estimated from simulation to be 0.83 $\pm$ 0.02. The hadron misidentification probability

has been measured on the real data to be of (0.68 ± 0.03) %.

Electron candidates have been selected using a Neural Network based on the response of the HPC e.m. calorimeter and on the measured specific ionization in the TPC [16]. The efficiency of the selection criteria chosen for this analysis have been measured on real data, using Compton events, obtaining 0.70 ± 0.02 with misidentification probability of (0.38 ± 0.03) %. In order to reduce the background from $b \to c \to \ell$ and $c \to \ell$ transitions the lepton candidates have been required to have $p_t^{in} > 0.5$ GeV/c.

Strange mesons are produced in the cascade $b \to c \to s$ decay and have been therefore used to reduce the background from charmed b decays. Charged kaons, with $p > 2.5$ GeV/c, have been identified by the combination of the response of the DELPHI Ring Imaging CHerenkov (RICH) detectors and the dE/dx in the TPC [17]. K_s^0 have been reconstructed in their $\pi^+\pi^-$ decay mode. Candidate $\pi^0 \to \gamma\gamma$ decays have also been tagged either through their decay in two reconstructed photons or by an analysis of the shower profile in the HPC as discussed in Chapter 2.

The analysis is based on the reconstruction of the secondary hadronic system emitted with the lepton in the B decay. This system has been reconstructed using an inclusive method. First the probability for a given particle to be a B decay product has been computed. This

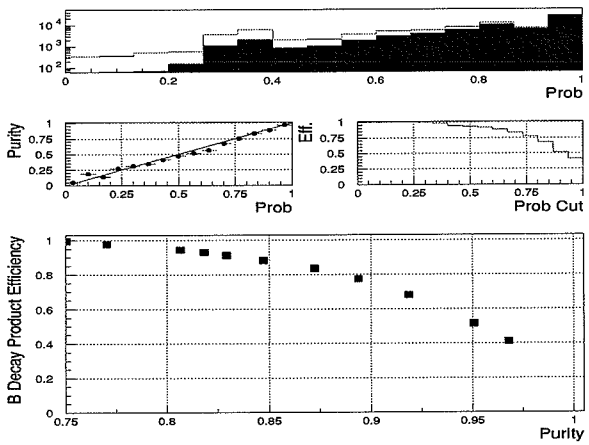

Figure 3.3: *The probability for a particle to originate from a B decay (upper plot). The filled histogram shows the distribution for genuine B decay products. The purity (left) and efficiency (right) as a function of the value of the probability are shown by the central plots while the lower histogram shows the efficiency as a function of the obtained purity.*

probability is expressed by a likelihood, defined as the normalised product of the probabilities, computed individually for a set of discriminating variables, that the particle originates from the B decay w.r.t. the hypothesis that it has been produced in the primary hadronisation. The discriminating variables have been divided into two categories. The first consists of the following six kinematical variables: the transverse momentum p_t, the ratio p/E_{jet}, particle mass, particle rapidity, particle rank in decreasing energy order and contribution to the invariant mass of the jet inclusive secondary vertex. These variables have been computed for all charged particles with momentum greater than 0.5 GeV/c and neutral particles with energy above 1.0 GeV. The second category groups four topological variables computed only for those charged particle tracks with

$p > 0.7$ GeV/c and associated hits in the Vertex Detector. These variables are the track impact parameters w.r.t. the event primary vertex in the $R - \phi$ and z projections normalised to their errors, the χ^2 contribution of the track to the jet inclusive secondary vertex and the distance of the point at which the track trajectory has the closest approach to the jet axis from the primary vertex normalised to the distance between the primary and secondary vertex. The likelihood has been computed for the particles produced in the same hemisphere as the lepton candidate (see Figure 3.3).

The hadronic secondary system has been reconstructed using an iterative algorithm that used the charged particles sorted by decreasing value of the likelihood variable. The two particles, with largest probability, compatible with forming a common secondary vertex have been taken as seed for the subsequent iterations. Once the vertex has been defined, charged particle tracks with likelihood larger than 0.75 have been tested for compatibility. Those giving a contribution to the χ^2 of the secondary vertex fit smaller than 4 and a total invariant mass M_X smaller than 3.0 GeV/c^2 have been accepted. After the charged hadronic system has been defined, identified K^0 and π^0 candidates with likelihood larger than 0.65 have been tested. A maximum of two π^0's have been accepted at each vertex, if the total vertex mass did not exceed 3.0 GeV/c^2 . Reconstructed secondary hadronic systems with only neutral particles, with absolute value of the charge larger than 1, with a total energy smaller than 4 GeV or with a total energy smaller than 75 % of the jet energy have been rejected. This procedure gives a reconstructed hadronic system in 75% of simulated $b \to c\ell\nu$ decays, in events fulfilling the event selection criteria described above.

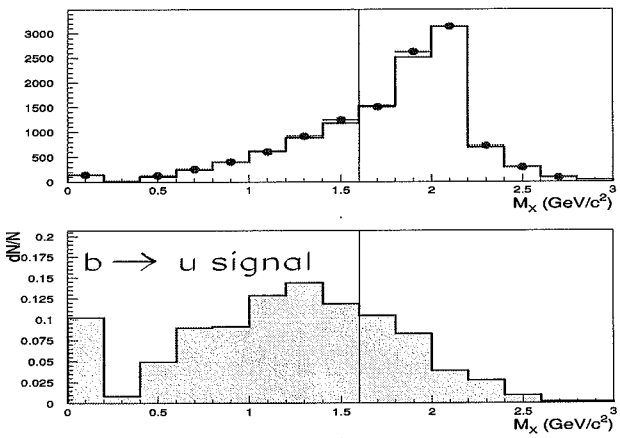

Figure 3.4: *The distribution of the hadronic mass M_X for real data and simulation (upper plot) and simulated signal $b \to u\ell\nu$ decays (lower plot).*

The total mass of the candidate B decay $M_{X\ell\nu}$ has been estimated from the invariant mass of the system formed by the secondary hadronic system, the lepton and the neutrino as discussed below. For simulated $b \to u\ell\nu$ and fully reconstructed $b \to c\ell\nu$ decays the distribution of this mass peaks at 5.0 GeV/c^2 and has a resolution of 0.9 GeV/c^2. On the contrary in partially reconstructed D decays this distribution peaks at 4.5 GeV/c^2. These decays contribute a background at values of M_X below the charm mass. They can be partially identified because of their lower value of $M_{X\ell\nu}$ compared with fully reconstructed decays. Therefore decays with

$M_{X\ell\nu} < 3.0$ GeV/c^2 have been removed and, for decays with $M_{X\ell\nu} < 4.5$ GeV/c^2 and $M_X < 1.6$ GeV/c^2, the measured hadronic mass M_X has been rescaled by the ratio $M_B/M_{X\ell\nu}$ (see Figure 3.4). In order to further remove partially reconstructed D decays, the compatibility of all charged particle tracks, in the lepton hemisphere having $p > 1.5$ GeV/c and not associated to the secondary vertex, with originating at the primary vertex has been tested. Decays having this probability below 0.025 have been removed. Also decays with two identified leptons in the same hemisphere have been removed because double semileptonic $b \to c\ell\nu$, $c \to s\ell\nu$ result in a low mass hadronic system and represent a background to this analysis.

In addition, an inclusive search for $D^* \to D\pi$ has been performed. Charged particle tracks with 0.4 GeV/c $< p <$ 3.0 GeV/c and $p_t < 0.7$ GeV/c and π^0 candidates with 1.5 GeV $< E <$ 3.0 GeV and $E_t < 0.7$ GeV have been iteratively added to the secondary system and the mass difference ΔM has been computed. Cases with 0.14 GeV/c^2 $< \Delta M <$ 0.16 GeV/c^2 and with a secondary hadronic mass larger than 0.6 GeV/c^2 have been accepted as candidate D^* decays. For these candidates the mass M_X has been set to 2.01 GeV/c^2. A study based on simulated events showed that these criteria correctly identified 22 % of semileptonic decays with a D^* meson.

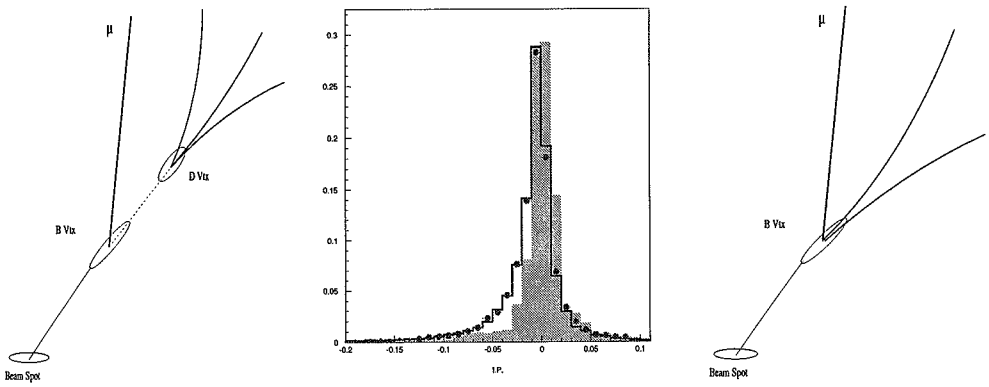

Figure 3.5: *The distribution of the lepton impact parameter computed w.r.t. the secondary vertex and the expected impact parameter configuration for $b \to c$ (left) and $b \to u$ (right) decays . The real data (dots with error bars) and the simulation background (histogram) show the enhancement at negative values due to the charm lifetime while the expected distribution for the signal (filled histogram) is centered around zero with a width corresponding to the impact parameter resolution*

In order to improve the separation of $b \to u\ell\nu$ from $b \to c\ell\nu$ and other background sources, the lepton energy in the B rest frame has been determined. The energy of the B hadron has been estimated, for each decay, as the sum of the energies of the identified lepton, of the secondary hadronic system and of the neutrino energy in the hemisphere. The neutrino energy has been computed from the missing energy using an hemisphere invariant mass correction term. Neutrino energies in the range of 1.5 GeV $< E_\nu <$ 25 GeV and a minimum B energy of 25 GeV have been required. The resolution on the neutrino energy in $b \to X\ell\nu$ decays has been estimated to be 3.6 GeV. The resulting resolution on the B energy has been studied on simulation and found to be 9.8 % for 80 % of inclusive semileptonic B decays and 15.4 % for the remaining of the decays. The B direction has been taken as the vector joining the primary vertex to the jet secondary

vertex. For those decays without a reconstructed secondary vertex, the sum of the momentum vectors of the hadronic system, of the lepton and of the missing momentum has been used. The angular resolution on the B direction has been estimated to 3.2° for semileptonic B decays.

The lepton energy E_ℓ^* has been computed in the frame defined by the estimated B energy and direction. The resolution on the E_ℓ^* reconstruction has been studied on simulated events and found to be 14 % for 81 % of the selected decays. The values of the resolution function obtained analysing $b \to u\ell\nu$ and $b \to c\ell\nu$ events separately have been found to be consistent.

A procedure to select separate samples, enriched or depleted in $b \to u$ transitions, independently of the reconstructed hadronic mass has been developed. It relies on the sign of the lepton impact parameter w.r.t. the secondary vertex and on the presence of identified kaons in the same hemisphere as the lepton. For each lepton hemisphere with a reconstructed secondary vertex the impact parameter has been computed w.r.t. this vertex and a sign has been attributed using the lifetime convention. The lepton impact parameter has been signed negative if it appeared to originate between the primary and the secondary vertex and positive in the case it originated in front of the secondary vertex. In $b \to c\ell\nu$ decays the secondary vertex corresponds to the D decay vertex. Therefore $b \to c$ semileptonic transitions preferably give leptons with negatively signed impact parameters since the lepton comes from the B decay vertex. On the contrary in the $b \to u\ell\nu$ transitions, the secondary vertex coincides with the B decay vertex and thus with the lepton production point (see Figure 3.5). In this case, the impact parameter signing depends only on resolution effects and has either positive or negative values with equal probabilities. Decays with a reconstructed secondary vertex and a significantly negative lepton impact parameter have been assigned to the $b \to u$ depleted class. A cut on $d_{sec}^{\ell} <$ -0.015 cm has been chosen.

The detection of a strange particle in the semileptonic B decay has been also used to separate cascade $b \to c\ell\nu$ followed by $c \to s$ decays from $b \to u$ transitions where the production of strange particle is suppressed because they may only originate from the spectator s quark in B_s decays or from $s\bar{s}$ popping. In simulated events 37% of $b \to c$ decays are characterised by the presence of an identified kaon, to be compared with 14% of $b \to u$ transitions. Therefore decays with an identified $K^{\pm}$ or K_s^0 with $p > 2.5$ GeV/c in the same hemisphere as the lepton have also been assigned to the $b \to u$ depleted class.

3.1.2 Results and Discussion

Candidate semileptonic B decays have been further selected by imposing the following cuts in order to remove background and poorly reconstructed decays. The sum of the energies of the hadronic system and of the lepton has been required to be larger than 12 GeV and decays with an invariant mass of the secondary hadronic system and of the lepton below 2.0 GeV/c^2 have been also removed. Finally decays in which the lepton charge had a sign equal to that of the hadronic system have been discarded. These criteria selected 12134 decays in real data and 11898 in the simulation with an estimated efficiency for $b \to u\ell\nu$, with $\ell = e, \mu$, of 0.165 ± 0.004. The background composition has been studied on simulation and found to consists of 91% of $b \to c\ell\nu$ decays, 7% of cascade $b \to c \to s\ell\nu$ decays and 2% of $c \to \ell$ decays and misidentified hadrons for $E_\ell^* > 1.0$ GeV.

The selected decays have been divided into four independent classes according to the reconstructed secondary hadronic mass M_X (see Figure 3.4) and the $b \to u$ enrichment criteria. These are: i) $b \to u$ enriched decays with $M_X < 1.6$ GeV/c^2, ii) $b \to u$ enriched decays with $M_X >$ 1.6 GeV/c^2, iii) $b \to u$ depleted decays with $M_X < 1.6$ GeV/c^2, and iv) $b \to u$ depleted decays with $M_X > 1.6$ GeV/c^2. The M_X cut at 1.6 GeV/c^2 has been chosen on the basis of studies showing that this value ensures a reduced model dependence in the extraction of $|V_{ub}|$ [9, 13] while being sufficiently below the D mass to suppress the bulk of $b \to c\ell\nu$ decays.

The number of events selected in the real data, the expected background events and the

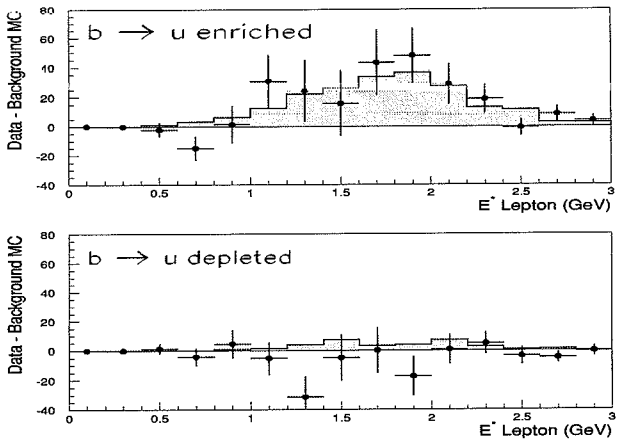

Figure 3.6: *The background subtracted distributions of the lepton energy in the B rest frame E_ℓ^*, for decays with $M_X < 1.6$ GeV/c^2, for the $b \to u$ enriched (upper plot) and depleted (lower plot) classes. The real data is shown by the dots with error bars while the histgram represents the expected signal from $b \to u\ell\nu$ decays normalised to the fitted value of $|V_{ub}|/|V_{cb}|$.*

Table 3.1: *Number of events selected in the real data, expected background events and fraction of the total number of signal events. The background has been rescaled by the normalisation factor obtained from the fit and the ± 0.01 error on this normalisation has been included.*

Data/Back./Sign.	$b \to u$ enriched	$b \to u$ depleted
$M_X < 1.6$ GeV/c^2	2292 ± 48 / 2087± 30 / 68%	1081 ± 33 / 1143 ± 19 / 9%
$M_X > 1.6$ GeV/c^2	5017 ± 71 / 4901 ± 58 / 17%	3744 ± 61 / 3648 ± 45 / 6%

fraction of the total number of signal events in the four categories are summarised in Table 3.1. The background has been rescaled by the normalisation factor obtained from the fit described below and the ± 0.01 error on this normalisation has been included. For decays selected in the low M_X, $b \to u$ enriched class that is expected to contain 68% of the $b \to u$ signal, an excess of 205 ± 56 events has been found in the real data compared to the expected background (see Figure 3.6). No significant excess has been observed in the other classes.

As a cross-check, the analysis has been repeated using both anti-b tagged events and decays with same-sign lepton and hadronic vertex combinations. All other selection criteria have been kept as in the main analysis. Both these samples are expected to be depleted in signal $b \to u$ decays but are sensitive to possible discrepancies between real data and simulation in the description of backgrounds. The numbers of selected decays in the low M_X, $b \to u$ class have been computed. For the anti-b tagged sample there have been 32 ± 6 events observed in the real data compared to 33 ± 3 expected from background. The same-sign sample consisted of 340 ± 18 events in real data with 319 ± 8 expected from backgrounds. No excess of events in the real data has been observed in either of these samples.

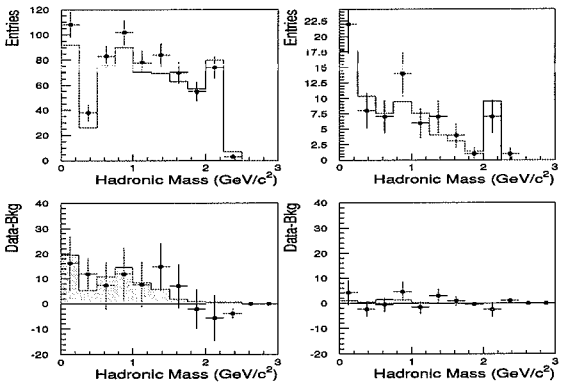

Figure 3.7: *Invariant mass M_X distribution for $b \to u$ enriched decays with secondary hadronic system consisting of either a single charged particle tracks or two particles forming a neutral or unit charge secondary system for opposite sign (left) and same sign (right) hadronic-lepton system. The upper histograms show the expected distribution from background, the points with error bars the real data. In the lower histograms the background subtracted data are compared with the expected distribution from signal $b \to u\ell\nu$ events.*

In order to support the interpretation of the excess of events in the low M_X, $b \to u$ enriched sample as signal of $b \to u\ell\nu$ transitions, a search for decays into the $B \to \pi\ell\nu$ and $B \to \rho\ell\nu$ exclusive final states have been performed. Decays with 1.0 GeV $< E_\ell^* <$ 3.0 GeV and a reconstructed hadronic system consisting of either a single charged particle or two particles with total charge zero or one have been selected. Further combinations with same-sign hadronic system and lepton have been rejected. The π and ρ mass region have been defined as $M_X <$ 0.2 GeV/c^2 and 0.55 GeV/c^2 $< M_X <$ 1.05 GeV/c^2. The distributions of M_X for genuine $B \to \pi\ell\nu$ and $B \to \rho\ell\nu$ signal events, satisfying the selection criteria, have been studied on simulation. It has been found that 69% (82%) of $\pi(\rho)\ell\nu$ decays have been reconstructed with values of the hadronic mass within these regions.

The M_X distribution shows an excess of events in the real data compared to the expected backgrounds in correspondance to the π and ρ masses compatible with that expected in $B \to X_u\ell\nu$ decays (see Figure 3.7). As a cross-check the analysis has been repeated for same-sign hadronic system and lepton combinations. This class receives contribution only from partially reconstructed decays as $B^+ \to \pi^+(\pi^-)\ell^+\nu$ and background events. No significant excess of events have been observed.

For each decay class, the number of events and their E_ℓ^* distributions have been used to extract the value of $|V_{ub}|/|V_{cb}|$ by a simultaneous binned maximum likelihood fit. The fraction of $b \to u\ell\nu$ decays in the sample is proportional to:

$$\frac{|V_{ub}|^2}{|V_{cb}|^2} \times \frac{f(m_u/m_b)}{f(m_c/m_b)} \times \frac{1 + a_1^u \frac{\alpha_s(m_b)}{\pi} + a_2^u \frac{\alpha_s^2(m_b)}{\pi^2} + ...}{1 + a_1^c \frac{\alpha_s(\sqrt{m_b m_c})}{\pi} + a_2^c \frac{\alpha_s^2(\sqrt{m_b m_c})}{\pi^2} + ...} \tag{3.1}$$

where the term $f(x)$ represents the phase space factor and the other term accounts for perturbative corrections. In the fit, the overall simulation to real data normalisation and the value of $|V_{ub}|/|V_{cb}|$ have been left free to vary. By leaving the normalization free, the systematic un-

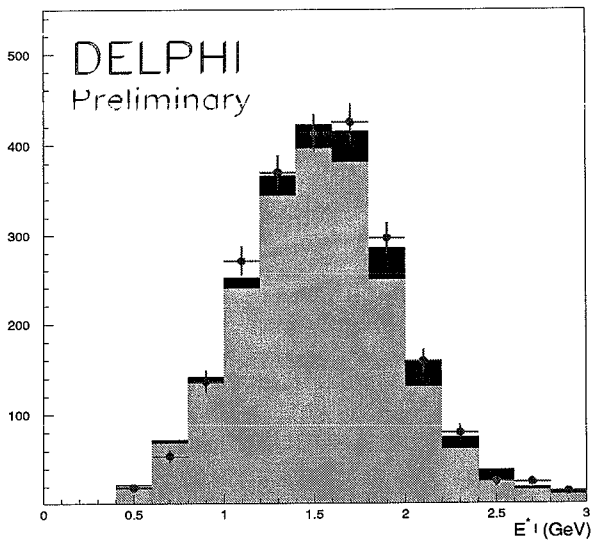

Figure 3.8: *E_ℓ^* distribution for the decays in the $b \to u$ enriched class with $M_X < 1.6$ GeV/c^2. Real data are indicated by the points with error bars, the background by the light shaded histogram and the $b \to u\ell\nu$ signal by the dark shaded histogram normalised to the fitted fraction of events.*

certainties from the lepton identification and other sources have been significantly reduced by absorbing their effects in this overall normalisation factor. The result of the fit was:

$$\frac{|V_{ub}|}{|V_{cb}|} = 0.104 \pm 0.012 \text{ (stat)}$$

with the normalisation factor 0.985 ± 0.010 (see Figure 3.8).

The stability of the result has been checked by changing the cut on M_X. This cut has been varied from 1.25 GeV/c^2 to 1.75 GeV/c^2, corresponding to a variation of the signal-to-background ratio from 0.11 to 0.06. The result of the fit has been found to be $\frac{|V_{ub}|}{|V_{cb}|} = 0.101 \pm 0.013$ and 0.092 ± 0.017 respectively. Several cuts used in the selection of the events have been varied or dropped and the fit has been repeated. These included the event b-tagging, lepton p_t, $E_{X\ell}$, $M_{X\ell}$, E_B and the secondary vertex decay distance significance. The results have been found to agree within the errors.

Several sources of systematic uncertainties have been considered. In the following these are discussed in four groups and the results are summarised in Table 3.2.

The first contains **systematics from the charm decays**. The description of charm decays affects the fraction of $b \to c\ell\nu$ transitions that have been accepted in the $b \to u$ enriched sample. First the branching ratios for D decays in low charged multiplicity final states have been considered. These are $D \to K^0$ and D decays in 0 and 1 prong final states. From the simulation studies the first class of decays represents 40 % of the background from charmed semileptonic b decays for the $b \to u$ enriched sample and the sum of the 0 and 1 prong decays 46 %. Their branching ratios have been varied within the uncertainties of the MARK III measurement [18]. The corresponding variations of the fitted value of $|V_{ub}|/|V_{cb}|$ have been found to be 0.0062 and 0.0020 respectively. Then the fraction of leptons from cascade $b \to c \to s\ell\nu$ decays has been

varied by the uncertainty on the ratio BR($b \to \ell$) / BR($c \to \ell$) = 0.112 ± 0.002 / 0.094 ± 0.010. This contributed a systematic uncertainty of 0.0063. Summing these contributions in quadrature, the systematic uncertainties from the charm decay have been found to be 0.0090.

The next source of systematic errors is due to **uncertainties in the B hadron production and decay**. The first component is due to the fraction of B_s and beauty baryons produced. Due to the rejection of kaons associated with the lepton hemisphere and of the shorter Λ_b lifetime these beauty hadrons are not significantly contributing to the $b \to u$ enriched sample. The production rates of B_u, B_d and B_s mesons have been extracted by a dedicated analysis [19]. The residual uncertainty of ± 0.026 on the sum of B_u and B_d meson fractions has been propagated and contributed a systematic of 0.0049.

The ϵ_b in the Peterson b fragmentation function has also been varied according to the uncertainty in the fraction of the beam energy taken by the beauty hadron $< x_b > = 0.702 \pm 0.008$. The corresponding systematic error was 0.0010. The inclusive b lifetime has been varied within the uncertainty of the present world average of 1.566 ± 0.018 ps [20]. The effect on the result has been found to be 0.0014. The branching ratio for inclusive double charm production in B decays has been fixed to 0.15 and varied by ±0.03. This has induced a change of the fit result by ±0.003. Finally, the dependance on the production rate of D^* and D^{**} mesons in semileptonic B decays, that is still quite poorly known, has been studied. These states flip charge of the resulting D meson and increase the charged B multiplicity. The production rate for the sum of D^* and D^{**} has been therefore varied by ± 14 %. The error represents the uncertainty due to both the present precision on the $B \to D^* \ell \nu$ and $B \to D^{**} \ell \nu$ branching ratios and that due to the fact that the sum of the exclusive final states, measured so far, does not saturate the B semileptonic branching ratio. The contribution to the systematic error has been found to be 0.0048. Summing these contributions in quadrature, the systematic uncertainties from the B production have been found to be 0.0076.

The third source of uncertainties is related to **detector dependent systematics**. The first source is due to the efficiency and purity in the lepton identification. Efficiency and misidentification probability for muon and electron tagging have been extracted from both the simulation and real data as discussed in 2.2. The central values for the simulation have been changed within these errors and the corresponding changes on $|V_{ub}|/|V_{cb}|$ have been found to be 0.0015 and 0.0020 respectively.

The second component of detector systematics is due to the hadronic mass resolution. This resolution depends on both the secondary hadronic multiplicity and the single particle energy resolution. The secondary hadronic multiplicity has been studied on the $b \to u$ depleted sample to avoid possible biases from the presence of signal events in the real data. The total (charged) secondary multiplicity have been measured to be 3.64 ± 0.01 (2.74 ± 0.01) in the real data and 3.63 ± 0.01 (2.72 ± 0.01) in the simulation. The systematic uncertainty has been evaluated by inducing a change of ±0.02 units of multiplicity. This has resulted in a variation of $|V_{ub}|/|V_{cb}|$ of 0.0065. The component due to the particle energy resolution is dominated by the resolution for neutral particles. The systematic effects has been checked by worsening by 2% the resolution on M_X for those decays including neutral particles. This range has been defined by a χ^2 analysis of the hadronic mass in real and simulated $b \to u$ depleted decays. It also corresponds to the typical event e.m. energy resolution in Z^0 decays. The corresponding systematic uncertainty has been found to be 0.0010 resulting in a total systematics from the hadronic mass resolution of 0.0066. The resolution on the neutrino energy reconstruction has been varied by 10 % and the effect has been propagated to the E_ℓ^* resolution obtaining a systematic error contribution of 0.0010. Finally the possible systematics in the decay classification have been studied. These systematics depend both on the measurement and signing of the lepton impact parameter w.r.t. the secondary vertex and on the kaon identification. The lepton impact parameter systematics receive contributions from two components. The first is due to the lepton extrapolation and the second to the secondary vertex reconstruction. The effect of changing the resolution on the

lepton track extrapolation has been computed by smearing the resolution on the lepton impact parameter by 5% which corresponds to the maximum discrepancy in the resolution function between the real data and the simulation [21]. The corresponding variation on $|V_{ub}|/|V_{cb}|$ is 0.0007. The component due to the secondary vertex position has been evaluated worsening by 50 μm the resolution on its decay length and the corresponding variation on $|V_{ub}|/|V_{cb}|$ has been found to be 0.0070. The kaon tagging efficiency has been varied by $\pm 5\%$ and the corresponding uncertainty on the result of the fit was 0.0017. Summing these contributions in quadrature, the detector systematics have been found to be 0.0100.

Table 3.2: *Summary of the sources of systematic uncertainties.*

Source	Value $\pm$ Range	Syst. Error
BR($D \to K^0 X$)	0.53 ± 0.05	.0062
BR($D \to 0,1$ prong)	0.22 ± 0.02	.0020
B($b \to \ell$)/BR($c \to \ell$)	$\frac{0.112 \pm 0.002}{0.094 \pm 0.010}$	.0063
$f(B_u) + f(B_d)$	0.834 ± 0.026	.0049
$< x_b >$	0.702 ± 0.008	.0010
b lifetime	1.566 ± 0.018	.0014
BR($b \to c\bar{c}s$)	0.15 ± 0.03	.0025
BR($B \to D^* \ell\nu + D^{**} \ell\nu$)	0.069 ± 0.010	.0048
e / μ id. Efficiency	$\pm 2.5\%$	.0015
e / μ id. Purity	$\pm 10\%$ / $\pm 4.5\%$	.0020
Hadronic Multiplicity		.0065
Neutral Energy Resolution		.0010
Missing Energy Resolution		.0010
ℓ Impact Parameter Sign		.0070
K id. Efficiency	$\pm 5\%$	.0017
Signal Efficiency	$\pm$ 2.4%	.0012
m_b	4.82 ± 0.10	.0057
$< p_b^2 >$	0.4 ± 0.1	.0012
b Kinematic Model		.0010
Hadronisation Model		.0060
Total		**.0177**

Finally the last source of systematics originates from the **uncertainties in the $b \to u\ell\nu$ model**. First the statistical error on the efficiency for selecting signal events has been propagated obtaining a contribution of ± 0.0012 to the systematic uncertainty. The predicted shape of the invariant mass distribution in the $b \to u\ell\nu$ decay, depends mainly on the kinematics of the heavy and spectator quarks inside the B hadron and on the b quark pole mass. Further, the hadronisation process, transforming the $u\bar{q}$ system into the observable hadronic final state, represents an additional source of model uncertainties.

The systematic uncertainties due to the $b \to u\ell\nu$ decay model have been studied using a dedicated generator that implements different prescriptions for the initial state kinematics and the resonance decomposition of the hadronic final states [13]. Three different sources of systematics have been considered.

The first is due to the values of the b quark mass m_b and of the expectation value of the kinetic energy operator. The b quark mass has been varied in the range 4.72 GeV/c^2 $< m_b <$ 4.92 GeV/c^2 corresponding to a systematic error of ± 0.0048. The value of the b quark mass introduces also an uncertainty in the extraction of $|V_{ub}|$ from the observed $b \to u\ell\nu$ rate.

However this uncertainty has been shown to be not larger than 3% [22] which corresponds to a total contribution to the error of 0.0057.

There have been several evaluations of $< p_b^2 >$ from both theory and fits to experimental data. Results are scheme or model dependent and, depending on the method used in their derivation, they point to values of μ_π^2 in the range from 0.4 GeV^2 to 0.2 GeV^2. In this study the value $< p_b^2 > = (0.4 \pm 0.1)$ $(GeV/c)^2$ has been adopted. The contribution to the systematic uncertainties has been found to be ± 0.0012.

A second source of systematic effect is due to the ansatz for the description of the motion of the b quark inside the heavy hadron. The momentum distributions obtained using the ACCMM model [23], a QCD universal structure function [24, 25] and the parton model [26] have been compared. The mass of the b quark has been kept fixed at its central value of $m_b = 4.82$ GeV/c^2, the p_F value and the a and c coefficients in the $f(z) = z^a(1-cz)e^{-cz}$ structure function have been chosen to reproduce the same value of $< p_b^2 >$. For the parton model, the Peterson form [27] of the fragmentation function has been adopted with $\epsilon_b = 0.0040$. A systematics uncertainty of ± 0.0010 has been evaluated.

Finally the production of the hadronic final states from the $u\bar{q}$ pair has been simulated according to both the ISGW2 [28] exclusive and a fully inclusive model based on parton shower fragmentation [12]. The ISGW2 model approximates the inclusive $b \to u\ell\nu$ decay width by the sum over resonant final states, taking into account leading corrections to the heavy quark symmetry limit. The predicted branching ratios for the different resonant final states have been used to define the hadronic system emitted with the lepton. Another approach is to assume that, at large enough recoil u quark energies, the $u\bar{q}$ system moves away fast enough to resemble the evolution of a jet initiated by a light quark q in $e^+e^- \to q\bar{q}$ annihilation. This has been simulated by first arranging the $u\bar{q}$ system in a string configuration and then making it to fragment according to the parton shower model. Due to the extreme assumptions of the two models adopted, the resulting difference in the fitted value of $|V_{ub}|/|V_{cb}|$ has been assumed to correspond to a 90 % confidence region and the $\pm 1\sigma_{syst}$ has been derived to be ± 0.0060. This study has quantified the systematic uncertainties from the $b \to u\ell\nu$ decay model as 0.0084.

In conclusion the value of the ratio $|V_{ub}|/|V_{cb}|$ has been measured to be:

$$|V_{ub}|/|V_{cb}| = 0.104 \pm 0.012 \text{ (stat)} \pm 0.015 \text{ (syst)} \pm 0.009 \text{ (model)}.$$

Table 3.3: *Recent Measurements of* $|V_{ub}|/|V_{cb}|$

Experiment	Method	$\lvert V_{ub}\rvert/\lvert V_{cb}\rvert$
ARGUS + CLEO	E_ℓ^* Endpoint	0.080 ± 0.020
CLEO	Exclusive	0.080 ± 0.020
ALEPH [29]	Neural Network	0.098 ± 0.024
L3 [30]	Decay Kinematics	$0.159\ ^{+0.042}_{-0.058}$
DELPHI	This Analysis	0.104 ± 0.021

This analysis has shown that it is possible to determine the $|V_{ub}|$ with model dependent systematic uncertainties at the 10% level. Part of the systematics from B and D decays originates from uncertainties on branching ratios that are going to be improved in the near future. In table 3.3 the result of this analysis is compared with those from other determinations both at the $\Upsilon(4S)$ using the end-point of the lepton spectrum and exclusive decays and also by other LEP experiments. All results are compatible and this measurement is the single most precise determination of $|V_{ub}|/|V_{cb}|$ presently available. The value of $|V_{ub}|$ can be extracted by using the recent DELPHI determinaton of $|V_{cb}|$, based on the analysis of $B \to D^*\ell\nu$ decays, giving

$|V_{cb}| = 0.0412 \pm 0.0015$ (stat) + 0.0018 (syst exp) $\pm$ 0.0014 (syst th) [11]. The result is $|V_{ub}| = 0.0042 \pm 0.0009$. Alternatively, using the LEP average value of $|V_{cb}| = 0.0378 \pm 0.0018$ (exp.) $\pm$ 0.0011 (model) $\pm$ 0.0013 (th.) the value of $|V_{ub}|$ is found to be:

$$|V_{ub}| = 0.0039 \pm 0.0008.$$

A preliminary average of the $|V_{ub}|$ determinations by DELPHI with those by ALEPH, L3, CLEO and ARGUS has also been obtained. In performing this average it is important to study the correlation of systematic uncertainties in the different measurements. For this preliminary study the uncertainties have been divided in three categories: i) statistical errors and ii) experimental systematics depending on the detector responses, that have been taken as uncorrelated, while iii) model systematics have been assumed to be fully correlated. The average has been computed, using the best unbiased linear estimator technique, as the weighted mean of the individual measurements V_i: $\sum_{i=1}^{7} w_i V_i$ where the weights w_i have been defined by minimising the total error. This total variance can be expressed as $S^2 = (S_{uncor})^2 + (S_{cor})^2$ with $(S_{uncor})^2 = \sum_{i=1}^{7}(w_i S_{i,uncor})^2$ and $(S_{cor})^2 = (\sum_{i=1}^{7} w_i S_{i,cor})^2$. The result has been found to be $|V_{ub}| = 0.0038 \pm 0.0006$.

It is possible to obtain an estimate of the contribution of this measurement to the constraints on the unitarity triangle discussed in Chapter 1. Figure 3.9 shows the constraints for the ρ and η parameters in the CKM matrix parametrisation as obtained by using the value of $|V_{ub}|/|V_{cb}| = 0.08 \pm 0.02$ from CLEO and ARGUS analyses and after adding the DELPHI measurement to obtain $|V_{ub}|/|V_{cb}| = 0.093 \pm 0.013$. The relative errors on ρ and η improves from $\pm$ 57% to $\pm$ 43% and from $\pm$ 16% to $\pm$ 14% respectively.

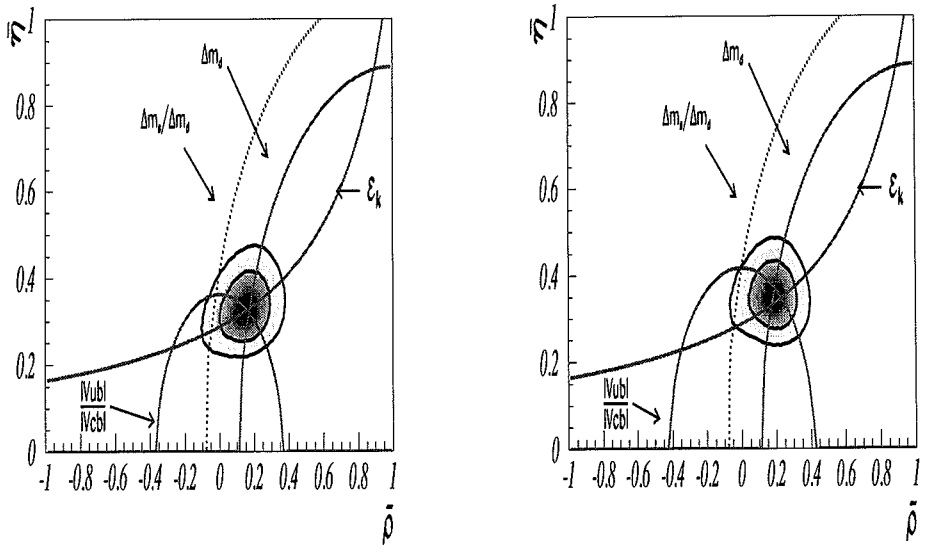

Figure 3.9: *The constraints on the unitarity triangle using the ARGUS and CLEO result on V_{ub} derived from the lepton end-point spectrum (left) and after averaging with the result of the present analysis (right) (from [6]).*

$$B^0 \to \pi^+ \mu^- \bar{\nu}$$

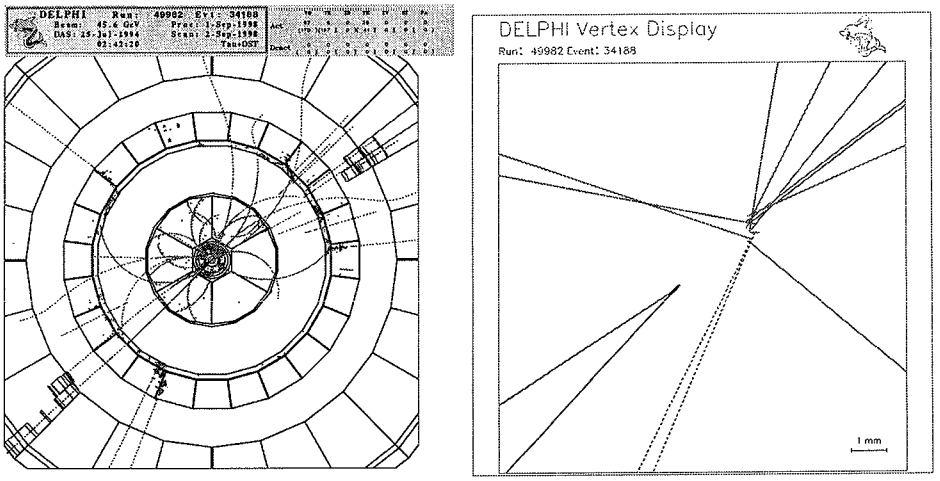

$$B^0 \to \rho^- \mu^+ \nu,\ \rho^- \to \pi^- \pi^0$$

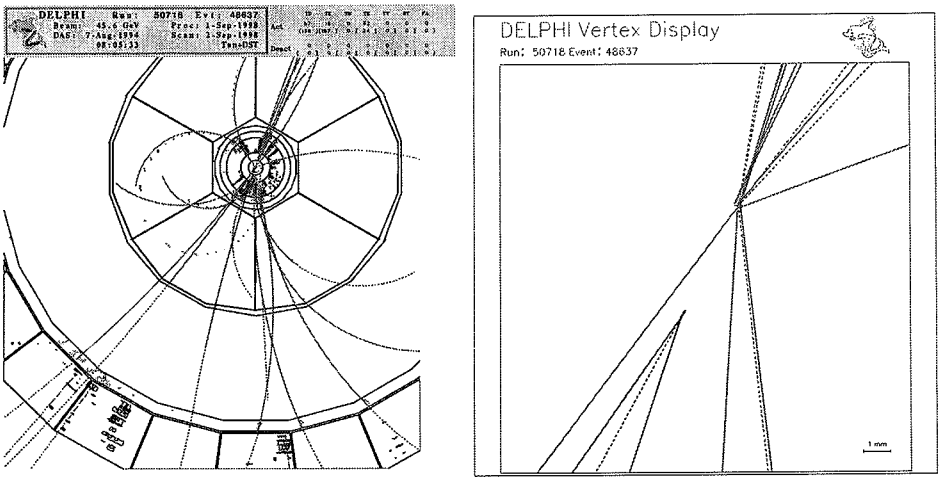

Figure 3.10: *Displays of two fully reconstructed exclusive $\pi\ell\nu$ and $\rho\ell\nu$ candidate decays with magnifications of the vertex region.*

Bibliography

[1] H. Albrecht *et al.* (ARGUS Collaboration), *Phys. Lett.* **B 234** (1990), 409.

[2] R. Fulton *et al.* (CLEO Collaboration), *Phys. Rev. Lett.* **64** (1990), 16.

[3] J.P. Alexander *et al.* (CLEO Collaboration), *First Measurement of the* $B \to \pi\ell\nu$ *and* $B \to \rho(\omega)\ell\nu$ *Branching Fractions*, CLEO 96-6.

[4] M. Artuso *et al.* (CLEO Collaboration), *A New Measurement of the* $b \to u$ *Semileptonic Decays* $B \to \pi\ell\nu$ *and* $B \to \rho\ell\nu$ CLEO CONF 97-30, EPS 97-343.

[5] P. Paganini, F. Parodi, P. Roudeau and A. Stocchi, *Phys. Scripta* **58** (1998), 556.

[6] A. Stocchi, private communication.

[7] V. Barger, C.S. Kim and R.J.N. Phillips, *Phys. Lett.* **B 251** (1990), 629.

[8] A.F. Falk, Z. Ligeti and M.B. Wise, V_{ub} *from the Hadronic Invariant Mass Spectrum in Semileptonic B Decay*, CALT-68-2110, hep-ph/9705235.

[9] I. Bigi, R.D. Dikeman and N. Uraltsev, *The Hadronic Recoil Mass Spectrum in Semileptonic B Decays and Extracting* $|V_{ub}|$ *in a Model-Insensitive Way*, TPI-MINN-97/21-T, hep-ph/9706250.

[10] M. Battaglia, P. Kluit and E. Piotto, *Measurement of* $|V_{ub}|/|V_{cb}|$ *with DELPHI at LEP*, DELPHI 98-97 CONF 165, paper submitted to the *ICHEP 98* Conference, Vancouver B.C. (Canada), July 1998.

[11] M. Battaglia, *New Measurements of* $|V_{ub}|$ *and* $|V_{cb}|$ *with DELPHI at LEP*, HIP-1998-74/EXP, to appear on the Proc. of the *XXIX Int. Conf. of High Energy Physics, ICHEP-98*, Vancouver B.C. (Canada), July 1998.

[12] T. Sjöstrand, *Comp. Phys. Comm.* **82** (1994), 74.

[13] M. Battaglia, *Study of* $b \to u\ell\nu$ *Decays with an Inclusive Generator*, DELPHI 98-42 PHYS 772.

[14] G. Borisov, *Lifetime tags of* $Z^0 \to b\bar{b}$ *with the DELPHI detector*, DELPHI 94-125 PROG 208.

[15] G.R. Wilkinson, *Improvements to the Muon identification in the 94C2 Short DST production*, DELPHI 97-37 PHY 690.

[16] C. Kreuter, *Electron Identification using a Neural Network*, DELPHI 96-169 PHYS 658.

[17] M. Battaglia and P.M. Kluit, *Particle identification using the RICH detectors based on the RIBMEAN package*, DELPHI 96-133 RICH 90.

[18] D. Coffmann *et al.* (Mark III Collaboration), *Phys. Lett.* **B 263** (1991), 135.

[19] M. Feindt and C. Weiser, contributed paper to the ICHEP 97 Conference.

[20] C. Caso *et al.* (Particle Data Group), *Review of Particle Properties*, *Eur. Phys. J.* **C 3** (1998).

[21] G. Borisov and C. Mariotti, *Nucl. Instr. and Meth. in Phys. Res.* **A 372** (1996), 181.

[22] N.G. Uraltsev, *Int. J. Mod. Phys.* **11** (1996), 515.

[23] G. Altarelli *et al.*, *Nucl. Phys.* **B 208** (1982), 365.

[24] R.D. Dikeman, M. Shifman and N.G. Uraltsev, *Int. J. Mod. Phys.* **11** (1996), 571.

[25] M. Neubert, *Phys. Rev.* **D 49** (1994), 4623 and
Phys. Rev. **D 50** (1994), 2037.

[26] A. Bareiss and E.A. Paschos, *Nucl. Phys.* **B 327** (1989), 353.

[27] C. Peterson *et al.*, Phys. Rev. **D 27** (1983), 105.

[28] D. Scora and N. Isgur, *Phys. Rev.* **D 52** (1995), 2783.

[29] R. Barate *et al.* (ALEPH Collaboration), *Determination of $|V_{ub}|$ from the Measurement of the Inclusive Charmless Semileptonic Branching Ratio of b hadrons*, CERN EP/98-67 to appear on *Eur. Phys. J.* **C**.

[30] M. Acciarri *et al.* (L3 Collaboration), *Phys. Lett.* **B 436** (1998) 174.

Chapter 4

Hadronic Charmless b Decays

Hadronic charmless decays originate both from the tree level spectator $b \to u$ transition and from the one-loop penguin process in which the b decays to a s quark via a loop including a virtual W^- boson and a virtual t quark (Figure 4.1). A gluon is also emitted from one of the lines giving the $b \to sg$, sg^*, sgg and $b \to sq\bar{q}$ processes [1]. Tree level dominated decays

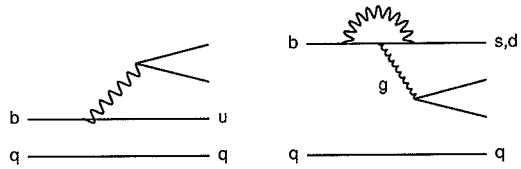

Figure 4.1: *Feynman diagrams of the tree level (left) and the penguin loop (right) transitions contributing to hadronic charmless decays of B mesons.*

confirm the non-zero value of $|V_{ub}|$ in the CKM mixing matrix while those induced by penguin $b \to s$ processes provide tests of the loop structure of the Standard Model. Signals for hadronic charmless b quark decays were first reported by the CLEO experiment at CESR [2] in the sum of the $B \to \pi\pi$ and $K\pi$ decay modes. At LEP analyses have been performed by all the four collaborations [3, 4, 5, 6]. At present it is important to confirm the existence of these decays in exclusive two body modes, to extend the search to as wide a variety of exclusive channels as possible and to search for the inclusive $b \to sg$ process. The determination of the fraction of exclusive charmless events containing a kaon in the final state probes the relative contribution of the tree level and penguin loop processes to the rate of rare hadronic charmless modes. Searches for $b \to sg$ provide with constraints on the rare b decay width Γ_{rare} and on its possible enhancements due to new physics beyond the Standard Model. This analysis is complementary to that performed searching for the $b \to s\gamma$ process discussed in Chapter 5.

4.1 Exclusive $B \to n\pi$, $Kn\pi$ Decays

Exclusive charmless hadronic decays can be reconstructed with good efficiency profiting of the significant decay distance of B mesons and the decay identified using the particle tagging capabilities of the DELPHI detector. Final states with a kaon are due to either $b \to s$ transitions or Cabibbo suppressed $b \to us\bar{u}$ decays where the K meson originates from the W boson. Those with only pions are mainly due to the $b \to u$ tree level diagram. For example, exclusive channels as $B^0 \to \pi^+\pi^-$ are mostly $b \to u$ decays with a possible contribution from suppressed $b \to d$ loop transitions. The decay $B^0 \to K^+\pi^-$ is due to a mixture of the $b \to s$ and the $b \to us\bar{u}$ decays. Finally decays with a neutral kaon as $B^- \to K^{*0}\pi^-$ do not receive tree level contributions and are pure penguin processes. Branching ratios for a large number of two-body exclusive decay modes have been predicted and are in the range of $(0.1 - 1.8) \times 10^{-4}$[8, 7, 9, 10].

With large enough statistics, the interference of the penguin and tree level amplitudes in hadronic charmless B decays could be studied, thereby providing a mean of analyzing the final state strong interactions in B decays [11]. These studies are of special relevance for the interpretation of CP asymmetries in B decays. In fact one of the weak phases of the CKM mixing matrix α can be determined by studying the time-dependance of the asymmetry in the rate of $B_d^0 \to \pi^+\pi^-$ and of its CP conjugate. This channel has a clean experimental signature and its study is the focus of the next generation of B physics experiments. Its interpretation is not affected by important theoretical uncertainties if the decay is dominated by the tree level weak amplitude. On the contrary, a sizeable penguin $b \to d$ contribution (known as "penguin pollution") to $B \to \pi\pi$ with a different weak phase would lead to a significant uncertainty in the extraction of the phase α.

Multi-body charmless decays are subject to larger uncertainties for both their theoretical predictions [12] and the looser constraints provided so far by experimental data. However hadronic charmless b decays are expected to have a large charged multiplicity both when induced by $b \to u$ [13] and by $b \to s$ [14] transitions. This makes the $n\pi$ $(n > 2)$ and $Km\pi$ with $(m > 1)$ final states particularly sensitive to charmless b decays compared to $\pi\pi$ and $K\pi$.

The results of the analysis of the DELPHI data for the exclusive $B \to n\pi$, $(n = 1, 4)$ and $B \to Km\pi$, $(m = 1, 3)$ and of an inclusive search for the $b \to sg$ decay are presented [15]. The particle identification capabilities of the DELPHI Ring Imaging Cherenkov detector allow the separaton of channels with charged kaons from the multi-pion final states. Their implications on the phenomenology of rare b decays are also discussed.

4.1.1 Data Analysis

The analysis is based on the topological reconstruction of exclusive B meson decays in b-tagged hadronic Z^0 decays. Hadronic events, with a probability from the b-tagging algorithm below 0.03, were divided into two hemispheres defined by the plane perpendicular to the event thrust axis. For each hemisphere the leading charged particle was used to start the secondary vertex reconstruction. The other charged particles were iteratively tested to form a common n-prong detached vertex with this leading particle. These were selected within the $(n+1)$ most energetic charged particles, which had momenta above 0.8 GeV/c and were within a 1.0 rad angle from the leading track. In order to preserve an accurate extrapolation to the vertex region, only tracks with at least one hit in the VD were considered. For each event the primary vertex was fitted using an iterative procedure as discussed in Chapter 2. The impact parameters for particle tracks were computed in the $R\phi$ plane with respect to this primary vertex. Tracks having impact parameters larger than 0.5 cm were rejected, because they could be due to a long-lived particle decay or to a problem in the pattern recognition. Vertices with a fit probability below 10^{-5} were discarded. Secondary vertices with one or more lepton candidates were also rejected as the lepton may come from either a semileptonic heavy quark decay or a charmonium decay.

Kinematic cuts were applied to exploit the hard b fragmentation. The total energy of the B candidate was required to be larger than 20 GeV and not to exceed the beam energy. For two (greater than two) prong topologies, the momentum of the leading track had to be larger than 10 (8) GeV/c and that of the other secondary tracks larger than 1.0 (0.8) GeV/c.

There are two main sources of background in the reconstruction of exclusive B decays. The first comes from combinatorial background and originates from all Z^0 hadronic decays. This component was suppressed by requiring that the candidate secondary vertex is separated by more than 2.5 σ from the reconstructed primary vertex in the $R\phi$ plane and that the decay distance was smaller than 2.0 cm. This second cut removes background from long-lived particles.

The second source of background is due to partially reconstructed B decays. This gives a mass distribution that falls steeply up to about 5.0 GeV/c^2 for B mesons. Above this value, a rather flat tail extending to higher masses is present. While partially reconstructed decays of beauty baryons also contribute below the Λ_b mass value, this tail is due mainly to tracks from the primary vertex being incorrectly assigned to the secondary vertex. This was suppressed by requiring that every track used in the secondary vertex reconstruction has an impact parameter with respect to the primary vertex larger than 1.5 times its associated error. In the 1994 data both the $R\phi$ and the z projections of the impact parameters were tested and at least one of the two was required to fulfill this cut. For earlier data only the $R\phi$ projection, where the track extrapolation accuracy was determined by the VD, was used. In two prong topologies this cut was not applied to the leading track. In fact in low multiplicity B decays the leading track is a B decay product in more than 98 % of the cases. Therefore it is not necessary to ensure the rejection of fragmentation tracks by cutting on its impact parameter significance.

As this analysis looks for fully reconstructed decays, special attention was paid to the compatibility of the tracks within the same hemisphere and not used in the secondary vertex reconstruction ("unassociated tracks") to the secondary and the primary vertex. Secondary tracks were defined as tracks with an impact parameter w.r.t. the primary vertex larger than 2.0 times its error. These tracks could originate from secondary decays that were not considered in the reconstruction of the n-prong vertex. Tracks with a smaller impact parameter were assumed to be primary particles originated in the hadronization. In case such tracks were close to the reconstructed secondary vertex, it is not possible to exclude that they might originate from this decay. The compatibility of unassociated tracks with the secondary vertex was studied by computing their χ^2 contribution to the secondary vertex. A candidate was rejected if any track not used in the secondary vertex reconstruction either missed the primary vertex by more than 2.0 times its error or fitted to the secondary vertex within 1.0 σ.

These criteria selected a pure sample of secondary vertices from b particle decays. A detailed simulation study showed that 99%, 98% and 94% of the selected two, three and four-prong vertices with invariant mass above 4.5 GeV/c^2 belong to beauty decays and respectively 2%, 12% and 32% of these have one or more primary particles wrongly assigned to the secondary vertex.

The following decay modes and their corresponding charge conjugates were investigated:

- Two-body decays:
  - $B_d^0 \to \pi^+\pi^-$
  - $B_u^- \to \rho(770)^0\pi^-, \quad \rho(770)^0 \to \pi^+\pi^-$
  - $B_{d,s}^0 \to K^+\pi^-$
  - $\Lambda_b^0 \to pK^-$
  - $B_u^- \to K^-\rho(770)^0, \quad \rho(770)^0 \to \pi^+\pi^-$
  - $B_{d,s}^0 \to K^+a_1(1270)^-, \quad a_1(1270)^- \to \pi^-\pi^+\pi^-$
  - $B_u^- \to \bar{K}^*(892)^0\pi^-, \quad \bar{K}^*(892)^0 \to K^-\pi^+$

- $B^0_{d,s} \to K^+K^-$
- $B^-_u \to \phi(1020)K^-, \quad \phi(1020) \to K^+K^-$

• Three-body decays:

- $B^-_u \to \pi^-\pi^+\pi^-$
- $B^-_u \to K^-\pi^+\pi^-$
- $B^-_u \to K^-K^+K^-$

• Four body decays:

- $B^0_d \to \pi^+\pi^-\pi^+\pi^-$
- $B^0_{d,s} \to K^+\pi^-\pi^+\pi^-$

In two-body decay channels involving a vector and a pseudo-scalar meson, such as $B \to K^*\pi$ and $\rho\pi$, the vector meson is fully polarized. The distribution of the decay helicity angle θ^* in the vector meson rest frame is proportional to $\cos^2\theta^*$ while the background is more isotropic. Therefore in these channels $|\cos\theta^*|$ was required to be larger than 0.5.

In multi-prong final states, B decays with fully reconstructed charmed intermediate states were removed by requiring that no pair of particles had an invariant mass close to either the ψ or the $\psi(2S)$ mass if given electron or muon mass, or close to the D^0 if assigned either $K\pi$ or $\pi\pi$ masses. The widths of the invariant mass intervals around the charm states corresponded to a 3 σ cut, using the measured mass. Triplets of particles from the four-prong vertices were checked also for compatibility with the D^- mass by testing all the possible $K^+\pi^-\pi^-$ and $\pi^-\pi^+\pi^-$ mass combinations, and for compatibility with the D^-_s mass by testing all possible $K^+K^-\pi^-$ combinations. Again events were removed accordingly. All possible combinations of mass assignments were tested provided the corresponding invariant mass of the multi-prong vertex was compatible with the signal mass regions. The efficiency of these criteria in rejecting beauty decays to charm has been evaluated with simulation by studying the fractions of rejected events, for which all the tracks used at the secondary vertex came from a $b \to c$ decay. These fractions were (94 ± 3) % and (96 ± 2) % for three and four-prong topology respectively. A further suppression of the charm intermediate states was achieved by applying the particle identification requirements and intermediate resonance constraints relevant to the channel considered. The charm states passing the selection criteria were taken into account in the evaluation of the background.

The mass resolution was found to be 85 MeV/c^2, 60 MeV/c^2 and 45 MeV/c^2 for two, three and four prong decays respectively. The $B_{d,u}$ (B_s) candidates were accepted in the invariant mass region defined by the intervals $5.15-5.55$ GeV/c^2 ($5.25-5.65$ GeV/c^2) and $5.20-5.50$ GeV/c^2 ($5.30-5.60$ GeV/c^2) for two and more than two prongs respectively. Λ^0_b candidates were accepted in the region between 5.45 GeV/c^2 and 5.9 GeV/c^2. Since the main source of background is partially reconstructed B decays, the background is higher for masses below the $B_{d,u}$ meson mass. For this reason the signal mass regions were chosen to be asymmetric around the mass values of the different b species.

4.1.2 Results

The characteristics of the candidate events found for the two, three and four body decays are given in Tables 4.1,4.2,4.3.

In two-body modes eight candidates of charmless decays of B mesons were reconstructed on the full 1991 - 1994 statistics: two in the $\pi^+\pi^-$ channel, three in $K^+\pi^-$, one in $\rho^0\pi^-$ and two in $K^{*0}\pi^-$ (see Figure 4.2). One of the two candidates classified as $B \to \pi^+\pi^-$ decay is ambiguous with the $K^+\pi^-$ hypothesis since the lower momentum hadron has no particle identification

Table 4.1: Characteristics of the candidate events in two-body decay modes.

Channel	Mass [GeV/c^2]	E_B [GeV]	d/σ_d	τ_B [ps]	$\lvert\cos\theta^*\rvert$	Distance in σ from resonant mass
$\pi\pi$	5.18 ± 0.11	23.0	6.4	3.1	-	-
$\pi\pi$	5.24 ± 0.07	21.2	6.4	2.6	-	-
$K\pi$	5.19 ± 0.08	27.5	3.2	0.3	-	-
$K\pi$	5.20 ± 0.08	39.3	3.0	0.3	-	-
$K\pi$	5.47 ± 0.10	43.7	8.5	1.5	-	-
$\rho\pi$	5.34 ± 0.09	42.0	70.4	3.4	0.68	+0.45
$K^*\pi$	5.21 ± 0.06	40.0	17.6	1.2	0.59	+0.78
$K^*\pi$	5.38 ± 0.07	39.0	44.6	2.3	0.63	+1.60

Table 4.2: Characteristics of the candidate events in three-body decay modes.

Channel	Mass [GeV/c^2]	E_B [GeV]	d/σ_d	τ_B [ps]
$\pi\pi\pi$	5.26 ± 0.05	34.6	27.2	2.1
$K\pi\pi$	5.23 ± 0.05	40.8	5.1	2.4
$K\pi\pi$	5.39 ± 0.04	20.3	17.6	3.0
$K\pi\pi$	5.27 ± 0.06	40.2	11.6	1.0
$K\pi\pi$	5.32 ± 0.04	21.6	11.8	1.2

Table 4.3: Characteristics of the candidate events in four-body decay modes.

Channel	Mass [GeV/c^2]	E_B [GeV]	d/σ_d	τ_B [ps]
$\pi\pi\pi\pi$	5.43 ± 0.05	39.6	13.2	1.4
$\pi\pi\pi\pi$	5.21 ± 0.05	41.4	16.8	0.9
$K\pi\pi\pi$	5.23 ± 0.11	44.5	46.0	0.3

information. Changing from the $\pi\pi$ to the $K\pi$ mass assignment moves its total mass from 5.18 GeV/c^2 to 5.32 GeV/c^2 which is also inside the signal mass region. No candidates for Λ_b charmless decays were found. The background was estimated by studying the rejection factors on simulated $q\bar{q}$ events for independent sets of the cuts applied in the analysis. The secondary vertex selection criteria were relaxed for the two-prong sample. The effect of intermediate mass and the helicity angle constraints were also studied in the multi-prong sample. In addition the background suppression coming from kaon or proton identification was measured for all the channels giving 0.68 ± 0.15 events. The rejection factors obtained from simulated events were compared with those obtained for real data and found to be consistent. The background estimate was also checked with the number of simulated events fulfilling all the selection cuts in the mass interval from 5.1 GeV/c^2 to 6.0 GeV/c^2, normalised to the signal region and to the equivalent data statistics. The result was 0.75 ± 0.25 events, in agreement with the value estimated using the rejection factors.

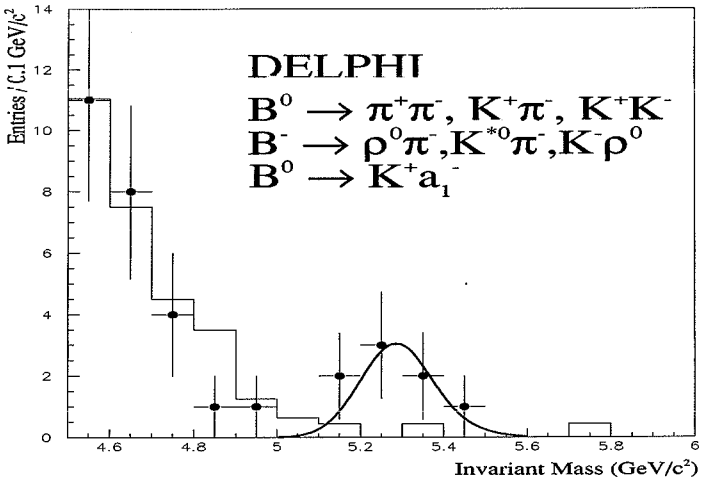

Figure 4.2: *Invariant mass distributions for two body B decay channels. Points with error bars represent the real data and the histograms the expected mass distributions in the absence of charmless hadronic B decays, as obtained from simulation. The curve represents the expected shape for the signal events normalised to the number of candidates selected in real data in the signal mass region.*

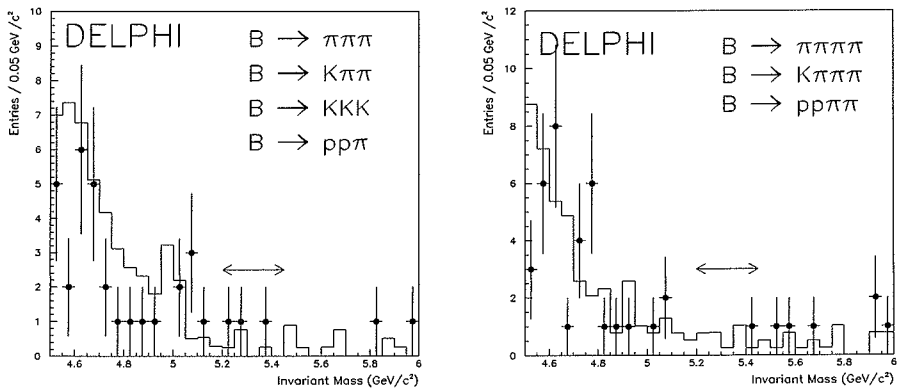

Figure 4.3: *Invariant mass distributions for three and four-body B decay channels. Points with error bars represent the real data and the histograms the expected mass distributions in the absence of charmless hadronic B decays, as obtained from simulation.*

Five and three candidate decays were found in three and four-body decay modes respectively. The numbers are consistent with the estimated background of respectively 3.5 ± 1.0 and 5.3 ± 1.2 events from other processes.

4.1.3 Discussion

Eight charmless decay candidates were selected in two-body hadronic modes in real data with an estimated background of 0.68 ± 0.15 events. The probability that all the events seen are due to a fluctuation of this background is 10^{-6}. This result is the first independent confirmation of the evidence for rare b decays in hadronic charmless modes already reported by the CLEO Collaboration. In the $\pi^+\pi^-$ and $K^+\pi^-$ modes five events were observed with an estimated background of 0.15 ± 0.05 events corresponding to a probability of originating from a background fluctuation of 5×10^{-5}. The efficiency for reconstructing either $B^0 \to \pi^+\pi^-$ or $B^0 \to K^+\pi^-$ decays without distinguishing between the two final states was evaluated to be 0.25 ± 0.01 using simulated data. The uncertainty on the reconstruction efficiency was taken into account as systematic error. Interpreting all the five observed events as signal, the corresponding branching ratio is:

$$\mathrm{BR}(B^0_{d,s} \to \pi^+\pi^-, K^+\pi^-) = (2.8\ ^{+1.5}_{-1.0}\ (\mathrm{stat.}) \pm 0.2\ (\mathrm{syst.})) \times 10^{-5}$$

This result agrees with the first measurement reported by the CLEO Collaboration of $(2.4 \pm 0.8) \times 10^{-5}$ [2]. The exclusive $K^+\pi^-$ channel has three events with an estimated background of 0.06 ± 0.03. This corresponds to a probability of being a fluctuation of the background of 10^{-4}. The three events give a branching ratio for the exclusive channel of:

$$\mathrm{BR}(B^0_{d,s} \to K^+\pi^-) = (2.4\ ^{+1.7}_{-1.1}\ (\mathrm{stat.}) \pm 0.2\ (\mathrm{syst.})) \times 10^{-5}$$

For the decay into three-prong final states, the combination of the $\rho\pi$ and $K^*\pi$ channels gave three events in real data with an expected background of 0.15 ± 0.04 events. This excess is also significant, while for either of the individual channels the probability of a background fluctuation is above 10^{-3}. Again considering the three candidates as signal events, the value for the combined branching ratio is:

$$\mathrm{BR}(B^-_u \to \rho\pi, K^*\pi) = (1.7\ ^{+1.2}_{-0.8}\ (\mathrm{stat.}) \pm 0.2\ (\mathrm{syst.})) \times 10^{-4}$$

In three and four-body modes, where no excess of events was observed, the upper limits set by this analysis are within a factor two of the expectations for these channels. The number of candidates for each of the channels, the estimated backgrounds, the reconstruction efficiencies and the corresponding results for the decay branching ratios are summarised in Tables 4.4, 4.5 and 4.66 for two, three and four-body decays respectively. The present upper limits are within a factor two to three above the expected rates in Standard Model.

The DELPHI data can be used to estimate the relative contribution from tree level $b \to u$ transitions and penguin $b \to s$, $b \to d$ loops to charmless hadronic b decays. This depends on the value of the relevant $|V_{ij}|$ elements in the CKM mixing matrix and on the penguin decay width. The fraction of candidate hadronic charmless decays containing a kaon in the final state is sensitive to the process responsible for the decay. In fact considering only the leading graphs, tree level $b \to u$ decays of $B_{u,d}$ mesons produce multi-pion $(u\bar{d})(d\bar{u})$... final states while loop $b \to s$ transitions give either a charged or a neutral kaon in the final state. Kaon production in $b \to u$ decays proceeds only through the Cabibbo suppressed $b \to u(s\bar{u})_W$ process. Similarly multi-pion final states in penguin $b \to d$ decays are suppressed by a factor $|V_{td}|^2/|V_{ts}|^2$ compared to the kaon final states. These effects from non-leading graphs can be parametrised. At LEP this picture becomes more complicated due to the decays of the strange beauty B^0_s meson. In fact in the case of hadronic charmless B^0_s decays, a kaon can originate from the spectator s quark also in the Cabibbo allowed tree level $b \to u d\bar{u}$ transition.

An unbinned maximum likelihood fit was performed using the reconstructed invariant mass m_B, the average Cherenkov angle $\bar{\theta}_c$ and the specific ionization dE/dx as inputs (Figure 4.4). All the events with at least one of the π, K mass assignments, independently of the hadron

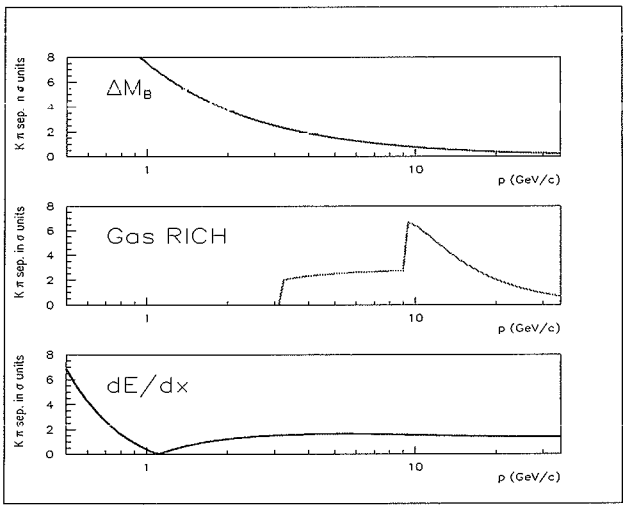

Figure 4.4: *The K-π separation obtained with the B mass difference, the average Cherenkov angle $\bar{\theta}_c$ in the RICH gas radiator and the specific ionisation dE/dx in the TPC as a function of the particle momentum. This figure shows the complementarity of the three variables used, providing a separation between the two mass hypothesis better than 1.5 σ over the full kinematical range of interest.*

tagging, giving an invariant mass in the B mass signal region were used in the fit. The efficiency for a signal event to be accepted in the fit is 0.26 ± 0.01. No events other than the eight candidates were accepted with this looser requirement. The fraction $F(K\pi,(K\pi)\pi)) = N(K\pi,(K\pi)\pi)/(N(\pi\pi,(\pi\pi)\pi)+N(K\pi,(K\pi)\pi))$ was left free in the fit. The result was $0.68^{+0.13}_{-0.16}$. The kaon contribution from B_s^0 decays was then taken into account in the fit to estimate the fraction of decays $b \to K$ for which a charged kaon in the final state is not due to a spectator s quark. The fraction of events containing a kaon and the fraction of B_s^0 candidates were fitted at the same time. Figure 4.5 shows the result of this fit and the fraction of B decays with a kaon in the final states as a function of the $b \to s$ fraction in charmless decays.

As a result, the fraction of candidate charmless hadronic B decays for which a charged kaon in the final state is not due to a spectator s quark $F(b \to K)$ is:

$$F(b \to K) = 0.58 \pm 0.18 \text{ (stat.)}.$$

The fit gave $1.3^{+1.5}_{-1.3}$ for the number of B_s^0 candidates in the sample to be compared with 1.5 expected assuming the B_s/B_d production rate of $f_s/f_d = 0.30$. Restricting the analysis only to the five candidates in the two prong modes $B^0 \to \pi^+\pi^-$, $K^+\pi^-$, the corresponding fraction $F(B_d^0 \to K^+\pi^-) = N(B_d^0 \to K^+\pi^-)/(N(B^0 \to \pi^+\pi^-) + N(B^0 \to K^+\pi^-))$ is determined to be 0.52 ± 0.21.

A similar analysis was performed by CLEO on their sample of candidate $B \to \pi\pi$, $K\pi$ decays. The number of signal events and the fraction $F(B_d^0 \to K^+\pi^-)$ were extracted by a likelihood fit to the B mass and to the dE/dx response. The result was 17 ± 6 signal events with $F(B_d^0 \to K^+\pi^-) = 0.54 \pm 0.20$ [16]. The CLEO and DELPHI results are in good agreement. The DELPHI result has a statistical uncertainty similar to that obtained by the fit to the CLEO data despite the smaller statistics; this is due to the superior K-π separation provided by the use of the RICH detector.

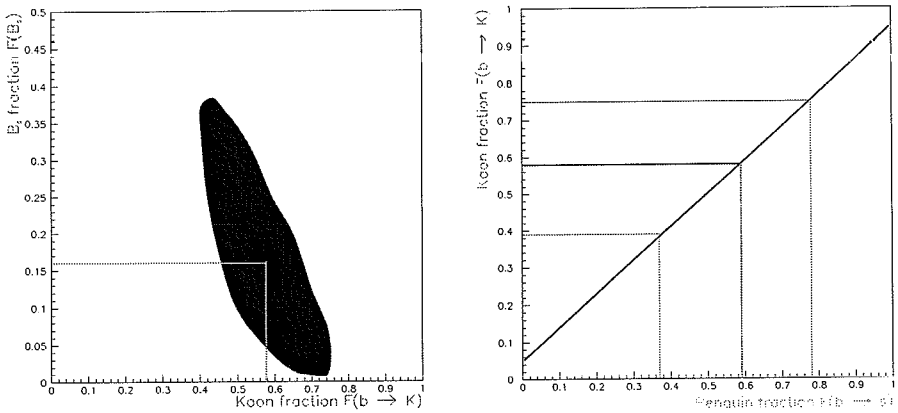

Figure 4.5: *Left: The result of the likelihood fit to the fraction of decays with a kaon $F(b \to K)$ and the fraction of B_s^0 decays in the reconstructed sample. The curve gives the contour of the 68 % confidence level. Right: The dependance of $F(b \to K)$ on the penguin fraction of $b \to s$ decays taking into account the effect of suppressed decays. The lines correspond to the DELPHI result for $F(b \to K)$.*

Averaging the DELPHI and CLEO results gives 0.56 ± 0.14 (stat.). These values agree well with the theoretical estimate of $0.57^{+0.36}_{-0.23}$ obtained in Chapter 1 by assuming $|V_{ub}|/|V_{cb}| = 0.10 \pm 0.02$ consistent with the recent DELPHI result discussed in Chapter 3. This argument can be reversed to extract an estimate of $|V_{ub}|/|V_{cb}|$ from the measured contribution of $b \to u$ transitions to the charmless hadronic decay rate as:

$$\frac{|V_{ub}|}{|V_{cb}|} = 0.10 \sqrt{\frac{BR(b \to s)^{th}_{had}}{BR(b \to s)^{th}_{had} + BR(b \to u)^{th}_{had}} \times \frac{1 - F(b \to K)}{F(b \to K)}} \tag{4.1}$$

Using $BR(b \to s)^{th}_{had} = 0.98^{+0.51}_{-0.30} \times 10^{-2}$ and $BR(b \to u)^{th}_{had} = 0.73^{+0.16}_{-0.12} \times 10^{-2}$ for $|V_{ub}|/|V_{cb}| = 0.10$ [17] and assuming equal final final state charged multiplicities for the $b \to u$ and $b \to s$ hadronic decays [14], the DELPHI + CLEO average for $F(b \to K)$ gives:

$$\frac{|V_{ub}|}{|V_{cb}|} = 0.103^{+0.031}_{-0.028} \tag{4.2}$$

again in good agreement with the result obtained using semileptonic decays.

The hypotheses that multi-pion decays or decays with a non spectator kaon saturate the hadronic charmless rate can be excluded at the 99.994% and 99.95% confidence level respectively. This result has two important consequences. The first is that the non zero value of the $|V_{ub}|$ element in the CKM matrix, as obtained from the study of charmless semileptonic inclusive decays discussed in the previous chapter, is confirmed. Further, it provides additional evidence of the contribution of loop diagrams to the b decay width. This is the only independent confirmation of the first observation of loop induced b decays in $B \to K^*\gamma$ [18] as discussed in the next chapter. More recently, the CLEO Collaboration has confirmed the observation of the $B^0 \to K^+\pi^-$ decay, first obtained in this study, and reported $\mathrm{BR}(B_d^0 \to K^+\pi^-) = (1.5 \pm 0.5\ (\mathrm{comb.})) \times 10^{-5}$ from the analysis of 3.3×10^6 $B\bar{B}$ events [19], in agreement with the DELPHI result.

$$B_u^- \to K^*(892)^0\pi^-$$

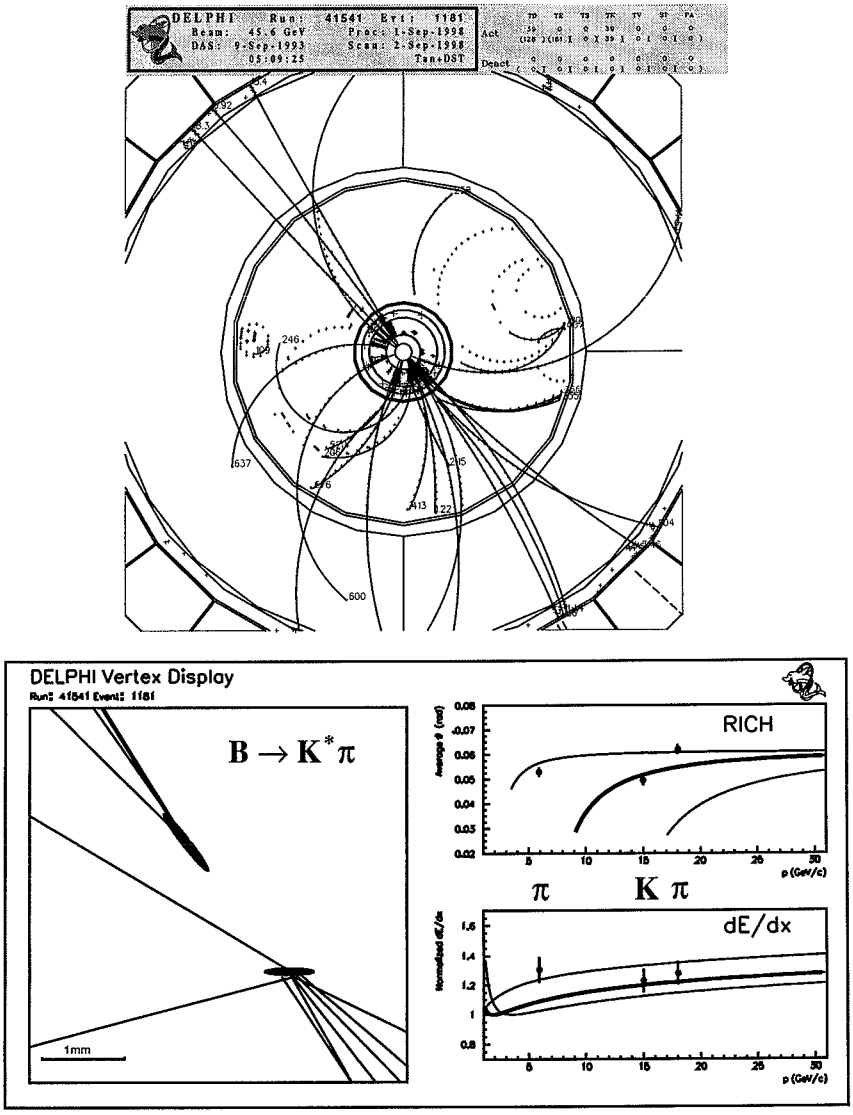

Figure 4.6: *Display of a fully reconstructed $B_u^- \to K^{*0}\pi^-$ candidate with a magnification of the vertex regions and the hadron identification responses for the particles originating at the secondary vertex.*

$$B_d^0 \to K^+\pi^-$$

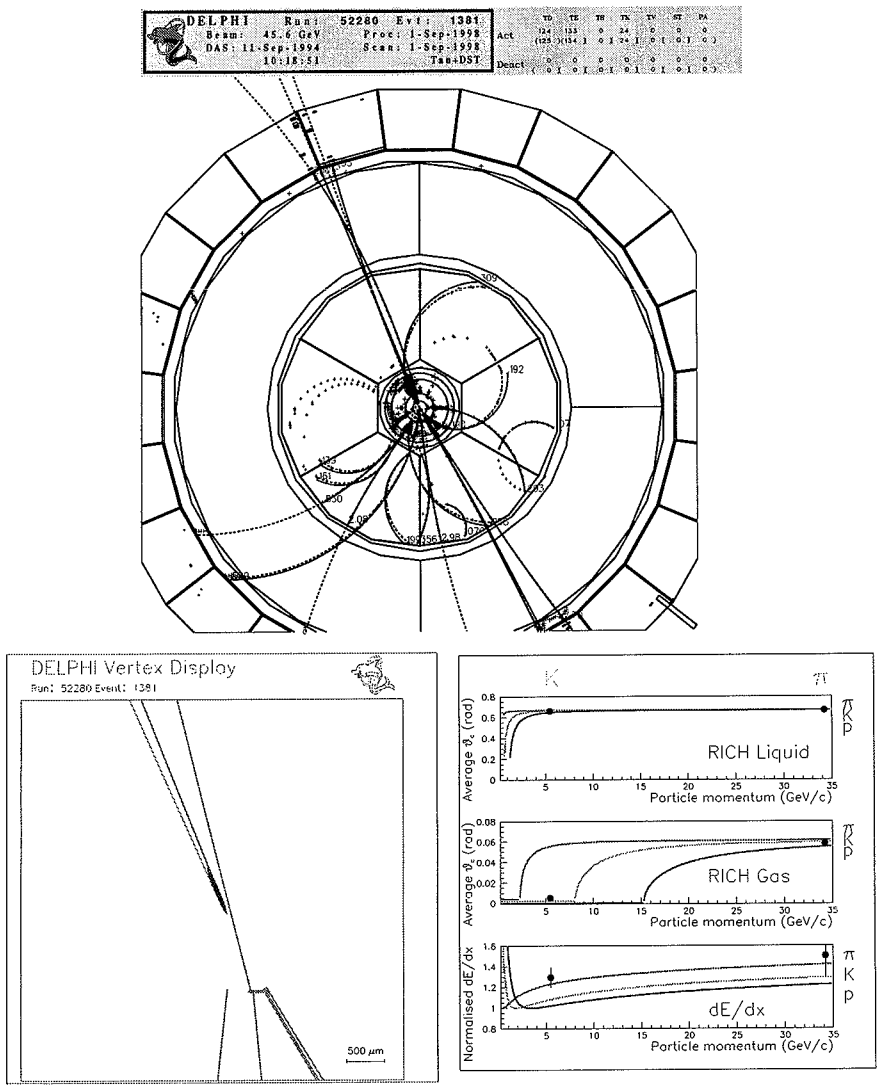

Figure 4.7: *Display of a fully reconstructed $B_d^0 \to K^+\pi^-$ candidate with a magnification of the vertex regions and the hadron identification responses for the particles originating at the secondary vertex.*

Table 4.4: Summary of the results for two-body decays.

Channel	Evts	Bkg	ϵ [%]	Signal Evts	Theory BR$\times 10^5$		DELPHI BR$\times 10^5$
$B_d^0 \to \pi^+\pi^-$	2	0.09	23.0	<5.2	1.1-1.8	[7, 9]	<4.5
$B_{d,s}^0 \to K^+\pi^-$	3	0.06	18.0	3	1.1-1.8	[7, 8, 9]	$2.4^{+1.7}_{-1.1} \pm 0.2$
$B_{d,s}^0 \to \pi^+\pi^-, K^+\pi^-$	5	0.15	25.0	5	-		$2.8^{+1.5}_{-1.0} \pm 0.2$
$B_{d,s}^0 \to K^+K^-$	0	0.01	8.0	<2.3	-		<4.6
$\Lambda_b^0 \to pK^-$	0	0.01	5.5	<2.3	-		<36
$B_u^- \to \rho^0\pi^-$	1	0.09	5.5	<3.8	0.4-1.4	[7, 9]	<16
$B_u^- \to K^{*0}\pi^-$	2	0.06	4.5	<5.3	0.6-0.9	[7, 8]	<39
$B_u^- \to \rho^0\pi^-, K^{*0}\pi^-$	3	0.15	6.0	3	-		$17^{+12}_{-8} \pm 2$
$B_u^- \to K^-\rho^0$	0	0.17	4.5	<2.3	.01-.06	[7, 8]	<12
$B_u^- \to K^-\phi$	0	0.01	4.0	<2.3	0.6-1.4	[7, 8, 10]	<28
$B_{d,s}^0 \to K^+a_1^-$	0	0.18	3.5	<2.3	-		<23

Table 4.5: Summary of the results for three-body decays.

Channel	Evts	Bkg.	ϵ [%]	Signal Event UL	Theory BR$\times 10^5$		DELPHI BR$\times 10^5$
$B_u^- \to \pi^+\pi^-\pi^-$	1	1.9	5.3	<3.0	6	[12]	<13
$B_u^- \to K^-\pi^+\pi^-$	4	1.6	4.3	<6.4	-		<33
$B_u^- \to K^+K^-K^-$	0	0.03	2.6	<2.3	-		<20

Table 4.6: Summary of the results four-body decays.

Channel	Evts	Bkg.	ϵ [%]	Signal Event UL	Theory BR$\times 10^5$		DELPHI BR$\times 10^5$
$B_d^0 \to \pi^+\pi^+\pi^-\pi^-$	2	2.9	3.8	<3.5	10	[12]	<23
$B_{d,s}^0 \to K^+\pi^+\pi^-\pi^-$	1	2.4	2.3	<2.9	-		<23

4.2 Inclusive $b \rightarrow sg$ Decays

The rates for $b \rightarrow s$ transitions have been estimated in Standard Model. QCD corrections have been computed at the leading order and have been found to enhance the $b \rightarrow sq\bar{q}$ rate and suppress the $b \rightarrow sg$ one. As a results the Standard Model expectation for $b \rightarrow sg$ is $(2.3 \pm 0.6) \times 10^{-3}$ [20].

The $b \rightarrow sg$ rate is poorly constrained by data on other $b \rightarrow s$ transitions. In fact it has been shown [20] that the $b \rightarrow sg$ rate is not bound by measurements and limits for the radiative decay $b \rightarrow s\gamma$. Further there is a substantial theoretical uncertainty on the relative branching ratios of exclusive modes that receive contributions from $b \rightarrow sg$ transitions. As an example, the branching ratios for $B \rightarrow Kn\pi$ with $(n = 1, 2, 3)$ final states have been estimated by means of an inclusive $b \rightarrow sg$ generator and turned out to be of the order of 10^{-3} - 10^{-4} of the inclusive BR($b \rightarrow s\gamma$). This shows that an inclusive analysis is necessary to set tight bounds on the $b \rightarrow sg$ rate.

Possible inconsistencies found in the analyses of the data on the inclusive $b \rightarrow c\ell\nu$ and the $b \rightarrow c\bar{c}s$ rates and on the kaon yield in B decays have prompted the developement of models with either an enhanced $b \rightarrow c\bar{c}s$ through the contribution of $B \rightarrow D\bar{D}KX$ [21] or a large $b \rightarrow sg$ rate [23]. More recently the CLEO Collaboration has reported evidence of $B \rightarrow \eta' X_s$

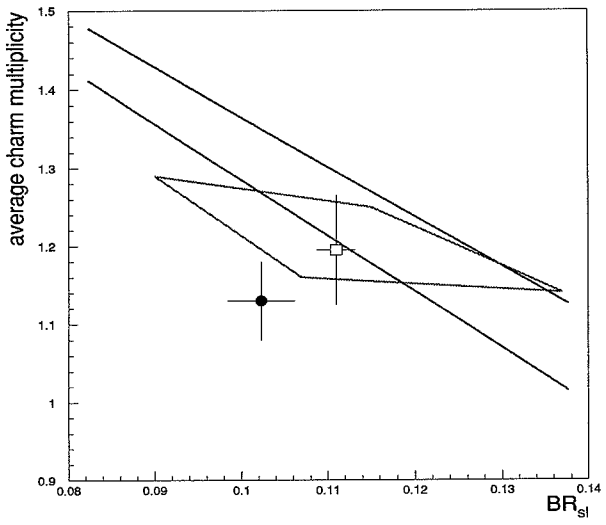

Figure 4.8: *The average number of charm particles in B decays n_c as a function of the semileptonic branching ratio BR_{sl}. The open square indicates the* LEP *results and the filled dot the average of the $\Upsilon(4S)$ results. The* LEP *result for BR_{sl} has been corrected for the different composition in B hadron species. The lines represent the theoretical predictions from [21, 22].*

with significantly enhanced branching ratio [24]. This can be explained either in terms of an enhanced yield of the $b \rightarrow sg^*$ process [25] or as a possible first signal of a large $b \rightarrow s$ from new physics contributions [26].

It is therefore important to acquire additional data on inclusive $b \to s$ transitions. The number of $K^{\pm}$ mesons produced in b decays and the distribution of their transverse momenta reflects the phase space and flavour dynamics in the B hadron decay and are therefore sensitive to the decay mechanisms. In fact $b \to c\bar{c}s$ decays are characterised by three strange hadrons in the final state and soft p_t spectra while an enhanced rate of loop mediated $b \to s$ transitions increases the yield of kaons at large values of p_t. The hadron identification capabilities of the DELPHI detector have been again exploited in this study to constrain models with large $b \to sg$ decay rates. This analysis is based on the study of identified charged kaons in b-tagged events [27] and it has been complemented by a study of the shape of the b-tagging probabilities [28] profiting of the small correlation of the resulting systematic uncertainties.

4.2.1 The Kaon p_t Analysis

A large rate of $b \to sg$ transitions can be detected by the distortion of the p_t spectrum of kaons from B decays. Due to the large phase space available in the $b \to sg$ transition, the momentum of the K in the B rest frame from these decays is typically larger than if the kaon originates in $b \to c \to s$ decays. An enhancement of the yield of kaons at large (p, p_t) values can therefore signal a large rate for the $b \to sg$ process [23].

The p and p_t distributions of kaons from B mesons decaying by the $b \to sg$ transition were studied on simulated B decays. The $b \to sg$ generator modelled these decays as follows [32]. In the B rest frame, a string was attached from the s to the g and from the g to the spectator quark, so that the gluon was a kink in the string. In the decay, the s quark and the gluon were emitted back to back with energies $m_b/2$, while the spectator quark momentum was determined by the Fermi momentum p_F. The system was then boosted and allowed to fragment using the JETSET model [31]. Results are presented assuming the kinematics of the kaons produced in $b \to sg$ decays is as described by this model.

A search for an excess of kaons from B decays at values of p_t above 1 GeV/c was performed in the DELPHI data. The analysis relied on *a)* the characteristic kinematics of B decays and *b)* the accurate extrapolation of charged particle tracks to their production vertices to separate B decay products from primary particles.

Charged kaons have been identified using the combined response of the RICH and TPC dE/dx as described in 2.2.3. Jets containing at least one tagged kaon with $p > 4.5$ GeV/c were selected in b-tagged events. Since the kaon produced in the hadronisation of the s quark from the b decay chain is the leading particle in 70% of cases, different selection criteria were applied for leading tagged kaons: the kaon was required to have a probability of belonging to the primary vertex of less than 0.15 if it was the leading particle in the jet or below 0.02 otherwise. The impact parameter of the kaon was signed according to the position of crossing with the estimated B flight direction using the lifetime sign convention. Kaons with negative impact parameter were rejected.

Background from misidentified pions as well as from kaons from double charm and B_s decays was partially suppressed by requiring the sign of the kaon charge to be equal to that of the b quark. This was estimated by the jet charge Q_{Jet}, defined as the momentum-weighted sum of the charges of the particles belonging to the jet. For those cases for which $|Q_{Jet}| > 0.10$, the kaon p_t was signed by the product of the kaon charge and the jet charge. If the jet charge was below the cut value of 0.10, therefore not providing useful discrimination on the b quark charge, the kaon p_t was signed positive. A total of 44500 tagged kaons fulfilling these selection criteria were selected in real data.

The ratio of selected particles in real data and simulation was 0.998 ± 0.007. From the simulation, the background of misidentified pions and of kaons not coming from B decays corresponds to 18% of the selected sample. The momentum distribution was checked to be in good agreement with the simulation. The fraction of $b \to sg$ decays was extracted by a χ^2 fit to the

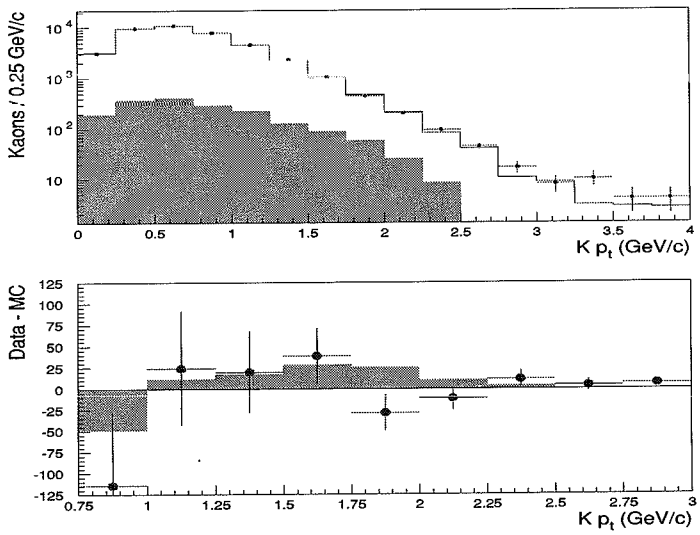

Figure 4.9: *The p_t distribution of selected kaons (upper plot). The points with error bars represent the real data and the histogram the simulation normalised to the same number of Z^0 hadronic decays. The lower plot shows the real data subtracted by the Monte Carlo prediction of $b \to c$ decays and background. The grey histograms are the expected contribution of $b \to sg$ corresponding to the fitted fraction.*

shape of the p_t distribution. The shape of the $b \to sg$ signal was obtained as the distribution for kaons from the decays produced with the generator described above and passed through the full DELPHI detector simulation. In the fit the fractions of $b \to sg$, $b \to c$ and $b \to c\bar{c}s$ and the background were left free. The relative ratio of double charm to single charm decays was fixed to the result of the previous analysis. The amount of charmless $b \to u, d$ transitions was fixed to 0.015.

The result of the fit was $\mathrm{BR}(b \to sg) = 0.005\ ^{+0.017}_{-0.005}$. with fit probability of 0.20. The amount of background from the fit was 0.16 ± 0.02, in agreement with the simulation prediction of 0.18. The p_t distribution for kaons with charge sign equal to that of the jet is shown in Figure 4.9 for real data and simulation, together with the simulation-subtracted distribution in the region sensitive to the presence of $b \to sg$ decays.

Several sources of systematic uncertainty have been taken into account. Firstly, it is important to verify that the simulation reproduces accurately the transverse momentum distribution of particles from B decays other than $b \to sg$ and from the background. The kaon momentum spectrum in the B rest frame was checked by comparing the distribution for K^0_s from the DELPHI simulation with ARGUS data [30] and they were found to agree well as shown in Figure 4.10. In addition the analysis was repeated for K's in jets containing an inclusively reconstructed D decay. The p_t spectra of real data and simulation agreed well over the full range used in the analysis and the result of the fit was $\mathrm{BR}(b \to sg) = 0.000\ ^{+0.026}_{-0.000}$. This shows that the modelling of the kinematics in $b \to c$ transition does not introduce any significant biases.

The B decay multiplicity also modifies the p_t spectrum of the decay products and it was therefore studied for its contribution to systematic uncertainties. Simulated events were re-

weighted such that the distribution of the $B\bar{B}$ charged decay multiplicity agreed with that recently measured by the CLEO experiment at the $\Upsilon(4S)$ resonance [29]. The average value was changed within the experimental errors and the width of the distribution was also varied within the constraint of the measured multiplicity distribution (see Figure 4.10).

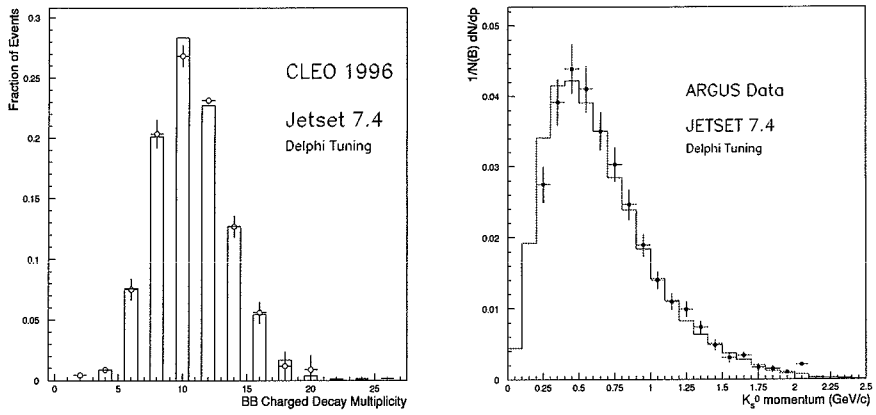

Figure 4.10: Comparison the simulation with published data for the charged BB decay multiplicity (left) and the momentum spectrum of K_s^0 from B decays (right).

The transverse momentum distribution of kaons from background, as $s\bar{s}$ pairs produced by fragmentation, was studied by selecting kaon candidates with negative signed impact parameter. While the p_t spectra agreed well up to about 2.0 GeV/c, the real data is enhanced at larger p_t values. This effect has already been noted in inclusive particle spectra. Therefore primary kaons in simulations were rescaled in order to reproduce the distribution observed on the real data. Since this discrepancy does not effect the region were the $b \rightarrow sg$ signal is enhanced, this correction did not change the result of the fit significantly. Finally, possible discrepancies in the p_t spectrum of B decay products were studied on a high statistics sample of tagged pions fulfilling the kaon selection criteria used in the analysis except for hadron identification. The distributions of transverse momenta for real data and simulation agreed well in the region 0.5 GeV/c $< p_t <$ 2.5 GeV/c. In the region p_t $<$ 0.5 GeV/c the simulation overestimated the data. A correction function was derived from this comparison and applied to the selected kaons in simulation. The fit was repeated and the result again agreed.

Finally the systematic uncertainty due to the modelling of the $b \rightarrow sg$ decays was evaluated. The effect of the uncertainty on the value of the Fermi momentum p_F measured at the $\Upsilon(4S)$ resonance in semileptonic and radiative decays [33, 34] was taken into account. Its variation modifies the broadening of the distribution of the K momentum in the B rest frame and therefore of the kaon p_t.

As a result of these studies a systematic error was estimated. This error takes into account both the change in the central value for the fitted $b \rightarrow sg$ fraction and that of the statistical error from the fit, reflecting a change in the experimental sensitivity. The resulting upper limit is:

$$\mathrm{BR}(b \rightarrow sg) < 0.05 \text{ (95 \% C.L.)}$$

The analysis has shown no excess of secondary kaons at large p_t in b-tagged events as expected from an anomalously large $b \rightarrow sg$ decay rate.

4.2.2 The Impact Parameter Analysis

The DELPHI kaon high p_t analysis has been complemented by a study of the inclusive impact parameter probability distribution [35] developed for the tagging of $Z^0 \to b\bar{b}$ events as discussed earlier in 2.2.1. Charmless b decays, including $b \to sg$ transitions, are characterised by a topology with a single secondary vertex at the B hadron decay point. On the contrary, due to the finite lifetime of charm hadrons, in $b \to c \to s$ decays there are distinct secondary and tertiary vertices. This characteristic results in a b-tagging probability distribution extending to larger values for cascade $b \to c$ decays compared to charmless decays as shown in Figure 4.11. The analysis was performed on 3.4 M selected Z^0 hadronic decays collected by DELPHI from 1992 to 1995. Events were divided into two hemispheres defined by the plane orthogonal to the event thrust axis and the b-tagging probability P_H^+ was computed for each hemispheres. The sample was then enriched in $b\bar{b}$ events by requiring at least one hemisphere in the event to give a probability $P_H^+ < 0.005$ (0.01 for 1992 and 1993 when only the $R-\phi$ coordinate of impact of the tracks was measured in the Vertex Detector. The hemisphere opposite to the one tagged was required to have at least to charged particles with associated hits in the Vertex Detector and positive impact parameter using the lifetime convention described in 2.2.1. A total of 389 k hemispheres was selected by these requirements. A fit to the shapes expected for the $b \to$ *no open charm* (0C), $b \to c$ and $b \to$ *open* $c\bar{c}s$ (2C)and the non-b background was performed on these hemispheres to determine the relative contribution of the three b decay classes. The $b \to$ *no open charm* class includes charmless $b \to u$, $b \to s$ transitions and decays with hidden charm like $B \to J/\psi X$ or decays to other charmonium states. The distributions of P_H^+ for inclusive $b \to sg$ decays simulated with the dedicated decay generator used for the previous analysis were also compared with those of generic $b \to u, s$ transitions and found to agree.

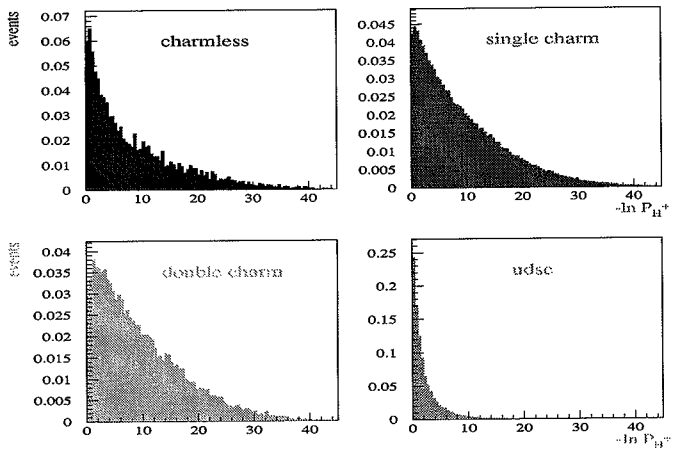

Figure 4.11: *The b-tagging probability distribution per hemisphere, P_H^+, from the 1994 simulation for charmless and hidden charm B hadron decays, B decays into one charm particle, B decays into two open charm particles, and the udsc background.*

The result of the fit was $BR_{0c} = 0.033 \pm 0.021$ (comb) and $BR_{2c} = 0.136 \pm 0.042$ (comb) where the errors account for both the statistical and systematic uncertainties (see Figure 4.12).

Subtracting the hidden charm contribution from B decays into charmonium states of 0.026 $\pm$ 0.004 [36] gives:

$$\mathrm{BR}(B \to no\ charm) = 0.007 \pm 0.021$$

to be compared with the SM expectation of 0.016 $\pm$ 0.008 (see 1.2.2). An upper limit on contribution to charmless B decays from new physics can be derived by subtracting the SM contribution and computing the 95 % upper limit obtaining

$$\mathrm{BR}(b \to no\ charm)^{NEW} < 0.037.$$

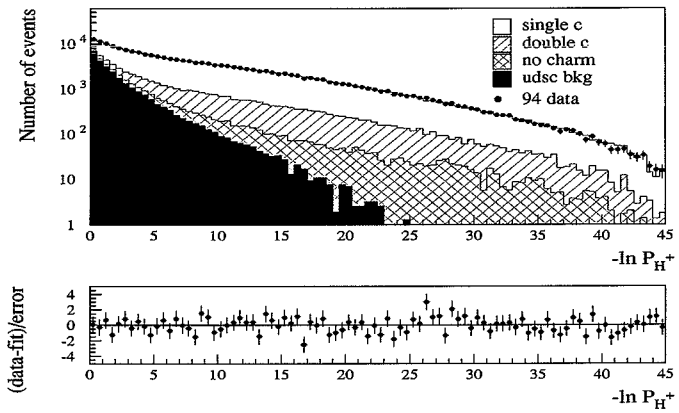

Figure 4.12: *The b-tagging probability distribution per hemisphere, P_H^+, from the 1994 data (points with error bars) compared with the simulation predictions for the different sources corresponding to the fit results.*

4.2.3 Conclusion

In conclusion, two independent analysis have been performed to search for a possible enhancement in the inclusive charmless b decay width. The kaon high p_t method, sensitive to $b \to sg$ decays, did not reveal any excess above the expected background from the analysis of about 50000 identified secondary charged kaons in b-tagged events. This corresponds to an upper limit at 95% C.L. of 0.05 for the $b \to sg$ decay branching ratio. This result is confirmed by the analysis of the b-tagging probability distribution that provides with a comparable constraint for any contributions of charmless b decays from new physics.

Searches for $b \to sg$ have been performed also by other experiments. The SLD Collaboration at the Stanford Linear Collider has performed an analysis of the p_t spectrum of identified kaons, similarly to that reported in this study, reporting no significant excess of events compared with the expected backgrounds [37]. The CLEO II experiment at CESR has derived a limit on $\mathrm{BR}(b \to sg)$ from a measurement of the double ratio of widths: $\frac{\Gamma(B\to\bar{D}X)}{\Gamma(B\to all)} / \frac{\Gamma(B\to\bar{D}X\ell\nu)}{\Gamma(B\to X\ell\nu)}$ [38]. The limit $\mathrm{BR}(b \to sg) < 0.082$ was obtained at 95% confidence level.

Bibliography

[1] W. Hou, *Nucl. Phys.* **B 308** (1988) 561.

[2] M. Battle *et al.*, *Phys. Rev. Lett.* **71** (1993) 3922.

[3] R. Akers *et al.*, *Phys. Lett.* **B 337** (1994) 393.

[4] P. Abreu,..., M. Battaglia *et al.*, *Phys. Lett.* **B 357** (1995) 255.

[5] M. Acciarri *et al.*, *Phys. Lett.* **B 363** (1995) 127.

[6] J. Boucrot *et al.*, EPS-0399, contributed paper to the EPS 1995 conference, Brussels, July 1995.

[7] L.L. Chau *et al.*, *Phys. Rev.* **D 43** (1991) 2176.

[8] N.G. Deshpande and J. Trampetic, *Phys. Rev.* **D 41** (1990) 895.

[9] A. Deandrea *et al.*, *Phys. Lett.* **B 320** (1994) 170.

[10] N.G. Deshpande and X.G. He, *Phys. Lett.* **B 336** (1994) 471.

[11] M. Bander, D. Silverman and A. Soni, *Phys. Rev. Lett.* **43** (1979) 242.
M. Gronau *et al.*, *Phys. Rev.* **D 50** (1994) 4529.

[12] K. Berkelman, *Hadronic Decays*, in *B Decays* ed. by S. Stone, World Scientific, Singapore 1992.

[13] A.V. Dobrovolskaya *et al.*, *Phys. Lett.* **B 229** (1989) 293.

[14] J. Swain, *Multiplicity distributions in* $b \to sgluon$ *Decays*, Northeastern University Preprint NUB-3101 (1995), hep-ph-9501415.

[15] P. Abreu,...,M. Battaglia *et al.*, *Zeit. Phys.* **C 72** (1996), 207.

[16] D.M. Asner *et al.*, CLEO CONF 95-7.

[17] A. Lenz, U. Nierste and G. Ostermayer, *Determination of the CKM angle* γ *and* $|V_{ub}/V_{cb}|$ *from inclusive direct CP asymmetries and branching ratios in charmless B decays*, DESY 97-208.

[18] R. Ammar *et al.*, *Phys. Rev. Lett.* **71** (1993) 674.

[19] R. Godang *et al.* (CLEO Collaboration), *Phys. Rev. Lett.* **80** (1998), 3456.

[20] M. Ciuchini *et al.*, *Phys. Rev.* **B 388** (1996), 353 and
Erratum, **B 393** (1997), 489.

[21] G. Buchalla *et al.*, *Hadronization of* $b \to c\bar{c}s$, FERMILAB-PUB-95/167-T and I. Dunietz *et al.*, *Large Charmless Yeld in B decays and Inclusive B Decay Puzzles*, FERMILAB-PUB-96/421-T.

[22] M. Neubert, *Nucl. Phys. Proc. Suppl.* **59** (1997), 101.

[23] A.L. Kagan, *Phys. Rev.* **D 51** (1995), 6169 and
A.L. Kagan and J. Rathsman, *Hints on Enhanced* $b \to sg$ *from Charm and Kaon Counting*, hep-ph 9701300 (1997).

[24] T. Browder *et al.*, *Observation of High Momentum* η' *Production in B Decay*, CLNS 98/1544 to appear in *Phys. Rev. Lett.*.

[25] D. Atwood and A. Soni, *Phys. Lett.* **B 405** (1997), 150.

[26] A. Kagan and A.A. Petrov, η' *production in B decays: Standard Model vs. New Physics*, UCHEP Preprint 27 and hep-ph/9707354.

[27] M. Battaglia, *Study of the Inclusive* $b \to c\bar{c}s$ *and* $b \to sg$ *Transitions with the DELPHI detector at LEP*, DELPHI 97-80 CONF 66, contributed paper to the *EPS-97 Conference*, Jerusalem (Israel), August 1997.

[28] P. Abreu,..., M. Battaglia *et al.* (DELPHI Collaboration), Phys. Lett. **B 426** (1998), 193.

[29] P. Avery *et al.* (CLEO Collaboration), *Charged Particle Multiplicity in B Meson Decay*, CLEO-CONF 96-28.

[30] H. Albrecht *et al.* (ARGUS Collaboration), *Z. Phys* **C62** (1994), 371.

[31] T. Sjostrand, *Comp. Phys. Comm.* **82** (1994), 74.

[32] A.L. Kagan and T. Sjostrand, private communications.

[33] M.S. Alam *et al.*, Phys. Rev. Lett. **74** (1995), 2885.

[34] A. Ali, C. Greub, *Photon Energy Spectrum in* $B \to X_s + \gamma$ *and Comparison with Data*, SLAC-PUB-6940.

[35] P. Abreu,...,M. Battaglia *et al.*, *Phys. Lett.* **B 426** (1998), 193.

[36] L. Gibbson *et al.* (CLEO Collaboration), *Phys. Rev.* **D 56** (1997), 3783.

[37] K. Abe *et al.* (SLD Collaboration), SLAC-PUB-7896, contributed paper 183 to the *ICHEP-98 Conference*, Vancouver B.C. (Canada), July 1998.

[38] T.E. Koan *et al.* (CLEO Collaboration), *Flavour-Specific Inclusive B Decays to Charm*, Cornell Preprint CLNS 97/1516 and CLEO 97-23.

Chapter 5

Radiative and Dineutrino Charmless b Decays

5.1 $b \rightarrow s\gamma$ Decays

The radiative decay $b \rightarrow s\gamma$ has recently been the focus of much interest from both theory and experiments. This decay proceeds through a one-loop penguin process, similar to the one contributing to the hadronic modes, in which a photon is radiated from either the W^- or the quark line (see Figure 5.1). The rate for this decay has been computed in the Standard Model

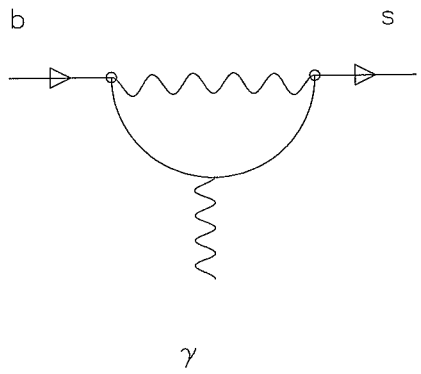

Figure 5.1: *Diagram of the penguin loop $b \rightarrow s\gamma$ transition*

including next-to-leading order QCD corrections as $BR(\ b \rightarrow s\gamma\ ) = (3.3 \pm 0.3) \times 10^{-4}$ [1]. Additional contributions can come from new particles in the loop, such as charged Higgs bosons or supersymmetric particles. This contribution can either enhance or decrease the $b \rightarrow s\gamma$ decay rate compared with the Standard Model expectation as discussed in details at the end of this chapter.

Evidence for $b \rightarrow s\gamma$ decays was reported by CLEO both in the exclusive channel $B \rightarrow K^*(892)\ \gamma$ [2] and in the inclusive mode [3] (see Figure 5.2). The inclusive analysis has been recently updated [4] giving $BR(b \rightarrow s\gamma)$ of $(3.15 \pm 0.54) \times 10^{-4}$, in good agreement with the Standard Model expectation. Searches for radiative charmless decays have already been performed at LEP by the ALEPH [5], DELPHI [6] and L3 [7] experiments.

In this chapter the results of the analysis of the DELPHI data, recorded at LEP from 1991 to 1994 are presented [8]. Radiative charmless decays were searched in both the inclusive $b \to s\gamma$ and the exclusive $B_d^0 \to K^{*0}\gamma$ channels. The $b \to s\gamma$ analysis uses an inclusive algorithm to reconstruct the hadronic system accompanying the photon in the decay of the B hadron. This method minimizes the dependence of the result on the size of the contribution from the individual exclusive decay channels and improves the rejection of charmed decays of the B hadron with an energetic photon or π^0. For the search of fully reconstructed exclusive decays two different procedures were followed and the results were combined. In the first one the events reconstructed using the inclusive algorithm were checked for the hypothesis of being fully reconstructed decays. The second analysis used a dedicated exclusive reconstruction procedure similar to the one used for the study of the charmless hadronic decays. After a description of the analysis technique and the results obtained, their implications on extensions of the Standard Model are also discussed.

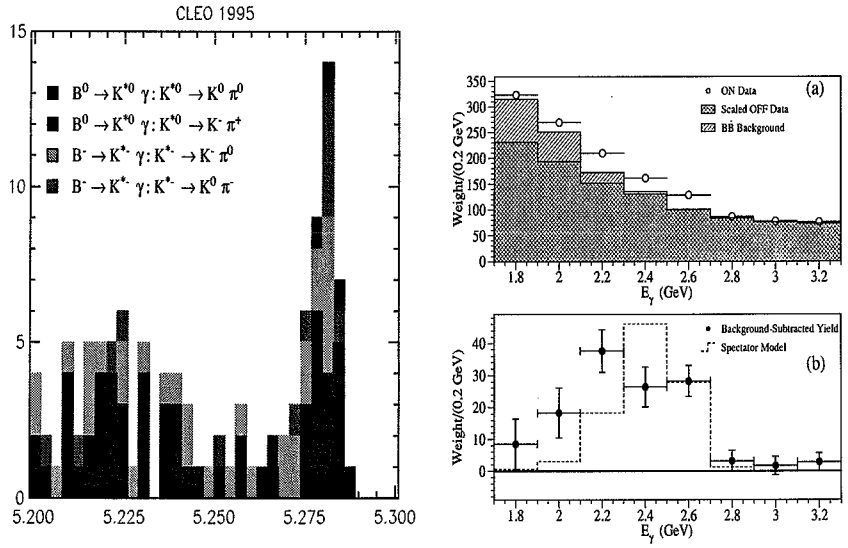

Figure 5.2: *The signal for $b \to s\gamma$ decays obtained by the CLEO experiment at the CESR storage ring for the exclusive (left) and the inclusive (right) channel [9]*

5.1.1 Data Analysis

Hadronic events satisfying with a probability from the impact parameter b-tagging below 0.01, a neutral electromagnetic shower reconstructed in the HPC calorimeter having an energy larger than 6 GeV and an energy component transverse to the jet axis E_t above 0.7 GeV were selected. Neutral pions were rejected by discarding all photons giving an invariant mass smaller than 0.25 GeV/c^2 when paired with another photon or by the shape of the electro-magnetic showers as described in chapter 2. The accompanying hadronic system was reconstructed using an inclusive procedure. Candidate secondary particles were selected among those contained in a cone of 0.7 rad around the photon direction and having a momentum larger than 1 GeV/c. Pairs of charged particle tracks, sorted in decreasing order of significance of their impact parameters with respect to the primary vertex, were iteratively tested for forming a common detached vertex. Vertices having low probability or a flight distance smaller than 0.5 times the associated error were

discarded. When a vertex was accepted, other charged particle tracks and reconstructed neutral pions and kaons, sorted in decreasing order of rapidity, were tested for inclusion. Charged particles compatible with the vertex position and neutrals with rapidity larger than 1.5 were added, provided the total invariant mass of the hadronic system and the photon did not exceed 6 GeV/c^2. No more than one neutral pion and one neutral kaon were associated to a vertex. Events with at least two particles selected in addition to the photon, a minimum mass of the hadronic system larger than the K^0 mass and a minimum total energy of 15 GeV, of which at least 5 GeV came from hadronic particles, were accepted. A study of simulated $b \to s\gamma$ events showed that on average 70 % of the selected particles were genuine B decay products.

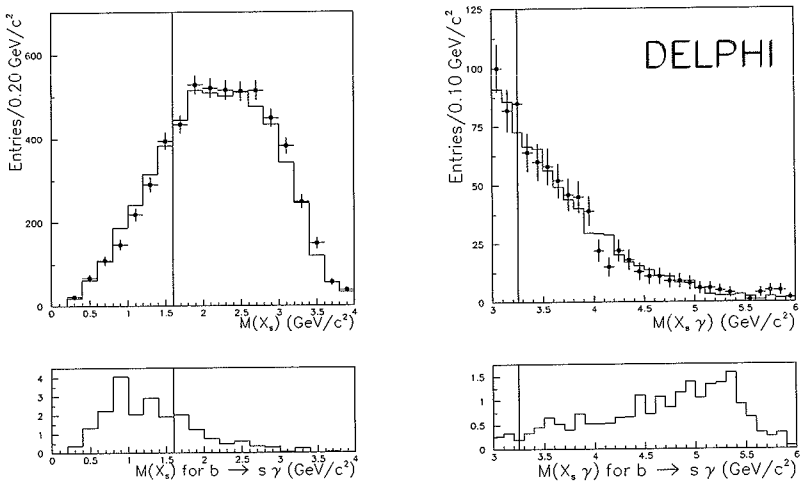

Figure 5.3: *The mass for the hadronic system X_s (upper left) and the total system $X_s\gamma$ (upper right) reconstructed using the inclusive algorithm for real and simulated b-tagged events. The same variables are plotted below for simulated $b \to s\gamma$ events. The horizontal lines correspond to the cuts applied in the analysis.*

Candidate events were selected by further requiring the total invariant mass to be between 3.25 GeV/c^2 and 6.0 GeV/c^2 and the mass of the selected hadronic system to be below 1.6 GeV/c^2 (see Figure 5.3). The dominant background is due to $b \to c$ decays with a misidentified π^0 or an energetic photon. The cut on the mass of the hadronic system removes the large fraction of this background, while it retains most of the signal, since the predicted invariant mass distribution of the hadronic system in $b \to s\gamma$ decays peaks below 1.5 GeV/c^2 [10].

The energy of the B hadron was estimated by scaling the sum of the energies of the selected particles and of the photon by the ratio of the total visible mass to the B meson mass. This procedure resulted in an energy resolution of about 7 % for the selected signal events.

Events with a scaled energy above 20 GeV were retained and the reconstructed photon was boosted into the B rest frame. At first approximation the two-body $b \to s\gamma$ decay gives a mono-energetic photon in this rest frame corresponding to the energy $E^{*max} = (m_b^2 - m_s^2)/(2\ m_b) \simeq 2.4$ GeV. The QCD corrections add a smearing to the photon energy spectrum due to gluon and photon emission. The detailed shape of the photon spectrum in $B \to X_s\gamma$ is not calculable from first principles. A fully inclusive spectator computation based on a B meson

wave function model was used [10, 11]. The photon energy spectrum at the partonic level $\frac{d\Gamma_b}{d\Gamma_\gamma}$ was obtained including gluon bremstrahlung and higher order radiative effects. The B meson was described by the Fermi motion model consisting of a b quark and a spectator q quark. In the wave function $\phi(p)$ the b quark has a Gaussian momentum distribution inside the meson with a width determined by the parameter p_F. The photon energy spectrum in the B meson rest frame is expressed in terms of the photon energy spectrum for the b quark decaying in flight as:

$$\frac{d\Gamma}{dE_\gamma} = \int_0^{p_{max}} \frac{d\Gamma_b}{d\Gamma_\gamma}(W(p), p, E_\gamma)\phi(p)p^2 dp \tag{5.1}$$

where W(p) is the momentum dependent b quark mass defined by: $W(p) = m_B^2 + m_q^2 - 2m_B\sqrt{p^2 + m_q^2}$. The input parameter values chosen were $m_B = 5.279$ GeV/c^2 and $p_F = 0.27$ GeV/c, while the spectator quark mass m_q was set to zero. These assumptions correspond to a value for the effective b quark mass of 4.97 GeV/c^2. The resulting photon spectrum is shown in Figure 5.4 together with the same spectrum after folding the detector effects.

In the simulation of the signal events, the branching ratios for the different K^* states were taken from the same model [12] except for the $K^*(892)$ for which the central value of the CLEO measurement [3] of $BR(B \to K^*(892)\gamma)/BR(B \to s\gamma) = 0.19$ was used. In addition 27% of the radiative decays were allowed to produce multi-body final states for which the JETSET fragmentation scheme was used [13]. The accuracy of the determination of the photon energy in the B rest frame E^* was studied using simulated $b \to s\gamma$ events. The resolution function was extracted from the difference between the values of reconstructed and generated E^* after all the selection cuts. This resolution function is well described by the sum of two gaussian distributions having σ widths of 40 MeV and 110 MeV with the narrower of the two distributions containing 40 % of the decays (see Figure 5.4). Using this simulation, the efficiency for the above reconstruction

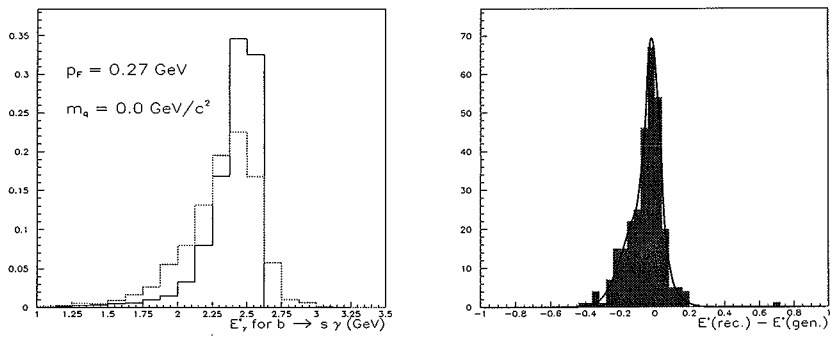

Figure 5.4: *Left: The spectrum for the photon energy in the B rest frame from the model of Ali and Mannel [10, 11] with the parameters described in the text (solid line) and the same spectrum after folding the E^* resolution function (dashed line). Right: The difference between the generated and the reconstructed values of E^* for simulated $b \to s\gamma$ fulfilling all the selection cuts applied in the inclusive analysis. The curve superimposed represents the fitted parametrisation of the resolution function.*

procedure was found to be 0.043 ± 0.002. For comparison, the central value measured by the

CLEO collaboration for $BR(b \rightarrow s\gamma)$ corresponds to about 11 signal events reconstructed in the DELPHI data.

Exclusive radiative b decays were searched for in the channels:

- $B_d^0 \rightarrow K^*(892)^0\gamma$, $K^*(892)^0 \rightarrow K^-\pi^+$
- $B_s^0 \rightarrow \phi\gamma$, $\phi \rightarrow K^+K^-$

Two reconstruction algorithms were used. In the first the events reconstructed for the $b \rightarrow s\gamma$ analysis were further selected by taking those for which the hadronic system was consistent with $K^*(892)^0 \rightarrow K^-\pi^+$ ($\phi \rightarrow K^+K^-$) and the $K\pi\gamma$ ($KK\gamma$) mass corresponded to the B meson mass. Candidate events where selected in the mass region 4.9 GeV/c^2 < M($K\pi\gamma$) < 5.7 GeV/c^2 and 5.0 GeV/c^2< M($KK\gamma$) < 5.8 GeV/c^2. A second analysis looked for displaced secondary $K\pi$ (KK) vertices associated with an energetic photon. This procedure profited from the clear signature of a charged kaon tagged by either the RICH detector or the dE/dx of the TPC emitted in a cone of 0.7 rad around the photon direction. The candidate kaon was tested to form a displaced secondary vertex with all other tracks having momenta above 1.0 GeV/c. Pairs having an invariant mass compatible with that of the $K^*(892)^0$ or ϕ meson were associated with the photon and the total mass of the $K\pi\gamma$ ($KK\gamma$) system was computed. The selection criteria were similar to those of the $b \rightarrow s\gamma$ analysis for the photon and to those of the hadronic charmless decays for the charged particles. The photon was required to have more than 6 GeV, the momentum of the tagged kaon had to be above 3.5 GeV/c and the sum of the photon and K^* energy had to exceed 25 GeV. The mass resolution obtained from simulated signal events was 0.25 GeV/c^2 for both the analyses. The efficiency was computed with fully simulated $B^0 \rightarrow K^*$ (ϕ) γ events. Taking into account the fraction of signal events tagged by both procedures, the total efficiency is 0.076 $\pm$ 0.008 (0.075 $\pm$ 0.010). Using this efficiency, the central value of the CLEO measurement of $BR(B \rightarrow K^*\gamma) = (4.0 \pm 1.0) \times 10^{-5}$ [2] corresponds to 2 fully reconstructed decays from the DELPHI data sample.

5.1.2 Inclusive $b \rightarrow s\gamma$

The fraction of inclusive $b \rightarrow s\gamma$ candidates selected in real data by these cuts was extracted by a fit to the shape of the spectrum of the boosted photon energy. The signal was described by the predicted photon spectrum described above smeared with the resolution function obtained using simulated signal events. The background was modelled using fully simulated hadronic events not containing $b \rightarrow s\gamma$ decays and fulfilling the same cuts as the real data. No excess of events in real data was observed and the fit gave 1.0 $\pm$ 11.8 signal events or BR($b \rightarrow s\gamma$) = (0.2 $\pm$ 2.5) $\times$ 10^{-4} (Figure 5.5).
This corresponds to an upper limit of 20.1 events at 90 % confidence level or $BR(\ b \rightarrow s\gamma\ )$ of 4.4 $\times$ 10^{-4}. The ratio of events selected in real and simulated data in the full spectrum of E^* was 1.03 $\pm$ 0.06. In the signal enriched region, defined by 2.25 < E^* < 3.00 GeV, 84 $\pm$ 9 events were found in real data with 91 $\pm$ 4 expected from simulation. The stability of this result changing the selection criteria was studied. In particular relaxing the b-tagging cut to 0.03, as for the other analyses, gave 5.0 $\pm$ 12.6 signal events or BR($b \rightarrow s\gamma$) = (1.0 $\pm$ 2.5) $\times$ 10^{-4} corresponding an upper limit of 5.2 $\times$ 10^{-4}. Making the b-tagging requirement tighter by cutting at 0.001 gave an upper limit of 4.6 $\times$ 10^{-4}. The cut on the minimum energy of the photon candidates was moved to 5 and 8 GeV, this did not change the result of the fit.

In the region 2.25 < E* < 2.60 GeV, where the signal to background ratio is more favourable, the main background is due to $B \rightarrow D^{(*)}\pi^0X$ decays and $q\bar{q}\gamma$ events. The branching ratios for the two-body $B \rightarrow D^{(*)}\pi^0$ were tuned in the simulation in order to agree with the present world averages [15]. Their uncertainty was included in the effect of the systematic errors. The inclusive π^0 background was checked by repeating the analysis selecting π^0 candidates instead of photons.

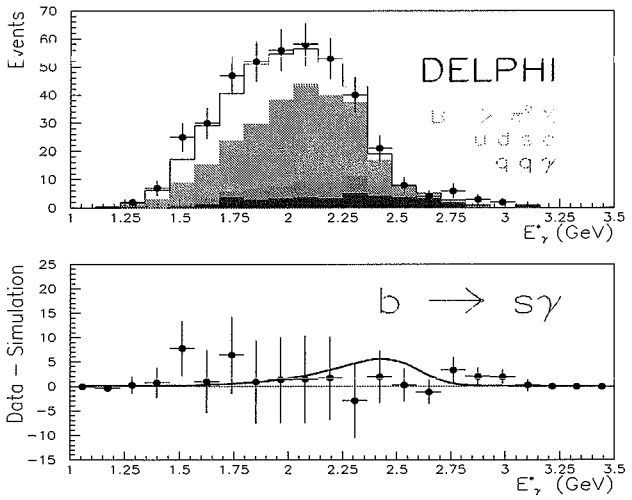

Figure 5.5: *Energy spectrum of the selected photons in the rest frame of the B meson. Real data and background from simulation are shown in the upper plot with the main background components highlighted. The data points after background subtraction are plotted below. The curve superimposed corresponds to the expected distribution for signal $b \to s\gamma$ events normalised to the number of events corresponding to the 90 % confidence level upper limit obtained from the fit.*

The shape of the E^* distribution for real data was found to be reproduced by simulation. In the region 2.25 GeV < E* < 2.60 GeV there were 101 ± 10 events in real data compared with 106 ± 5 expected from simulation. The ratio of the number of $q\bar{q}\gamma$ events in real data to the one in the simulation was estimated by a fit to the distribution of E_t/E for the selected photons . The $q\bar{q}\gamma$ events are characterised by a broad distribution of E_t/E extending to large values while other processes, including $b \to s\gamma$, are peaked at E_t/E below 0.35. An excess of events at E_t/E above 0.45 was present in real data. From the result of a fit leaving the fraction of $q\bar{q}\gamma$ events free, the ratio of $q\bar{q}\gamma$ events in the data to that in the simulation was found to be compatible with 1.0 with an error of 0.25. Changing this ratio from 1.00 to 1.25 would give $-7\pm$ 14 signal events, compatible with zero and thus with the present result. Lowering this ratio to 0.75 gives 5.3 ± 13.5 signal events corresponding to an upper limit of 5.7×10^{-4}.

The sensitivity of the upper limit to the predicted shape of the E^* distribution for $b \to s\gamma$ events was also studied by varying the value of p_F from 0.27 GeV/c, obtained from an analysis of the B semi-leptonic decay [16], to 0.45 GeV/c that gives the best fit to the photon spectrum obtained by CLEO [11]. The change in the value of p_F increases the smearing of the photon spectrum. The upper limit derived with the new value for p_F increased to 5.0×10^{-4}.

Several sources of systematic errors were taken into account. The resolution function, the absolute normalisation of real to simulated data, the reconstruction efficiency and the branching ratios for $B \to D^{(*)}\pi^0$ were changed within their uncertainties. The convolution of the changes in the fitted number of signal events was propagated to obtain the upper limit in presence of systematic errors. The final result was:

$$\mathrm{BR}(b \to s\gamma) < 5.1 \times 10^{-4}.$$

This result is compatible with the Standard Model expectations for $\mathrm{BR}(b \to s\gamma)$ and the results reported by the CLEO Collaboration.

5.1.3 Exclusive $B^0 \to K^*\gamma$, $\phi\gamma$

For the exclusive decay modes in the real data there are two events in the signal mass region with an expected background of 0.66 ± 0.17 events for the $K^{*0}\gamma$ mode (Figure 5.6). This corresponds

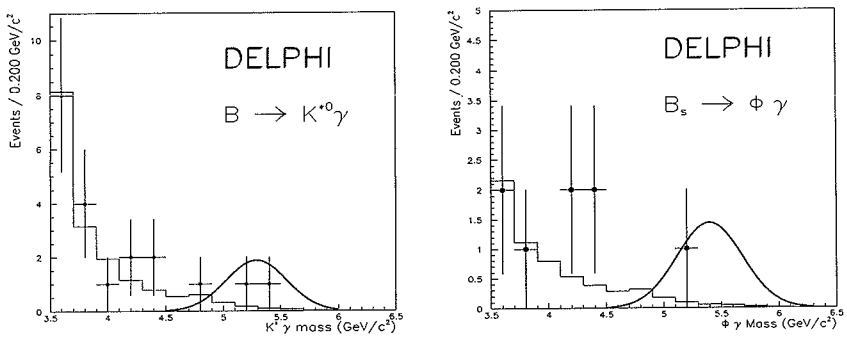

Figure 5.6: *The mass distribution for the $(K^+\pi^-)_{K^{*0}}\gamma$ (left) and $(K^+K^-)_\phi\gamma$ system. The curves represent the expected distributions for fully reconstructed $B^0_d \to K^{*0}\gamma$ and $B^0_s \to \phi\gamma$ decays normalised to the 90 % upper limit obtained for the number of signal events.*

to a probability for a background fluctuation of 0.14. Therefore no significant excess of events was observed and the upper limit on the number of signal events of 4.7 was derived at 90 % confidence level corresponding to $\mathrm{BR}(B^0_d \to K^*(892)^0\ \gamma) < 1.8 \times 10^{-4}$. The ratio of events in real and simulated data in the mass region from 3.5 GeV/c^2 to 6.5 GeV/c^2, excluding the signal region, was found to be 1.13 ± 0.30. This result was cross-checked by performing a fit to the spectrum of the photon energy in the B rest frame as was done for the inclusive $b \to s\gamma$ analysis. The fit gave $\mathrm{BR}(B^0_d \to K^*(892)^0\ \gamma) = (7.8 \pm 6.8) \times 10^{-5}$ that corresponds to an upper limit at 90 % confidence level compatible with the one obtained above. After including the effect of the systematic uncertainties on the background estimate and of the reconstruction efficiency, the final result is:

$$\mathrm{BR}(B^0_d \to K^*(892)^0\ \gamma) < 2.1 \times 10^{-4}.$$

For the $\phi\gamma$ mode there is one candidate selected in real data with an estimated background of 0.35 ± 0.13 events (see Figure 5.6). No excess of events was seen and the upper limit for the decay branching ratio was found to be:

$$\mathrm{BR}(B^0_s \to \phi\ \gamma) < 7.0 \times 10^{-4}.$$

at 90 % confidence level and including systematic uncertainties.

$$B_d^0 \to K^*(892)^0\gamma,\ K^{*0} \to K^+\pi^-$$

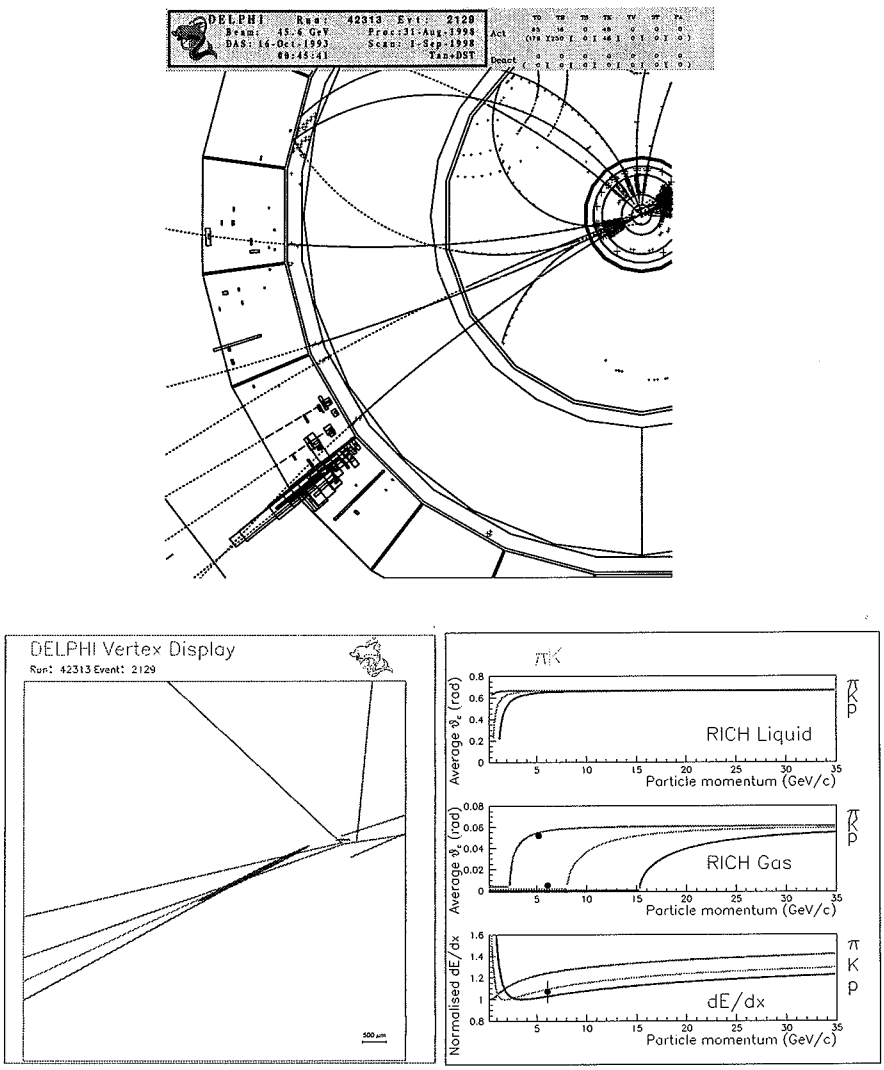

Figure 5.7: *Display of a fully reconstructed radiative decay* $B_d^0 \to K^*(892)^0\gamma$, $K^{*0} \to K^+\pi^-$ *candidate with a magnification of the vertex region and the hadron identification response for the two charged particles originating at the secondary vertex.*

5.2 Dineutrino charmless decays

Like the radiative $b \to s\gamma$ decays, $b \to sl\bar{l}$ decays with $l = e, \mu, \nu$ have also received considerable theoretical attention [21, 22, 23]. From the theoretical point of view, dineutrino decays $b \to s\nu\bar{\nu}$ are simpler to treat than other classes of rare decays involving dileptons, such as $b \to s\mu^+\mu^-$, and therefore the rates predicted in the Standard Model are subject to smaller uncertainties. The estimated rate for $b \to s\nu\bar{\nu}$ is in the range $0.4 - 1.0 \times 10^{-4}$ for $m_{top} = 180$ GeV/c^2 with about 30 % of the inclusive rate going through $B \to K^* \nu\bar{\nu}$ [23, 25]. Analogously to $b \to s\gamma$ decays, the rate for this decay can be modified by the contribution of new particles in the loop. In addition it has recently been pointed out that a new $U(1)$ gauge boson X, coupling predominantly to third family fermions, can give a large increase of the rate $b \to s\nu_\tau\bar{\nu}_\tau$ produced by tree level X boson exchange [24]. For specific combinations of the X boson mass M_X, its coupling g_X and the $Z - X$ mixing angle, this rate can become as large as the b semi-leptonic decay rate.

At LEP this process can be searched for in exclusive decays consisting of a secondary strange particle accompanied by large missing energy due to the presence of the two neutrinos. At LEP energies, the decay products of the two b quarks are contained in opposite hemispheres. This is essential for tagging the presence of a beauty hadron decaying into $s\nu\bar{\nu}$ using the missing energy. To suppress the large backgrounds from partially reconstructed s, c and b decays, the analysis was performed using the exclusive final states $K^*\nu\bar{\nu}$ and $\phi\nu\bar{\nu}$. The cuts on the invariant mass of the strange mesons and the secondary vertex reconstruction reduce the combinatorial and other backgrounds.

5.2.1 Event reconstruction

Hadronic events satisfying the b-tagging criteria were selected as in the two previous analysis. The $b \to s\nu\bar{\nu}$ decays were searched for in the exclusive channels:

- $B_d^0 \to K^*(892)^0\nu\bar{\nu}$, $K^*(892)^0 \to K^+\pi^-$
- $B_s^0 \to \phi(1020)\nu\bar{\nu}$, $\phi(1020) \to K^+K^-$.

The reconstruction started with an identified charged K having momentum larger than 3.5 GeV/c. Oppositely charged particles belonging to the same jet and having momentum above 1 GeV/c were tested for forming a common vertex with the charged kaon. Vertices with a low fit probability or a decay distance with respect to the primary vertex normalized to its error below 2.5 were rejected. Pairs having $K\pi$ invariant mass between 0.80 GeV/c^2 and 1.00 GeV/c^2 and K K invariant mass between 1.00 GeV/c^2 and 1.04 GeV/c^2 respectively were taken as $K^*(892)^0 \to K^+\pi^-$ and $\phi(1020) \to K^+K^-$ candidates.

The characteristics of signal $B \to K^*$ (ϕ) $\nu\bar{\nu}$ were studied on fully simulated events. For this simulation the JETSET event generator was used and events were reweighted in order to reproduce the predicted mass distribution of the $\nu\bar{\nu}$ system [23]. Signal $b \to s\nu\bar{\nu}$ events can be separated from most of the background sources by using the energy detected in the hemisphere. The visible energy E_{vis} in the hemisphere containing the strange meson candidate was determined as the sum of the energy in charged particles E_{cha}, in electromagnetic showers measured in the HPC calorimeter E_{HPC} and in neutral hadrons detected by the hadron calorimeter E_{HCAL}. The missing energy was defined as $E_{miss} = E_{hem} - E_{vis}$. The total energy in the hemisphere E_{hem} was determined imposing four-momentum conservation and it is given by $E_{hem} = E_{beam} - (M_{oh}^2 - M_{sh}^2)/(4E_{beam})$ where E_{beam} is the beam energy and M_{sh}, M_{oh} the invariant mass of the same and of the opposite hemisphere with respect to the strange particle candidate. The resolution on the missing energy can be parametrised by a Gaussian distribution with a resolution σ of 5 GeV and a wider component extending to larger values

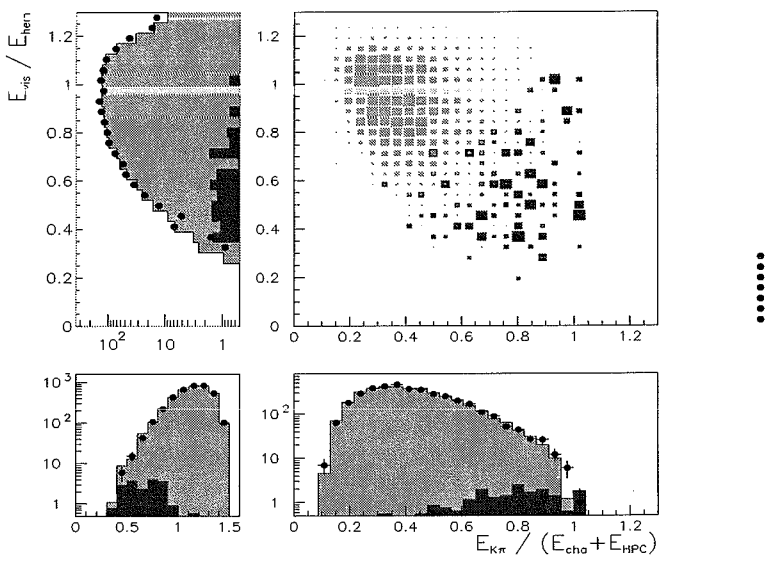

Figure 5.8: *Distributions for the E_{vis} / E_{hem} (upper left) and $E_{K\pi}$ / (E_{cha} + E_{HPC}) (lower right) variables used in the search for dineutrino charmless B decays. The angular variable α used to select the signal enriched region is in the left lower plot. Real data and background from simulation are shown with dots and the light grey histogram while the expected distributions for signal $B \rightarrow K^{*0}\nu\bar{\nu}$ events is described by the dark grey histograms.*

of missing energy. Signal events are characterized by a large missing energy corresponding to a low value of E_{vis}/E_{hem} and a large fraction of the energy in charged hadrons and photons taken by the strange meson candidate. Semi-leptonic decays of either b or c quarks can also give large missing energy due to the emission of a neutrino and therefore represent a potential source of background. These events were removed by rejecting all $K^+\pi^-$ and K^+K^- pairs having a tagged lepton in the same hemisphere. Events for which the missing momentum vector points outside the barrel region were rejected since the missing energy is likely to be due to neutrals outside the acceptance of the calorimeters. Events were also rejected if the invariant mass of the hemisphere containing the strange meson was above 10 GeV/c^2 since signal $b \rightarrow s\nu\bar{\nu}$ are characterised by a low jet mass due to the missing neutrinos.

5.2.2 Results

To separate possible signal candidates from the bulk of the background, the variable α describing the position of each selected entry in the $E_{K^*}/(E_{cha}+E_{HPC})$, E_{vis}/E_{hem} plane was defined (see Figure:5.8). For the events in the signal enriched region corresponding to α below 0.9 a binned likelihood fit to the $K\pi$ (KK) invariant mass distribution was performed to extract the number of events containing a K^* or ϕ strange meson resonance.

In real data 70 $\pm$ 18 (97 $\pm$ 16) events with a K^* (ϕ) were seen with an expected background of K^* (ϕ) from other processes of 76 $\pm$ 7 (94 $\pm$ 6) (see Figure 5.9). This corresponds to a 90

Table 5.1: Summary of the 90 % C.L. upper limits for dineutrino decays.

Channel	Evts	Bkg.	ϵ [%]	Signal Event UL	Theory BR$\times 10^5$		DELPHI BR$\times 10^5$
$B_d^0 \to K^{*0}\nu\bar{\nu}$	70	76	0.09	<32	1.0-3.0	[23, 25]	<97
$B_s^0 \to \phi\nu\bar{\nu}$	97	94	0.07	<30	-		<490

% confidence level upper limits for the number of signal events of 32 and 30. A study of the simulated signal sample showed that 0.09 $\pm$ 0.007 (0.07 $\pm$ 0.01) of signal $K^*\nu\bar{\nu}$ ($\phi\nu\bar{\nu}$) events satisfy these selection criteria. The following upper limits were derived (Table 8):

$$BR(B_d \to K^*\nu\bar{\nu}) \ < 9.7 \times 10^{-4}$$

and

$$BR(B_s \to \phi\nu\bar{\nu}) \ < 4.9 \times 10^{-3}.$$

The agreement between the data and the Monte Carlo in describing the background was verified. The ratios of the events in real data and simulation in the region of α above 0.9 is 1.02 $\pm$ 0.03 (0.95 $\pm$ 0.05) showing that the rejection factors of the selection cuts for real data are well reproduced by the simulation. Also the number of K^* and ϕ candidates obtained from the fits

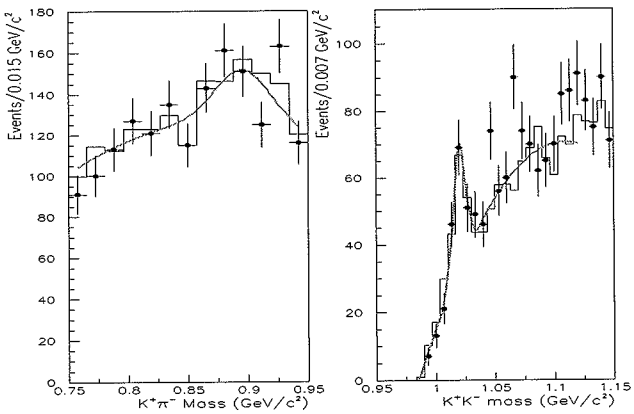

Figure 5.9: *The invariant mass distribution for $K^+\pi^-$ (left) and K^+K^- (right) pairs for events in the signal $b \to s\nu\bar{\nu}$ region of α below 0.9. The points with error bars show the distribution for real data and the histogram the one for simulation. The curves are the fits to the distributions used to extract the number of K^* and ϕ mesons in the real data.*

to the mass distributions in real data and simulation were found to be in agreement. Before applying the cut on the α angular variable, the ratios of these numbers were 1.00 $\pm$ 0.07 and 0.98 $\pm$ 0.07 for K^* and ϕ mesons respectively.

5.2.3 Conclusion

The analysis of the DELPHI data has revealed no excess of events with the signature expected for radiative charmless decays neither in the inclusive nor in its exclusive modes and of dineutrino decays. The exclusive analysis of radiative decays profited of the cleaner signature due to the full reconstruction of the B decay but its interpretation suffers of the large theoretical uncertainties in the estimate of the ratio $BR(B \to K^*\gamma)/BR(b \to s\gamma)$ [1, 12, 18, 19, 20]. The inclusive analysis, less sensitive to the description of the decay in terms of the exclusive $X_s\gamma$ final states, provides a result that can be directly compared with the predictions. The sensitivity of this search is close to the Standard Model value of 3.3×10^{-4} for the inclusive rate. The upper limit obtained of $BR(b \to s\gamma) < 5.1 \times 10^{-4}$ approaches also the 90 % exclusion limit of 4.1×10^{-4} implied by the updated CLEO result [4] and matches the 5.3×10^{-4} limit from the recent ALEPH result [5], thus confirming that the $b \to s\gamma$ decay does not exhibit any significant enhancement above the SM expectations. Their implications on the constraints on new physics beyond Standard Model are discussed in Chapter 6.

The first limits for the exclusive charmless dineutrino decays $B^0_d \to K^*\nu\bar{\nu}$ and $B^0_s \to \phi\nu\bar{\nu}$ have been obtained. They have been found to be less than 9.7×10^{-4} and 4.9×10^{-3} at 90 % confidence level. These limits have implications on models with an additional $U(1)$ gauge boson coupling predominantly to the third family as also discussed in Chapter 6.

Bibliography

[1] M. Chetyrkin, M. Misiak and M. Munz, *Phys. Lett.* **B 400** (1997), 206 and references therein.

[2] R. Ammar *et al.*, *Phys. Rev. Lett.* **71** (1993) 674 and
Idem et al., Radiative Penguin Decays of the B Meson, CLEO CONF 96-5, contributed paper to the ICHEP-96 Conference, Warsaw (Poland), August 1996.

[3] M.S. Alam *et al.*, *Phys. Rev. Lett.* **74** (1995) 2885.

[4] S. Glenn *et al.*, *Improved Measurement of BR($b \to s\gamma$)*, CLEO CONF 98-17, contributed paper to the ICHEP-98 Conference, Vancouver B.C. (Canada), July 1998.

[5] R. Barate *et al.*, *Phys. Lett.* **B 429** (1998), 169.

[6] M. Battaglia, in *Proceedings of the 5^{th} Int. Symp. on Heavy Flavour Physics*, edited by D.I. Britton, D.B. MacFarlane and P.M. Patel, Edition Frontieres, 1993.

[7] O. Adriani *et al.*, *Phys. Lett.* **B 317** (1993) 637.

[8] M. Battaglia *et al.*, *Nucl. Instr. and. Meth. in Phys. Res.* **A371** (1996) and
P. Abreu, ..., M. Battaglia *et al. Zeit. Phys.* **C 72** (1996), 207.

[9] Courtesy of Karen Lingel (CLEO Collaboration).

[10] A. Ali and C. Greub, *Phys. Lett.* **B 259** (1991) 182.

[11] A. Ali and C. Greub, *Phys. Lett.* **B 361** (1995) 146.

[12] A. Ali *et al.*, *Phys.Lett.* **B 298** (1993) 195.

[13] T. Sjöstrand, *Comp. Phys. Comm.* **82** (1994) 74.

[14] A. Ali and C. Greub, private communication.

[15] C. Caso *et al.* (Particle Data Group), *Review of Particle Properties, Eur. Phys. J.* **C 3** (1998).

[16] M.S. Alam *et al.*, *Phys. Rev. Lett.* **74** (1995) 2885.

[17] A. Ali, W. Braun and H. Simma, *Z. Phys.* **C 63** (1994) 437.

[18] B. Holdom and M. Sutherland, UTPT-93-22.

[19] C.W. Bernard, P.F. Hsieh and A. Soni, BNL-45033.

[20] P. Colangelo et al., *Phys. Lett.* **B317** (1993) 183

[21] S. Bertolini *et al.*, *Nucl. Phys.* **B 353** (1991), 591.

[22] N.G. Deshpande and J. Trampetic, *Phys. Rev. Lett.* **60** (1988), 2583.

[23] A. Ali and T. Mannel., *Phys. Lett.* **B 264** (1991) 447.

[24] B. Holdom and M.V. Ramana, *Phys.Lett.* **B 365** (1996) 309.

[25] G. Buchalla and A.J. Buras, *Nucl. Phys.* **B 400** (1993) 225.

Chapter 6

Rare b Decays and New Physics beyond Standard Model

In the previous chapters results on rare B decays obtained in the analysis of the data collected by DELPHI at LEP have been presented. These results are summarised in Table 6.1 where recent experimental data from other experiments and the Standard Model expectations for the rates of the different processes are also given for comparison.

Table 6.1: *Summary of results on Rare B Decays compared with other measurements and SM predictions. The column Other Experiments lists the latest measurements available for the same branching ratios or the best limit reported.*

Channel	DELPHI Results	Other Experiments.	SM Prediction
$\|V_{ub}\|/\|V_{cb}\|$	0.104 ± 0.021	0.080 ± 0.020 (CLEO+ARGUS)	-
		0.080 ± 0.020 (CLEO Excl.)	-
		0.098 ± 0.024 (ALEPH)	-
		$0.159\ ^{+0.042}_{-0.058}$ (L3)	-
$B^0_{d,s} \to \pi^+\pi^-,\ K^+\pi^-$	$(2.8^{+1.5}_{-1.1}) \times 10^{-5}$	1.5 ± 0.5 (CLEO)	$1.1 - 1.8$
$B^0_d \to \pi^+\pi^-$	$< 4.5 \times 10^{-5}$	< 1.5 (CLEO)	$1.1 - 1.8$
$B^0_{d,s} \to K^+\pi^-$	$(2.4^{+1.7}_{-1.1}) \times 10^{-5}$	1.5 ± 0.5 (CLEO)	$1.1 - 1.8$
$B^-_u \to \pi^+\pi^-\pi^-$	$< 1.3 \times 10^{-4}$	< 0.5 (ALEPH)	0.6
$B^-_u \to K^-\pi^+\pi^-$	$< 3.3 \times 10^{-4}$	-	-
$B^0_d \to \pi^+\pi^-\pi^+\pi^-$	$< 2.3 \times 10^{-4}$	< 2.6 (ALEPH)	1.0
$B^0_{d,s} \to K^+\pi^-\pi^+\pi^-$	$< 2.3 \times 10^{-4}$	-	-
$b \to K/b \to \pi + K$	0.58 ± 0.18	0.54 ± 0.20 (CLEO)	-
$b \to s\gamma$	$< 5.1 \times 10^{-3}$	3.15 ± 0.54 (CLEO)	3.28 ± 0.33
		3.38 ± 1.13 (ALEPH)	
$B^0_d \to K^{*0}\gamma$	$< 2.1 \times 10^{-4}$	(0.4 ± 0.1) (CLEO)	-
$B^0_s \to \phi\gamma$	$< 7.0 \times 10^{-4}$	-	-
$B^0_d \to K^{*0}\nu\nu$	$< 9.7 \times 10^{-4}$	-	0.1 - 0.3
$B^0_s \to \phi\nu\nu$	$< 54. \times 10^{-4}$	-	-
$b \to sg$	$< 5.0 \times 10^{-2}$	< 8.2 (CLEO)	0.5-2.0
$b \to no\ charm$	$(0.7 \pm 2.1) \times 10^{-2}$	-	1.6 ± 0.8

The results obtained in the search for the $b \to s$ transitions are an important source of information on possible new physics beyond the Standard Model. New virtual particles may in fact contribute to the penguin loop graphs and thus to the inclusive rate of these processes. In this chapter these implications are reviewed. The upper limit obtained from $BR(b \to s\gamma)$ on the mass of a charged Higgs boson is discussed both in the context of an extension of the Standard Model with an additional Higgs doublet (2HDM) and in the Minimal Supersymmetric Standard Model (MSSM). The limits derived are compared with those obtained from direct searches at LEP 2 and at the Tevatron. Further constraints of Supersymmetric scenarios are derived from the results from $b \to sg$ and inclusive charmless b decays. Finally, the limits on the exclusive decays mediated by $b \to s\nu\nu$ dineutrino transitions are discussed in the framework of Standard Model extensions with an additional $U(1)$ gauge boson.

6.1 Limits on Charged Higgs Bosons from $b \to s\gamma$

Several extensions of the Standard Model introduce a Higgs sector made of two Higgs doublets [1] and are known as Two Higgs Doublet Models (2HDM). The two doublets can be expressed as:

$$\phi_1 = \begin{pmatrix} \phi_1^+ \\ \phi_1^0 \end{pmatrix} \quad \phi_2 = \begin{pmatrix} \phi_2^+ \\ \phi_2^0 \end{pmatrix} \quad <\phi_1> = \frac{e^{i\eta_1}}{\sqrt{2}} \begin{pmatrix} 0 \\ v_1 \end{pmatrix} \quad <\phi_2> = \frac{e^{i\eta_2}}{\sqrt{2}} \begin{pmatrix} 0 \\ v_2 \end{pmatrix} \tag{6.1}$$

with $v_1^2 + v_2^2 = v^2$ and $v = 246$ GeV. The ratio of the vacuum expectation values (VEV) is indicated with $\tan\beta = v_2/v_1$. The phase difference between the two VEV's $\eta = \eta_2 - \eta_1$ introduces direct CP violation if taken to be non zero. After the symmetry breaking, the Higgs sector contains five physical particles, with two scalars grouped in a doublet $\binom{H^+}{H^-}$.

The introduction of an extended Higgs sector can be motivated for explaining the quark mass pattern $m_t >> m_b$ in terms of a hierarcy in the vacuum expectations values of the two doublets $v_2 >> v_1$, and for introducing spontaneous CP violation. Further, it naturally arises in Supersymmetry to give mass to both *up*− type and *down*−type quarks. 2HDM extensions of SM can be made to satisfy the low energy phenomenology. The constrain $\rho = \frac{m_W^2}{m_Z^2 \cos^2\theta_W} \simeq 1$ is fulfilled if the Higgs sector contains only doublets and the absence of flavour changing neutral currents (FCNC) processes can be guaranteed by requiring that fermions of a given charge couple to a single Higgs doublet [2]. Therefore, in the definition of the models, *up* and *down* type quarks get masses by their coupling to either the same doublet (Model I) or the *up* quarks get masses from the first doublet a nd the *down* quarks from the second doublet (Model II). In these models, two of the Yukawa matrices are exactly zero and each of the non zero matrices is proportional to the mass matrix of either the *up* or the *down* quarks. Now since the quark mass matrices are diagonal, by definition, in the physical basis and the Yukawa matrix is proportional to the mass matrix, the off diagonal Yukawa couplings are zero. This holds at any energy scales and protects the model from developing FCNC couplings. In particular the 2HDM Model II is of special interest, since it is naturally realised in the Minimal Supersymmetric Standard Model extension (MSSM). In the general 2HDM model there are no constraints on the charged Higgs mass $m_{H^\pm}$ while in minimal Supersymmetry $m_{H^\pm} > m_{W^\pm}$.

The structure of the Higgs-fermion coupling $H^+ f_i^u f_j^d$, proportional to the fermion mass m_f and the relevant CKM element V_{ij} implies a possible phenomenology in low energy processes. The charged Higgs can contribute to the box diagrams responsible for the $B^0 - \bar{B}^0$ mixing and CP violation in the K^0 system. Rare b decays as $B \to \tau\nu(X)$ and $b \to s$ transitions may also receive possible large contributions from charged Higgs bosons. In particular, the existence of a charged Higgs particle increases the $b \to s\gamma$ rate through the corresponding SM penguin diagram where the $H^\pm$ replaces the $W^\pm$ in the loop. The addition of a charged Higgs boson does not

imply the appearence of new operators in the effective Hamiltonian discussed in Chapter 1 and its contribution can be absorbed in an appropriate redefinition of the relevant Wilson coefficients.

6.1.1 Two Higgs Doublet Model (2HDM)

In the case of the two Higgs doublet model II with Higgs mass m_H and ratio of the vacuum expectation values $\tan\beta = v_2/v_1$ for the two doublets, the $A_{\gamma,g}^{2HDM}$ coefficients in the effective Lagrangian due to the additional contribution from the $H^\pm$ exchange are [3]:

$$A_{\gamma,g}^{2HDM} = \frac{1}{2}\left(\frac{m_t}{m_H}\right)^2\left(\frac{1}{\tan^2\beta} f_{\gamma,g}^{(1)}\left(\frac{m_t^2}{m_H^2}\right) + f_{\gamma,g}^{(2)}\left(\frac{m_t^2}{m_H^2}\right)\right). \tag{6.2}$$

The contributions from the $W^\pm$ and the $H^\pm$ exchange to the $b \to s\gamma$ rate are shown in Figure 6.1 for different values of $\tan\beta$ fixing $m_t = 180$ GeV/c^2.

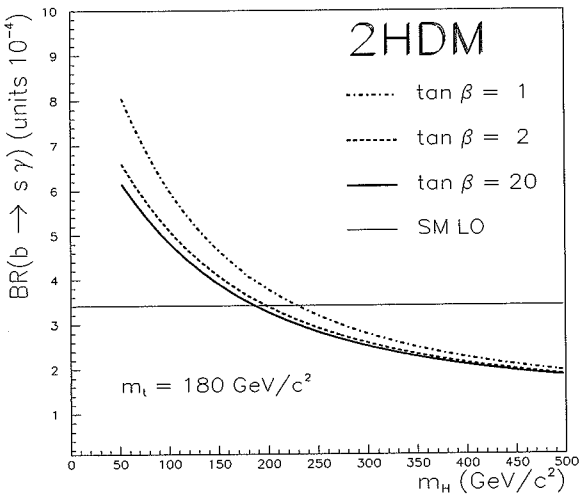

Figure 6.1: *The contribution from the virtual H emission to $BR(b \to s\gamma)$ in the 2HDM model as a function of the $H^\pm$ mass for different values of* $\tan\beta$. *The Standard Model value $BR(b \to s\gamma)_{SM}$ including the leading order QCD corrections is also shown for comparison.*

For $m_H < 300$ GeV/c^2 the Higgs contribution is important over a large range of $\tan\beta$ values and therefore the upper limit obtained for $BR(b \to s\gamma)$ can be translated in a lower limit on the $H^\pm$ mass. This is shown in Figure 6.2 where the upper limit at 90 % confidence level is shown as a function of m_H and $\tan\beta$. For large values of $\tan\beta$ the mass region $m_H < 200$ GeV/c^2 is excluded.

In the case of Model I the presence of a charged Higgs boson interfers with the W contribution and the resulting BR$(b \to s\gamma)$ is reduced at low $\tan\beta$ values while it approaches the SM prediction as $1/\tan^2\beta$.

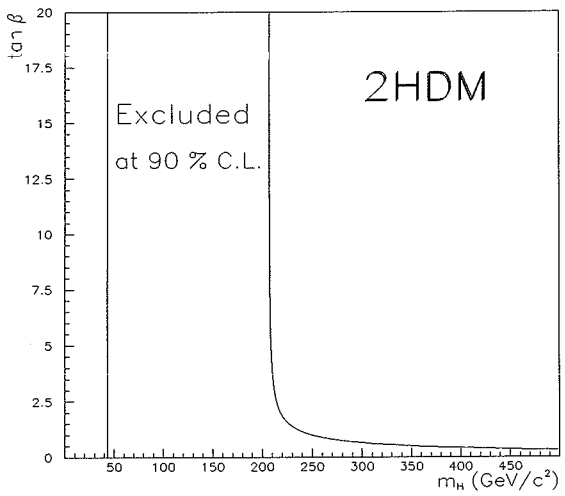

Figure 6.2: *Exclusion limit at 90 % confidence level in the m_H, $\tan\beta$ plane for the 2HDM Model II derived from the DELPHI upper limit $BR(b \to s\gamma) < 5.1 \times 10^{-4}$. The upper limit from the direct search for $H^{\pm}$ at LEP is also shown.*

6.1.2 Charged Higgs Bosons in MSSM

In the assumption that the dominant additional contribution to the penguin loop in the $b \to s\gamma$ transition is due to the virtual $H^{\pm}$ emission, results similar to those for the non supersymmetric 2HDM model can be derived. This generated a significant interests in the $b \to s\gamma$ transition as a sensitive test of the MSSM extending to a region of parameters complementary to the one accessible by the direct search at LEP 2 and at the LHC [4]. However, a detailed analysis of the effect of the other charged SUSY particles shows that the actual picture has to be modified and the constraints put by an analysis restricting only to the $W^{\pm}$ and $H^{\pm}$ graphs can be evaded in significant regions of the MSSM parameter space [5, 6, 7].

In fact, in the limit of exact supersymmetry all magnetic operators in the effective Hamiltonian vanish [8] and the rate for $b \to s\gamma$ is zero. Since SUSY is not an exact symmetry, $BR(b \to s\gamma)$ gets a non zero value due to the presence of supersymmetry-breaking terms [3]. Nevertheless the net contribution of supersymmetric particles to the loop is suppressed by large cancellation effects. This cancellation comes from loops with other supersymmetric particles replacing the $W^{\pm}$ and $H^{\pm}$ bosons. In the MSSM there are five different graphs mediating the $b \to s$ transition:

1. W boson emission: $b \to (W^{\pm}\ u, c, t) \to s$
2. H boson emission: $b \to (H^{\pm}\ u, c, t) \to s$
3. chargino emission: $b \to (\tilde{\chi}^{-}\ \tilde{u}, \tilde{c}, \tilde{t}) \to s$
4. gluino emission: $b \to (\tilde{g}\ \tilde{d}, \tilde{s}, \tilde{b}) \to s$ and
5. neutralino emission: $b \to (\tilde{\chi}^{0}\ \tilde{d}, \tilde{s}, \tilde{b}) \to s$.

The main contribution is due to the first three terms. The H emission adds always constructively to the W loop while the chargino contribution can have both signs. In particular for increasing values of $\tan\beta$, $BR(b \to s\gamma)_{MSSM}$ decreases. This is due both to the increasing value of m_H and thus to the suppression of the process 2) and to the fact that the chargino adds destructively to the loop for $\tan\beta > 10$, thus cancelling the $W^{\pm}$ contribution [6]. The picture can be simplified

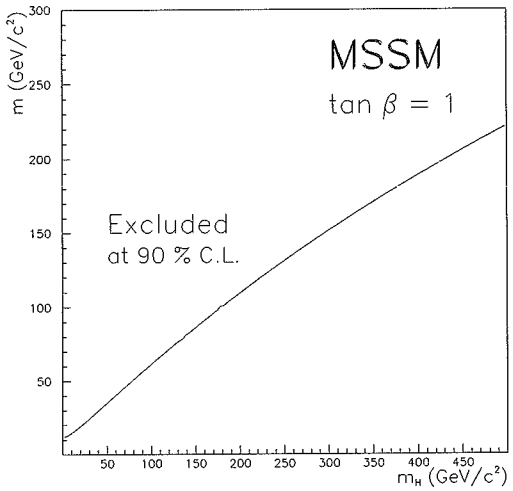

Figure 6.3: *Exclusion limit at 90 % confidence level in the m_H, $\tilde{m}$ plane for the MSSM model derived from the DELPHI upper limit $BR(b \to s\gamma) < 5.1 \times 10^{-4}$ for $\tan\beta = 1$ and the assumptions described in the text.*

with a limited set of additional assumptions, namely by taking: i) all squarks except the scalar partners of the top quark to be degenerate in mass to $m_{\text{squark}} = \tilde{m}$, ii) the two Higgs vacuum expectation values v_1 and v_2 to be equal giving $\tan\beta = 1$ and iii) the scalar top mass to be $m_{\tilde{t}}^2 = \tilde{m}^2 + m_t^2$ [3]. In this case the $A_{\gamma,g}$ coefficients in equation (6.2) can be written as a function of m_H and $\tilde{m}$ as:

$$A_{\gamma,g}^{MSSM} = \frac{3}{2}f_{\gamma,g}^{(1)} + \frac{y}{2}\Big(f_{\gamma,g}^{(1)}(y) + f_{\gamma,g}^{(2)}(y)\Big) + z\Big(f_{\gamma,g}^{(1)}(z) + \frac{1}{2}f_{\gamma,g}^{(2)}(z)\Big) - (2x+z)f_{\gamma,g}^{(1)}(x+z) - \frac{x+z}{2}f_{\gamma,g}^{(2)}(x+z) \tag{6.3}$$

with $x = \frac{m_t^2}{m_W^2}$, $y = \frac{m_t^2}{m_H^2}$, $z = \frac{\tilde{m}^2}{m_W^2}$. The limit of exact supersymmetry corresponds to vanishing values of $\tilde{m}$ or $z \to 0$ and $y \to x$ for which the equation exhibits complete cancellation. Away from this limit, the ratio $BR(b \to s\gamma)_{MSSM}/BR(b \to s\gamma)_{SM}$ can be either larger or smaller than one corresponding to the different sign and size of the Higgs and chargino contributions. Figure 6.3 shows the region of the $m_H, \tilde{m}$ plane excluded by the DELPHI result. The constraint becomes stronger for large values of $\tilde{m}$.

It can be pointed out that in the large $\tan\beta$ scenario the chargino loop effects become large and therefore it may dominate the $b \to s\gamma$ contribution from new physics. As the direct searches at LEP 2 are presently narrowing the available parameter space for MSSM solutions with small $\tan\beta$, increasing accuracy on $b \to s\gamma$ may reveal large $\tan\beta$ Supersymmetry.

6.1.3 Comparison with Limits from Direct Searches

*

The study of loop contributions to rare b decays provides with tight bounds on charged Higgs bosons. However these bounds are model dependent as their analysis in the case of SUSY models has shown. Direct searches complement this information with a more limited coverage of the mass spectrum but less model dependent results. Direct searches for charged Higgs bosons are being actively pursued both at LEP 2 and at the Tevatron.

At LEP, charged Higgs bosons can be produced in pairs in the process $e^+e^- \rightarrow H^+H^-$ for values of the Higgs mass $M_{H^\pm}$ up to $\sqrt{s}/2$. The production cross-section depends only on the Higgs mass, independently on its nature, as shown in Figure 6.4. The charged Higgs boson

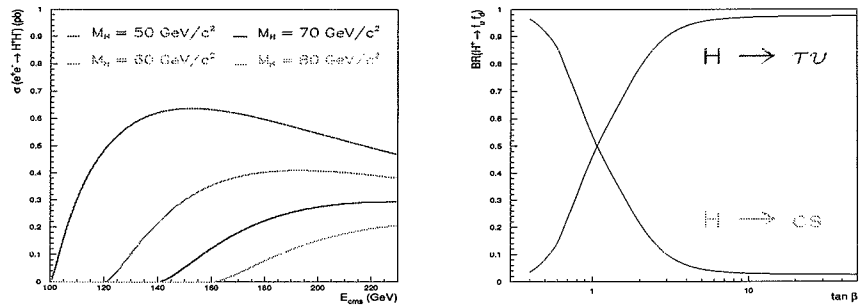

Figure 6.4: *The $H^\pm$ production cross-section as a function of the centre-of-mass energy for different values of the Higgs mass (left) and the decay branching ratios as a function of* $\tan\beta$ *in MSSM (right).*

predominantly couples to either $c\bar{s}$ or $\tau^+\nu$ fermion pairs, $\bar{b}c$ being suppressed by the small value of the $|V_{cb}|$ element and $t\bar{b}$ being kinematically forbidden for the mass values accessible at LEP 2. The relative contributions of the leptonic and hadronic channels depend on the value of $\tan\beta$ as shown in Figure 6.4 for the MSSM case. In the SUSY case, decays into supersymmetric particles are also possible but again they are not important for the mass region of interest. Searches for charged Higgs bosons have been performed by the four LEP experiments. In particular DELPHI has analysed the full LEP 2 data set recorded at $\sqrt{s} = 161$ GeV, 172 GeV and 183 GeV [9]. The main background for this search is represented by the $e^+e^- \rightarrow W^+W^-$ process that has a cross section about 60 times larger compared with that of H^+H^- production for $M_{H^\pm} = 60$ GeV/c^2 and $\sqrt{s} = 183$ GeV. Therefore efficient techniques have been developed to reject this background. They included the different distribution of production and decay angles for W and H and quark couplings. Since $|V_{ud}| \simeq |V_{cs}|$ the W boson couples equally to either $u\bar{d}$ or $c\bar{s}$ while the Higgs decays predominantly in the heavier fermion pair. Tagging of $c\bar{s}$ pairs in hadronic final states suppresses part of this background. The $c\bar{s}\bar{c}s$, $c\bar{s}\tau^-\bar{\nu}$ and $\tau^+\nu\tau^-\bar{\nu}$ final states have been analysed. No excess of candidates has been found compared to the expected backgrounds and this result has been expressed as the 95% C.L. lower mass limit as a function of BR($H^\pm \rightarrow$ *hadrons*) in Figure 6.5. A charged Higgs boson can be excluded, independently on its couplings, for mass values $M_{H^\pm} < 59$ GeV/c^2 at 95% C.L..

*The results presented in this section are being published in part in P. Abreu,...,M. Battaglia *et al.*, to appear *Phys. Lett.* **B**

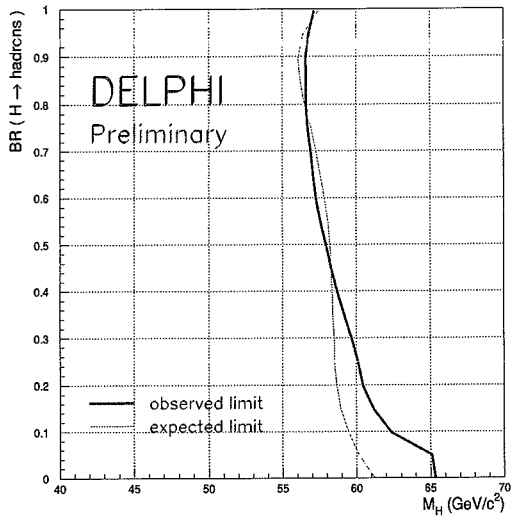

Figure 6.5: *The $H^{\pm}$ mass limits as a function of the Higgs hadronic decay branching ratio obtained from the analysis of the DELPHI data at LEP 2.*

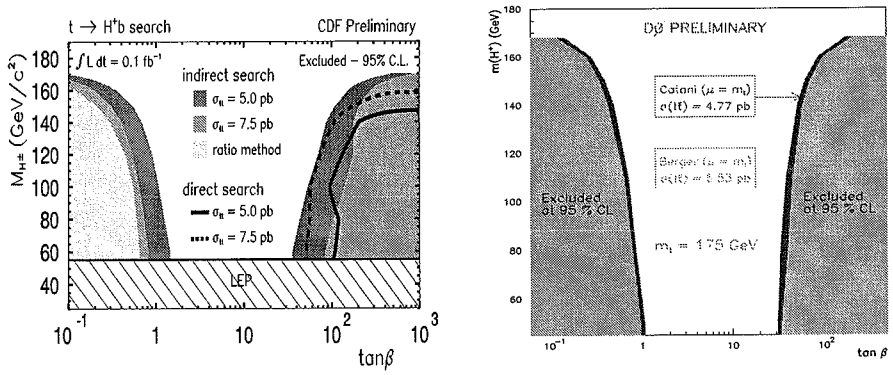

Figure 6.6: *The $H^{\pm}$ mass limits as a function of the* $\tan\beta$ *value obtained by the CDF (left) and D0 (right) Collaborations at the Tevatron (from ref [10]).*

At the Tevatron, charged Higgs bosons can be searched for in top decays $t \rightarrow H^{+}b$ for $M_{H^{\pm}} < m_t - m_b$. Depending on the value of $\tan\beta$ and therefore of the dominant $H^{\pm}$ decay mode the analysis is performed either in the inclusive $t\bar{t} \rightarrow \ell\ell X$, $\ell + Jets$ or in the exclusive channel $t\bar{t} \rightarrow \tau\nu j$. Contrary to the searches at LEP 2, the sensitivity of these channels is limited to the regions $\tan\beta < 1$ and $\tan\beta > 30$. This is evident from the lower mass limits derived from the CDF and D0 Collaborations shown, as a function of $\tan\beta$, in Figure 6.6.

6.2 Additional Constraints to SuperSymmetry from $b \rightarrow s$ *gluon*

While the $b \rightarrow s\gamma$ decay probes possible extensions of the Higgs sector, the bound derived for the $b \rightarrow sg$ rate can be used to set further constraints on SUSY models with enhanced $b \rightarrow s$ contributions. As discussed in Chapter 1, the $b \rightarrow sg$ rate in SM can be expressed at leading order as:

$$\frac{BR(b \rightarrow sg)}{BR(b \rightarrow c\ell\nu)} = \frac{|V_{ts}^* V_{tb}|^2}{|V_{cb}|^2} \frac{2\alpha_s(\mu)}{\pi f(\frac{m_c}{m_b})} |C_{11}^{SM}(\mu)|^2$$

where $C_{11}^{SM}(\mu)$ is the SM Wilson coefficient of the chromomagnetic operator in the operator product expansion. Following [11], it is possible to parametrise the deviations from the Standard Model prediction by introducing the ratio of the effective Wilson coefficient in the process, now also including possible new physics, to its SM value $r_g = C_{11}/C_{11}^{SM}$. The change in the leading order predictions for BR($b \rightarrow s\gamma$) and BR($b \rightarrow sg$) are shown in Figure 6.7 where it is evident that large enhancements of the $b \rightarrow sg$ rate are possible without violating the present constraints on $b \rightarrow s\gamma$ discussed in the previous section. As an example $r_g \simeq 10$ would correspond to BR($b \rightarrow sg$) = 0.07. The generation of a large coefficient of the chromomagnetic operator without affecting the radiative decay rate can be realised in SUSY for flavour changing transitions mediated by a gluino and a squark exchanged in the loop [11]. This requires also flavour non-diagonal entries in the squark mass matrix or flavour non-diagonal LR mixing terms as in the case when the flavour changing interaction is due to a quark-squark-gluino loop.

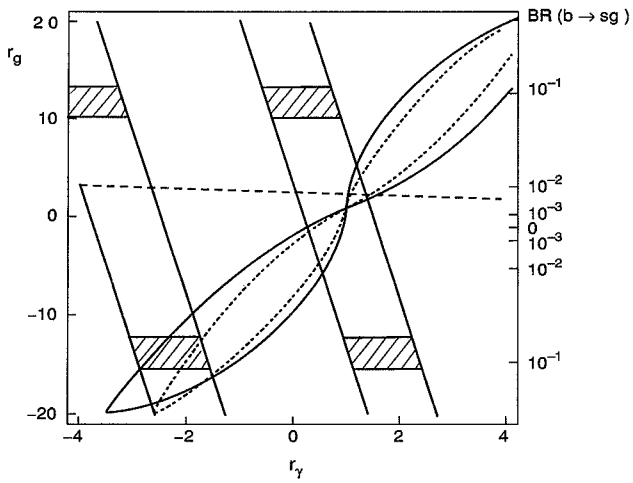

Figure 6.7: *The correlation of the r_g - r_γ enhancement factors. The regions outside the two oblique bands are excluded by the data on $b \rightarrow s\gamma$ decays from CLEO and DELPHI. The two oblated curves delimit the regions allowed in SUSY models with $m_{\tilde{g}} > 200$ GeV/c^2 and $\tilde{m} > 100$ GeV/c^2 (from ref. [11]). The DELPHI results on inclusive hadronic charmless decays exclude the region corresponding to BR($b \rightarrow sg$) > 0.05*

6.3 Constraints on a new $U(1)$ Gauge Boson from $b \to s\nu\bar{\nu}$

The study of rare b decays provides sensitivity to a large variety of models introducing new physics beyond the Standard Model. A different scenario in which new physics can be realised is represented by models seeking to explain the fermion mass hierarchy in a dynamical framework where the large *top* quark mass implies large isospin breaking for the *top* and *beauty* quarks. These models introduce new gauge bosons arising from additional broken symmetries. The lightest of such bosons is expected to be a $U(1)$ boson X coupling predominantly to the third family [12]. The X boson with coupling g_X receives a mass m_X fulfilling the relationship:

$$\frac{g_X^2}{m_X^2} = \frac{G_F}{2\sqrt{2}}. \tag{6.4}$$

Such a model introduces a peculiar phenomenology by shifting the Z^0 couplings to the third family and lowering the $\alpha_s(m_Z)$ value. This has motivated a careful check of its predictions in view of the observed anomaly in the $\Gamma_{b\bar{b}}/\Gamma_{had}$ value and the results on α_s from LEP. An additional gauge boson X coupling predominantly to the third family may enhance $b \to s\nu_\tau\bar{\nu}_\tau$ and $b \to s\tau^+\tau^-$ decays through treel level X emission diagrams [12]. While the $s\tau\tau$ channel is suppressed by phase space, the study of $b \to s\nu_\tau\bar{\nu}_\tau$ can set tight constraints for this class of models. The $b \to s\nu\nu$ decay proceeds in SM through a virtual Z^0 penguin diagram and its rate can be computed with small uncertainties. In fact the non perturbative $1/m_b^2$ corrections have been shown to be small and the decay is not affected by long distance contributions as it is the case for the similar process $b \to s\ell^+\ell^-$. The expected value of BR($b \to s\nu\bar{\nu}$) in SM is 5×10^{-5}. Introducing the new X boson adds a contribution to the Lagrangian given by:

$$L_X = g_X[\lambda_{23}^L \bar{b}_L \gamma^\mu s_L + \lambda_{23}^R \bar{b}_R \gamma^\mu s_R + \bar{\nu}_\tau^L \gamma^\mu \nu_\tau^L] X_\mu \tag{6.5}$$

where $g_X^2 = \frac{G_F m_X^2}{2\sqrt{2}}$ according to (6.4) and $\lambda_{23}^{R,L}$ are the mixing angles between the second and the third generations. The width of the decay $b \to s\nu_\tau\bar{\nu}_\tau$ can be therefore expressed as:

$$\Gamma(b \to s\nu\bar{\nu}) = (|\lambda_{23}^L|^2 + |\lambda_{23}^R|^2)(g_X/M_X)^4 m_b^5/1536\pi^3(1 - \frac{2\alpha_s(m_b)}{3\pi} f(0)). \tag{6.6}$$

To remove the large m_b^5 dependence, the branching ratio can be written in units of the semileptonic decay rate as:

$$\frac{\Gamma(b \to s\nu\bar{\nu})}{\Gamma(b \to ce\nu)} = \frac{1}{8G_F^2|V_{cb}|^2 g(\frac{m_c^2}{m_b^2})}(|\lambda_{23}^L|^2 + |\lambda_{23}^R|^2)(g_X/M_X)^4 \left[\frac{1 - \frac{2\alpha_s(m_b)}{3\pi} f(0)}{1 - \frac{2\alpha_s(m_b)}{3\pi} f(\frac{m_c}{m_b})}\right] \tag{6.7}$$

where the functions f and g can be found in reference [13]. These formulae may be used to obtain constraints on the combination:

$$(|\lambda_{23}^L|^2 + |\lambda_{23}^R|^2)(g_X/M_X)^4. \tag{6.8}$$

Assuming $(g_X/M_X)^2 = G/2\sqrt{2}$ and a ratio of the exclusive $B \to K^*\nu\bar{\nu}$ branching ratio to the inclusive $b \to s\nu\bar{\nu}$ rate of 0.30 [14], an upper bound for the mixing angle $|\lambda_{23}^L|^2 + |\lambda_{23}^R|^2$ of 1.0 $\times|V_{cb}|$ follows from the upper limit obtained for $B^0 \to K^*\nu\bar{\nu}$ (see Figure 6.8), taking $(M_X/g_X) = 1$ TeV this limit becomes 4.0 $\times|V_{cb}|$.

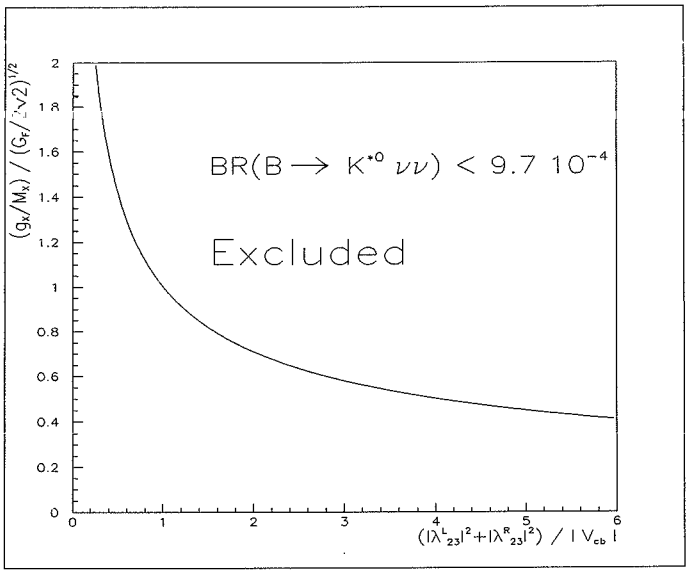

Figure 6.8: *Constrain to a new $U(1)$ gauge boson X from the $BR(B_d^0 \to K^{*0}\nu\bar{\nu})$ DELPHI upper limit. The 90% excluded region in the $(|\lambda_{23}^L|^2 + |\lambda_{23}^R|^2)$ - (g_X/M_X) plane is shown.*

Bibliography

[1] T.D. Lee, *Phys. Rev.* **D 8** (1973), 1226.

[2] S.L. Glashow and S. Weinberg, *Phys. Rev.* **D15** (1977), 1958.

[3] R. Barbieri and G.F. Giudice, CERN-TH.6830/93.

[4] V. Barger, M.S. Berger and R.J.N. Phillips, *Phys. Rev. Lett.* **70** (1993) 1368;
J.L. Hewett, ANL-HEP-PR-92-110.

[5] S. Bertolini, F. Borzumati, A. Masiero and G. Ridolfi, *Nucl. Phys.* **B 353** (1991) 591.

[6] R. Garisto and J.N. Ng, *Phys. Lett.* **B 315** (1993) 372.

[7] F.M. Borzumati, DESY 93-090.

[8] S. Ferrara and E. Remiddi, *Phys. Lett.* **B 53** (1974) 347.

[9] M. Battaglia *et al.* (DELPHI Collaboration), *Search for Charged Higgs Bosons at LEP 2*, DELPHI 98-96 CONF 164, submitted to the ICHEP-98 Conference, Vancouver B.C. (Canada), July 1998 and
P. Abreu, ..., M. Battaglia *et al.* (DELPHI Collaboration), to be submitted to *Phys. Lett.* **B**.

[10] A. Boenheim, *Searches for new phenomena at Fermilab Tevatron*, review talk at the 1997 APS Meeting and
I.A. Bertram, *Search for new phenomena at D0 and CDF*, in Proc. of the HADRON-97 Conference, Brookhaven National Laboratory, August 1997.

[11] M. Ciuchini *et al.*, *Phys. Rev.* **B 388** (1996), 353 and
Erratum, **B 393** (1997), 489.

[12] B. Holdom and M.V. Ramana, *Phys. Lett.* **B 365** (1996), 309.

[13] N. Cabibbo and L. Maiani, *Phys. Lett.* **B 79** (1978), 109.

[14] A. Ali and T. Mannel., *Phys. Lett.* **B 264** (1991) 447.

Conclusions

The study of rare B decays have been the scope of several years of investigations using the data collected with the DELPHI detector at LEP. These investigations relied on the response of the DELPHI apparatus in the detection and identification of leptons, photons and hadrons produced from the decay of Z^0 bosons. Demanding in terms of hadron identification, topological reconstruction of the decay chains of short lived hadrons and decay reconstruction efficiency, the study of rare B decays has promoted the developments of new analysis techniques based on the combined use of the high resolution silicon vertex detector for accurate tracking and the Ring Imaging Cherenkov detector for hadron identification.

The results obtained clarify the present picture of weak decays of B hadrons. The magnitude of the $|V_{ub}|$ element in the CKM quark mixing matrix has been determined to better than 20% accuracy using a new technique based on the inclusive reconstruction of the hadronic recoiling against the lepton in the semileptonic $b \to u\ell\nu$ decay. At present, this is the most precise single determination of the $|V_{ub}|$ element. Establishing the non-zero value of the small $|V_{ub}|$ element is a requisite for explaining CP violation in the framework of the Standard Model. Its precise determination is then essential for testing the origin of CP violation by comparing the values of the CP violating phases in B^0 meson decays with the Standard Model predictions.

Loop induced $b \to s$ hadronic transitions have been observed, thus confirming a significant contribution of penguin diagrams to rare B decays. A detailed analysis of the fraction of candidate decays including identified kaons has provided the first estimate of the relative contribution of penguin loops to tree level mediated charmless B decays. Loop transitions appear to be of the same order as tree level ones. This result has important consequences in the interpretation of the CP violating phases α that will be measured by studying the $B^0 \to \pi^+\pi^-$ decay at B factories. Contributions from both misidentified $b \to s$ decays $B^0 \to K^+\pi^-$ and $b \to d$ decays $B^0 \to \pi^+\pi^-$ will need to be disentangled in the interpretation of those results.

Searches for the other loop mediated $b \to sg$, $b \to s\gamma$ and $b \to s\nu\bar{\nu}$ decays have provided upper limits for the branching ratios of these processes. These limits set significant constraints on several scenarios introducing new physics beyond Standard Model and complement the results from direct searches for new physics at LEP 2 and at the Tevatron, as discussed in Chapter 6.

The start of data taking at dedicated low energy, high luminosity e^+e^- colliders in summer 1999, promises a continuation of the flourishing of studies in B physics beyond the turn of the millennium. These studies aim to establish the CP violation effects in the B system, predicted to be large by the Standard Model, and to study in details the size of the three CP violating phases α, β and γ. This will clarify the origin of CP violation by comparing the first direct measurements of the phases with the Standard Model predictions from the unitarity triangle and will specify the values for $f_B|V_{ub}|$, $|V_{ub}|/|V_{td}|$ and $|V_{ts}|/|V_{td}|$ with high accuracy. In addition, the continuation of the studies on rare B decays like $b \to sg$, $b \to s\gamma$, $b \to d\gamma$, $B^- \to \tau\nu$ will rely on the large data samples that will be recorded at these colliders. The CLEO-III [1] and BaBar [2] experiments, surrounding the interaction regions of the CESR and PEP-II colliders respectively, are all equipped with RICH detectors. This choice has been dictated by the challenging requirements in terms of particle identification of the physics interests and encouraged by the successful exploitation of RICH particle identification in the DELPHI and SLD experiments.

Beyond the reach of e^+e^- B factories, the investigation of CP violation in the B system will be accomplished at hadron machines providing even higher statistics and accessing B_s decays important for the determination of the γ angle. The HERA-B experiment [3] at DESY is presently installing a forward spectrometers for B physics using an internal target in the

HERA proton ring. Further in the future, the LHCb experiment [4] has been recently approved for operation at the CERN LHC collider while the BTeV collaboration has proposed a dedicated B experiment for the C0 interaction region of the Tevatron collider [5]. HERA-B has recently installed its RICH detector on the HERA beam-line, reporting the observation of clean Cherenkov rings. LHCb and BTeV also include RICH detectors in their designs. While the different experimental environment in terms of trigger rates, backgrounds, kinematical and geometrical coverage calls for different technical solutions for the Cherenkov radiators, for the photon detection and for the read-out schemes compared to those adopted by DELPHI, the case for RICH particle identification is the sams and similar are the particle identification algorithms being developed [6]. Therefore the particle detection principles and the analysis techniques pioneered by DELPHI and discussed in these chapters are insured a long lifetime of applications in the effort for improving our knowledge of the fundamental constituents of matter and of their interactions.

Bibliography

[1] The CLEO III Collaboration, *The CLEO III Detector - Design and Physics Goals*, Cornell University, February 1994.

[2] The BaBar Collaboration, *BaBar Technical Design Report*, SLAC, March 1995.

[3] The HERA-B Collaboration, *HERA-B: An Experiment to Study CP Violation in the B System using an Internal Target at the HERA Proton Ring*, DESY PRC 95/01.

[4] The LHCb Collaboration, *LHCb - Technical Proposal*, CERN LHCC 98-4.

[5] The BTeV Collaboration, *BTeV: An Expression of Interest for a Heavy Quark Program at C0*, Fermilab, May 1997.

[6] R. Forty, to appear on *Nucl. Instr. and Meth. in Phys. Res.* **A**.